SATELLITE EVIDENCE OF PHYSICAL FEATURES AND

PROCESSES IN THE BERING SEA

RECOMMENDED:

Chairman, Advisory Committee

Program Head

Director, Institute of Marine Science

APPROVED:

Vice Chancellor for Research and Advanced Study

March 10, 1982

Date

SATELLITE EVIDENCE OF PHYSICAL FEATURES AND PROCESSES IN THE BERING SEA

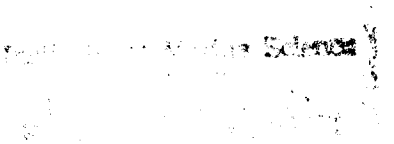

A

THESIS

Presented to the Faculty of the University of Alaska

in Partial Fulfillment of the Requirements

for the Degree of

MASTER OF SCIENCE

By

Theresa Paluszkiewicz, B.S.

Fairbanks, Alaska

May 1982

ABSTRACT

Satellite infrared imagery is used to study temporal and spatial relationships of physical features and processes in the Bering Sea. A two-year collection of enhanced infrared imagery reveals that the maximum extent of the ice corresponds with the location of the Bering Slope current. Sea surface temperature patterns visually correlate with the 50-m and 70-m bathymetric contours. Processes which establish fronts in these regions are possible explanations for this correlation. Warm surface water extending from the Gulf of Alaska, through the Aleutian passes into the Bering Sea, is found simultaneously with warm surface water and eddies along the shelf break. Spatial and temporal relationships of these patterns imply surface circulation in the Bering Sea basin with inflow of Gulf of Alaska water through the Aleutian passes, cyclonic flow in the basin, and flow along the shelf by the Bering Slope current. Several generating mechanisms for the eddies are proposed.

TABLE OF CONTENTS

LIST OF FIGURES

LIST OF FIGURES

(continued)

LIST OF FIGURES

(continued)

LIST OF FIGURES

(continued)

LIST OF FIGURES

(continued)

LIST OF TABLES

ACKNOWLEDGEMENTS

I would like to thank Dr. H. J. Niebauer, Dr. T. C. Royer, Dr. W. S. Reeburgh, and Dr. J. Goering for their advice, encouragement, and support during my study. Also, I would like to thank Kristina Ahlnäs, who taught me a great deal about infrared imagery and gave me moral support and friendship. I also appreciate the help and humor of Dr. W. Johnson and the encouragement of Dr. D. C. Burrell. Mr. G. Hufford of the Anchorage NESS station was helpful in providing data which I referred to in this thesis. Mr. G. White, Mr. D. Sundgren, and Mr. K. Meyer at the Gilmore Tracking Station were extremely helpful, and I appreciate their assistance. Most of all, I would like to thank Frank Flynn, my good friends who kept me rational, Nancy Ricci, the draftspeople, and the people in photographic services, without whom this finished product would not exist.

This study was funded by the National Science Foundation Contract DPP7623340 under the "Processes and Resources of the Bering Sea Shelf" program and by the NOAA Contract NA 795 AC00780 for the study "On the Use of SEASAT-A in Ongoing Fisheries Oceanography Programs in the Bering Sea."

INTRODUCTION

The Bering Sea is an area of increasing economic importance. The shelf area and Bristol Bay support productive fisheries and are also scheduled for oil and gas exploration. In order to preserve this environment and manage its resources properly, it is necessary to understand the circulation in the Bering Sea and adjacent water masses and the related effects on biological and chemical processes. Physical features, such as fronts, currents, and eddies, have been identified by investigators in the PROBES (Processes and Resources of the Bering Sea Shelf) program and other field investigations. It is important to understand how these physical features and processes within the Bering Sea relate in time and space.

The objective of this thesis is to use satellite infrared imagery to study the temporal and spatial relationships of physical features in the Bering Sea. The use of satellite infrared imagery enables one to see, in a "snapshot," sea surface temperature distributions over a large area and identify physical features. In the area of this study, one snapshot can include the area between the Bering Strait to the Aleutian Islands, encompassing the shelf, shelf break, and basin area of the Bering Sea (Figure 1). The infrared satellite imagery are obtained from the advanced, very high resolution radiometer (AVHRR) on board the NOAA-6 and TIROS-N polar orbiting satellites. The images provide a spatial resolution of 1 km and a temperature resolution of ± 1.5°C for absolute temperatures, ± 0.5°C for relative temperatures. This allows coverage of large-scale features and instantaneously shows the

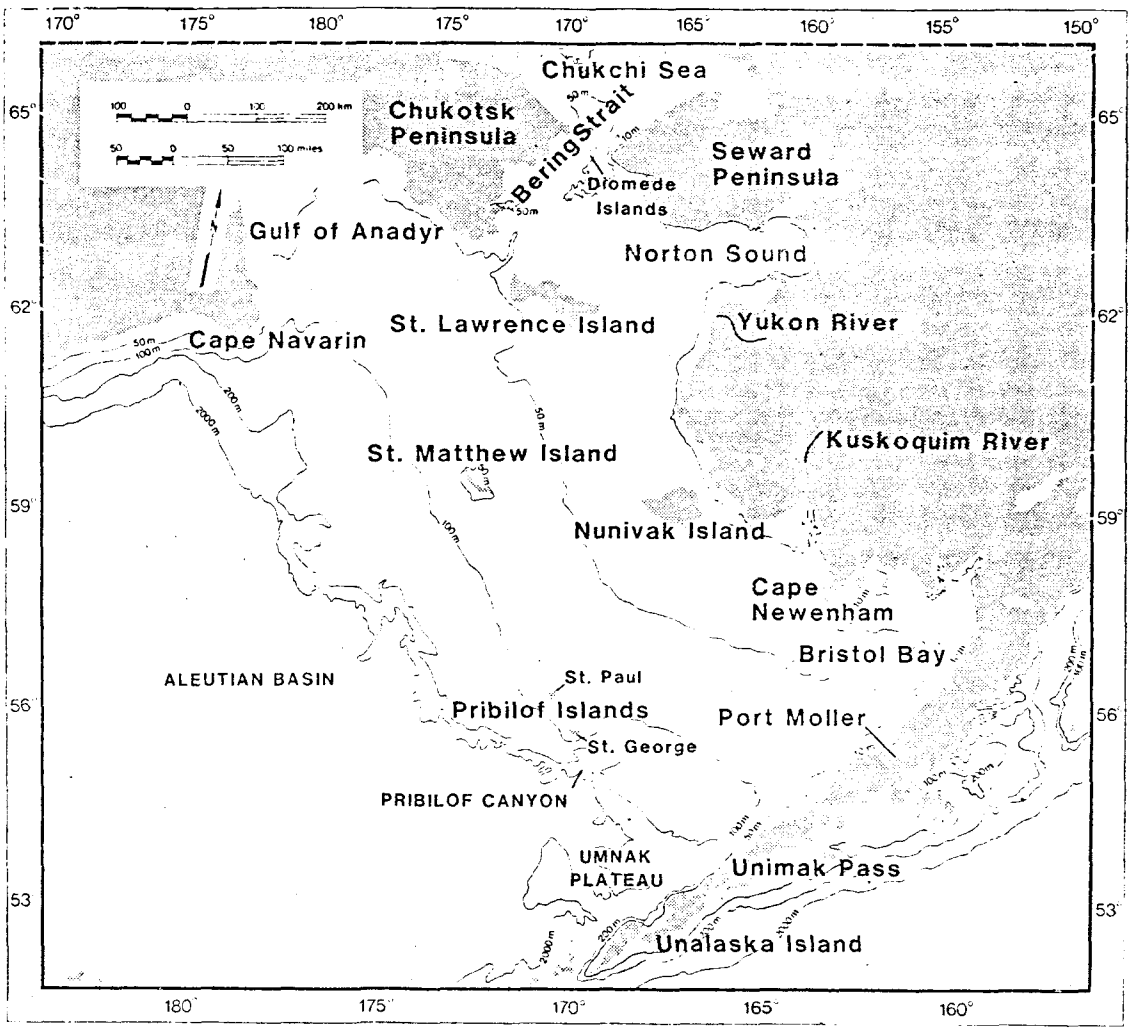

Figure 1. The eastern Bering Sea shelf. From Hood and Calder, 1981.

spatial relationships of surface water features on the shelf and in the basin. Although salinity is normally used in the North Pacific to identify physical processes, surface temperatures, as measured by the satellite, can prove very effective as an indicator of these same processes. The satellite uses many more data points to establish the temperature contours than is generally possible in hydrographic studies and can reveal large-scale features.

In this study satellite data over a two-year period reveals re-occurring features such as ice, fronts, eddies, and a broad warm band of water located in the shelf break region. In turn, there appears to be a spatial and temporal relationship between the warm band, possibly the result of the Bering Slope Current, and the maximum extent of the ice edge. Visual correlations between the fronts on the shelf and fronts in Bristol Bay and isobaths are also apparent. Information from the imagery indicates that the 100 m and 200 m fronts along the 100 m and 200 m isobaths could be a result of mixing with Gulf of Alaska water. The occurrence and location of eddies along the shelf break also appears related to the occurrence of the warm band of surface water over the shelf break. Information from the imagery implies that these eddies may arise from topographic interactions, baroclinic instabilities, or topographic Rossby waves. Relationships implied by the satellite imagery are supported by information supplied in the literature. A background section is included to introduce the information which was used to interpret and help explain the relationships implied by the satellite imagery.

BACKGROUND

Geography

The Bering Sea lies between 52°-66°N and 162°E-157°W. It is characterized by a wide continental shelf in the eastern half, a steep shelf break, and deep basin. The shelf is cut by several large canyons. Figures 2a and 2b show the bathymetry and topographic features of the Bering Sea. The shelf occupies 80% of the Bering Sea with an area of 2.25×10^6 km (Sharma, 1974). It is broad, bordering the Alaskan peninsula and continent, and extends seaward $\sim$ 250 km. The shelf is relatively featureless, except for a few depressions, and is gently sloping and relatively shallow with the shelf break at 170 m. The average slope is $1:10^5$. The topographic contours run generally southeast to northwest.

The continental margin in the Bering Sea stretches 1300 km in length from the tip of the Alaskan Peninsula to Cape Navarin in Siberia, and is rugged and canyon scarred (Scholl *et al.*, 1968). It is on the average 3200-3400 m deep and separates the shelf area from the abyssal plain. The three components of the margin are a flat outer shelf, steep continental slope, and the deeper, more gently sloping seaward continental rise. Scholl *et al.* (1968) divide the margin into provinces; the southeastern province, between Unimak Island to the Pribilof Canyon, has a gradual slope (1°-2°) with a gradual transition at 150-190 m, reaching the abyssal plain at 1800-1900 m. The central province is 720 km in length, and is between the Pribilof Canyon to Pervenets Canyon. Scholl *et al.* (1968) describe this section as

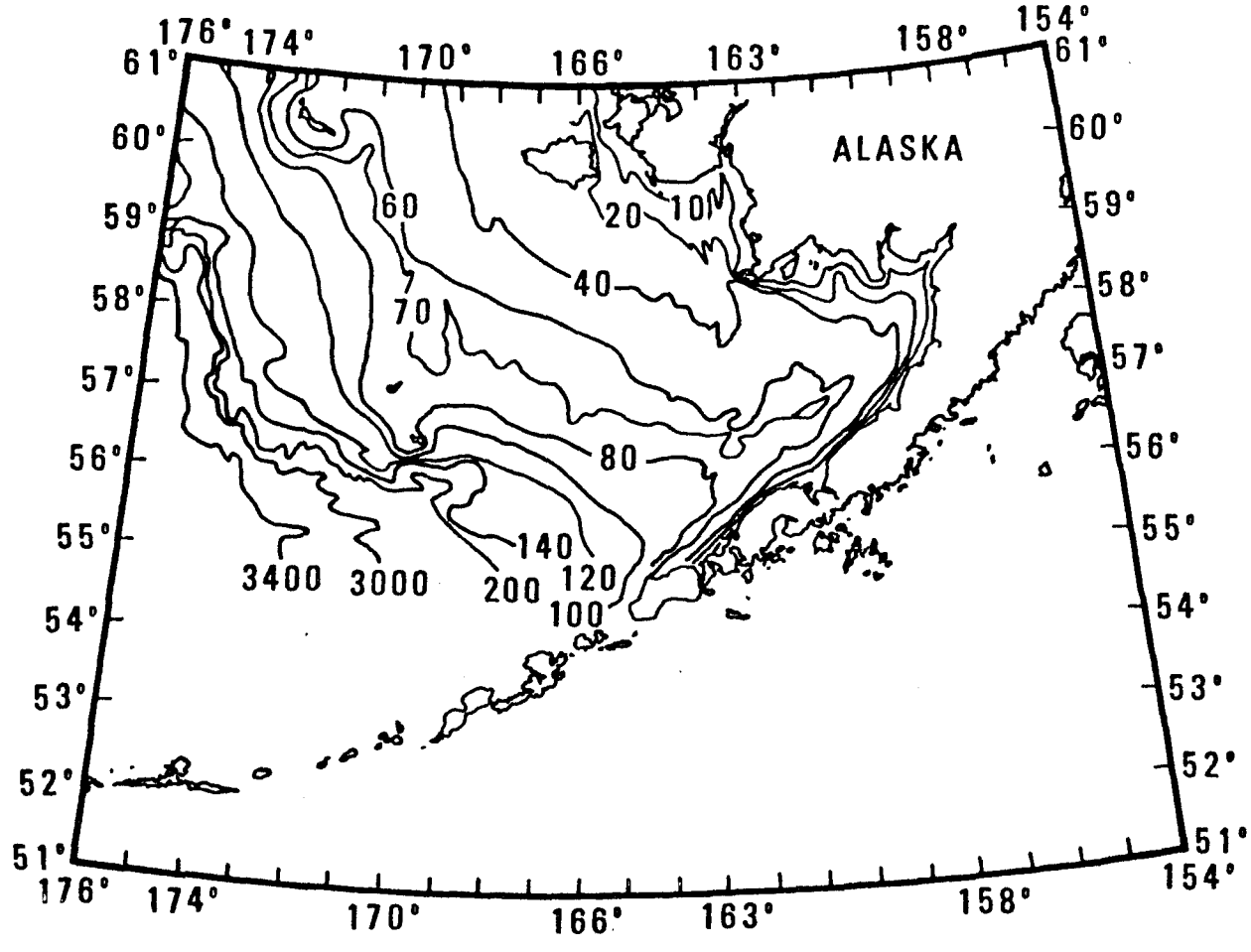

Figure 2a. Bathymetric contours on the Bering Sea shelf — An overlay produced from this map is used to visually correlate features on the satellite imagery with geographic location (reproduced after R. Pratt and F. Walton, National Oceanic Survey).

Figure 2b. Topography of the Aleutian Basin of the Bering Sea (after Scholl *et al.*, 1968).

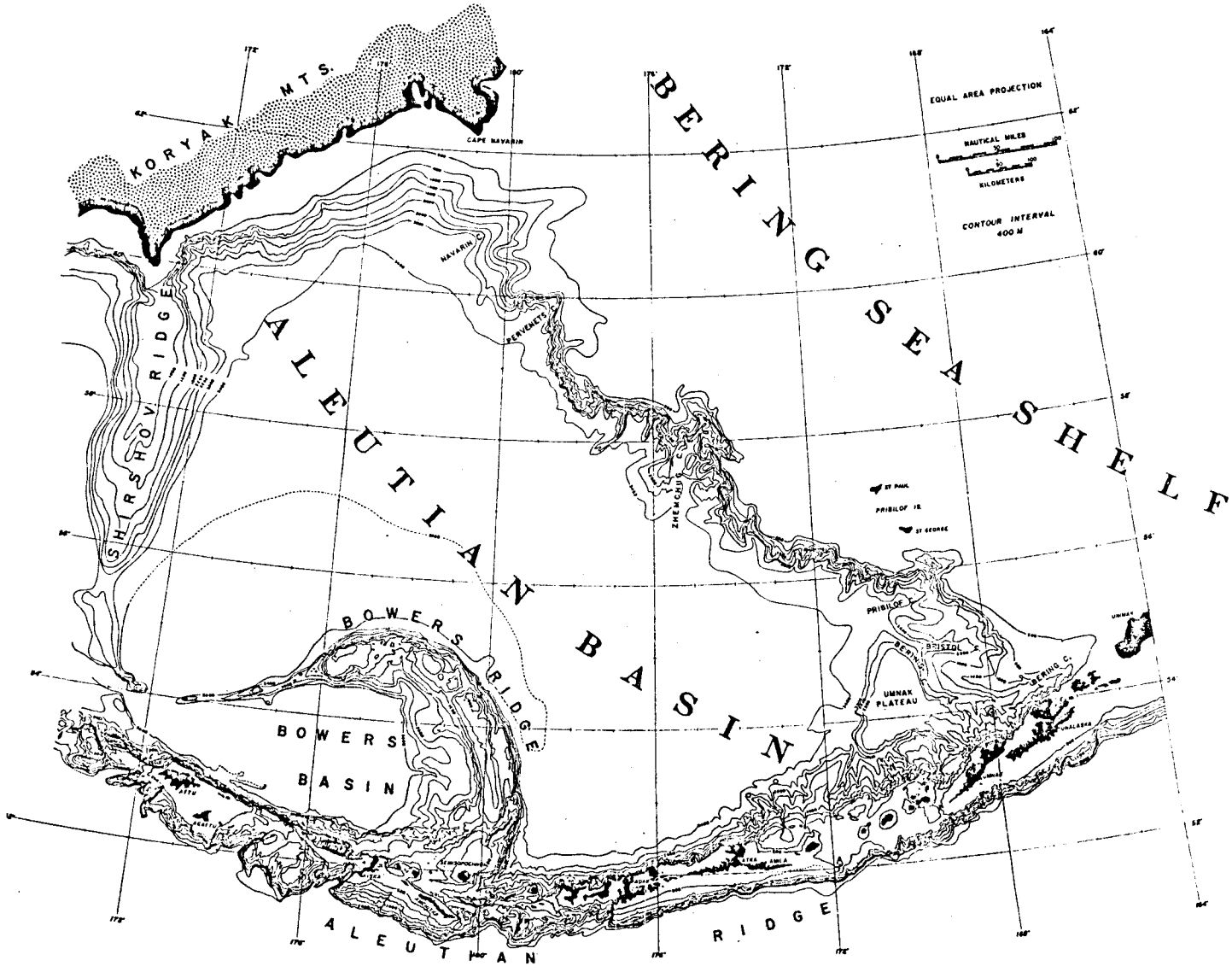
KORYAK MTS.
CAPE NAVARIN
NAVARIN
BERING SEA SHELF
EQUAL AREA PROJECTION
NAUTICAL MILES
KILOMETERS
CONTOUR INTERVAL
400 M
ALEUTIAN BASIN
SHIRSHOV RIDGE
BOWERS RIDGE
BOWERS BASIN
ZHEMCHUG C.
ST PAUL
PRIBILOF IS.
ST GEORGE
PRIBILOF
BERING C.
UMNAK PLATEAU
UMNAK
ALEUTIAN RIDGE

rugged, steep (5°-6°), scarred by canyons joining the shelf abruptly at 170 m merging with the abyssal plain at depths between 3200 m and 3300 m. Most of the canyons start at a depth just below the shelf break.

The Pribilof Canyon, as described by Scholl *et al.* (1968), is one of the world's largest submarine canyons. There is a broad outer-shelf trough formed by a headward bifurcation of the main canyon axis, which is behind the projected position of the shelf edge (Figure 3a). The canyon is approximately 150 km in length and has a volume of 1300 km^3. The trough is oriented northwest, approximately parallel to the line of the continental margin, and is 90 km long, 30 km wide, and 1500 m deep. At the position where it cuts through the projected position of the shelf edge, it is approximately 45 km wide and 1600 m deep. Proceeding westward along the continental slope, the canyon turns west and empties onto the continental rise at a depth near 3000 m.

The Zhemchug Canyon (Scholl *et al.*, 1968) is larger, with a volume of 8500 km^3, but basically is similar to the Pribilof Canyon. The central axis also bifurcates behind the slope face; the trough is oriented northwestward, and is 160 km long, 25-30 km wide, and 2600 m deep. The width of the canyon at the slope face is 100 km and is emptied on the continental rise at 3400 m. Overall, the continental margin provides an abrupt transition from deep (3000-4000 m) basin water to shallow (100-170 m) shelf water. The two canyons which incise the continental slope can be pictured as deep "bay-like" features along the shelf.

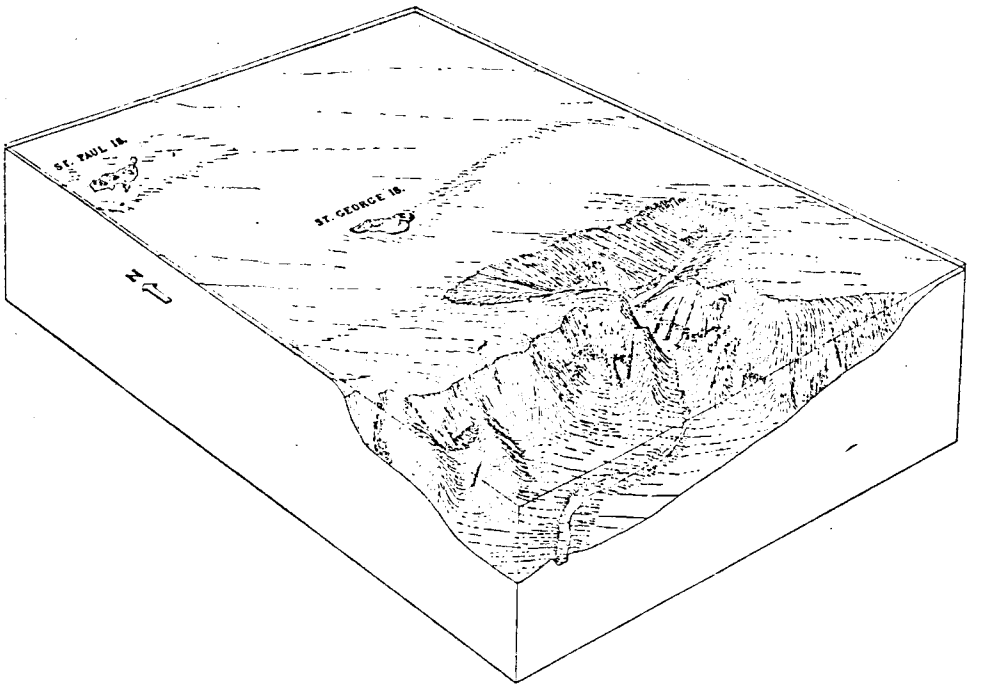

Figure 3a. Physiographic diagram of the Pribilof Canyon: view toward the Bering shelf (after Scholl *et al.*, 1970).

The basin area, known as the Aleutian Basin (Scholl *et al.*, 1968), intersects the continental rise at depths close to 3600 m. The central Aleutian Basin is a flat expanse of sea floor with slopes less than 1: 1000. In the region where the Bering Sea continental slope intersects the Aleutian ridge (Figure 2b) is a continental borderland named Umnak Plateau. Its surface lies between 1800 m and 1900 m (Figure 3b). The Bering Canyon and Bristol Canyon can also be found in the triangle formed by the intersection of the continental slope and the Aleutian ridge. The Bering Canyon is 400 km long and is located near the outer edge of the shelf near Unimak Island. The canyon follows the Aleutian ridge southwestward and then turns and runs below the eastern rim of Umnak Plateau. The canyon is located at a depth of 2800 m and deepens to about 3100 m where the Bristol canyon joins the Bering canyon. The point where these canyons meet the continental rise is only 30 km south of the mouth of the Pribilof Canyon. Another notable topographic feature is Bower's Ridge, located in the southwestern portion of the Aleutian Basin, near the Andreanof Islands. The ridge is a topographic high place located in 1400 m, descending to the basin floor at 3600 m. Other than these topographic features, the Aleutian Basin is a relatively featureless abyssal plain.

Climate

Overland (1981) notes that the marine climatology of the Bering Sea is classified as polar oceanic, meaning a region in which mean monthly temperatures for the warmest month are 10°C or less. The

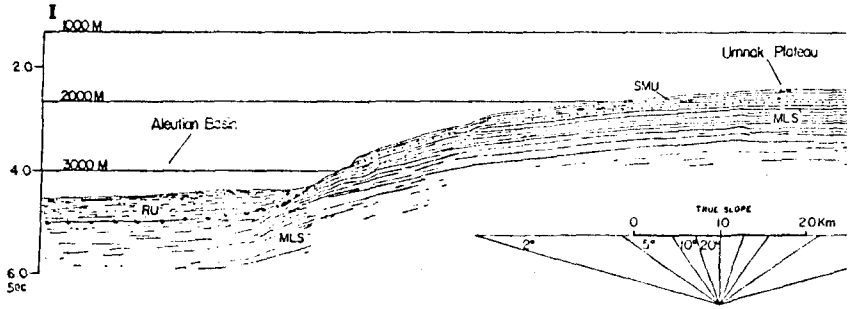

Figure 3b. Umnak Plateau (after Scholl *et al.*,

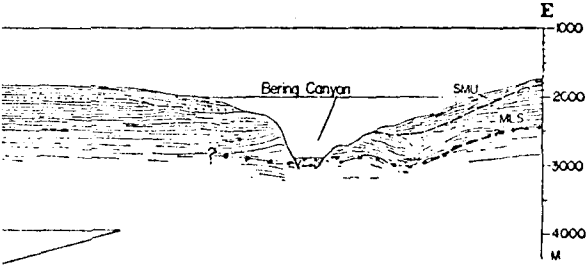

1968).

Bering Sea is affected by arctic, continental, and maritime air masses. In the winter, roughly September-May, the area receives the arctic/continental air which is cold and dry. The type of air overlying is determined largely by the pressure system influencing the Bering Sea area. In winter the Aleutian low is a major influence. Winds associated with this condition are generally greater than 17 knots coming from the north and northeast; the air is generally very dry and cold, and often this is associated with clear weather. Lows in winter are more frequent (4-5 per month) and more intense than summer (3-4 per month). Summer weather can be characterized by the maritime air mass and the warm, moist Pacific air. There is more precipitation, especially in the southern region, and clouds are more frequent. Severe atmospheric fronts can occur when the colder arctic/continental air mass and the Pacific air mass meet, but generally summer storms are less intense, and wind speeds are more moderate than in winter.

Winter weather conditions appear to be of importance in influencing sea surface temperature (SST) (Niebauer, 1981) and circulation (Hughes *et al.*, 1974). Niebauer (1981) related fluctuations in environmental conditions to fluctuations in SST. A rise in SST from 1974-1978 correlates well with increased southerly flow bringing in warmer air from the Pacific. In 1967-1971 a decrease in SST was noted and correlated with flows from the arctic into the Bering Sea. Niebauer (1981) proposed that heat gains and losses were primarily through air-sea interaction. Correlation between June shelf bottom temperatures, freezing degree days of the previous winter, and between mean winter cloud cover

with mean winter north-south wind components indicated that fluctuations in mean winter circulation drives the year-to-year fluctuations in SST.

Hughes *et al.* (1974) noted that the primary source of relative vorticity in the Bering Sea Basin is the torque generated by wind. The curl of the wind stress is then in balance with the advection by planetary vorticity. Hughes *et al.* (1974) calculated the Sverdrup transport (ratio of wind stress curl to variation with latitude of the Coriolis parameter) and noted an annual variation related to wind torque, with the Sverdrup transport being an order of magnitude greater in winter than summer. They also note that there is a predominant anticyclonic wind torque in the summer. In winter, there is a cyclonic wind torque due to the Aleutian Low. Hughes *et al.* (1974) believes that the intensification of atmospheric circulation in winter is related to the intensification of the winter circulation of water in the western Bering Sea.

The atmospheric circulation in the Bering Sea is thought to be an important controlling factor in the formation and movement of sea ice in the Bering Sea (Muench and Ahlnäs, 1976; Niebauer, 1981). The ice in the Bering Sea extends from the Bering Strait to near the shelf break at its maximum extent, a meridional variation of 1000 km. The ice is generally 0.5 m thick except when ridging occurs. The formation of ice occurs primarily by *in situ* freezing rather than advance through the Bering Strait. Muench and Ahlnäs (1976), Ahlnäs and Wendler (1977), Niebauer (1980, 1981) noted that ice and its movements are relationed to climatic variables; for example, Muench and Ahlnäs (1976) found that

local ice movement was due to variations in wind. They also believed that the Bering Slope Current played a role in heat transfer, and this was a possible reason for maintaining a relatively constant position of the ice edge at the southern boundary.

Hydrography

Kinder and Schumacher (1981) categorize and describe the various domains within the eastern Bering Sea (coastal, middle, and outer) (Figure 4a) largely by their horizontal structure and vertical dynamics (Figure 4b). The coastal domain is homogeneous to a depth of 50 m, which is equal to approximately the thickness of the tidal mixed layer. Schumacher *et al.* (1979) describe the front, which defines the boundary of this domain, as the front coinciding with the 50-m isobath, the width is approximately 10 km wide. This front, known as the inner front, separates the homogeneous coastal domain from the two-layer middle domain. Schumacher *et al.* (1979) refer to the inner front as a structural front to emphasize the change in vertical structure between the two domains. The temperature ranges between 8 and 12°C. In winter 60% of the area is covered by ice. The salinity is generally low ($< 31.5°/_{oo}$) during most of the year and is influenced by river runoff from the Kuskokwim and Kvichak Rivers. Periods of higher ($> 32°/_{oo}$) salinity can be found during winter as the ice forms and brine drainage occurs.

Both Schumacher *et al.* (1979) and Kinder and Schumacher (1981) point out that mean advection in the coastal domain is negligible,

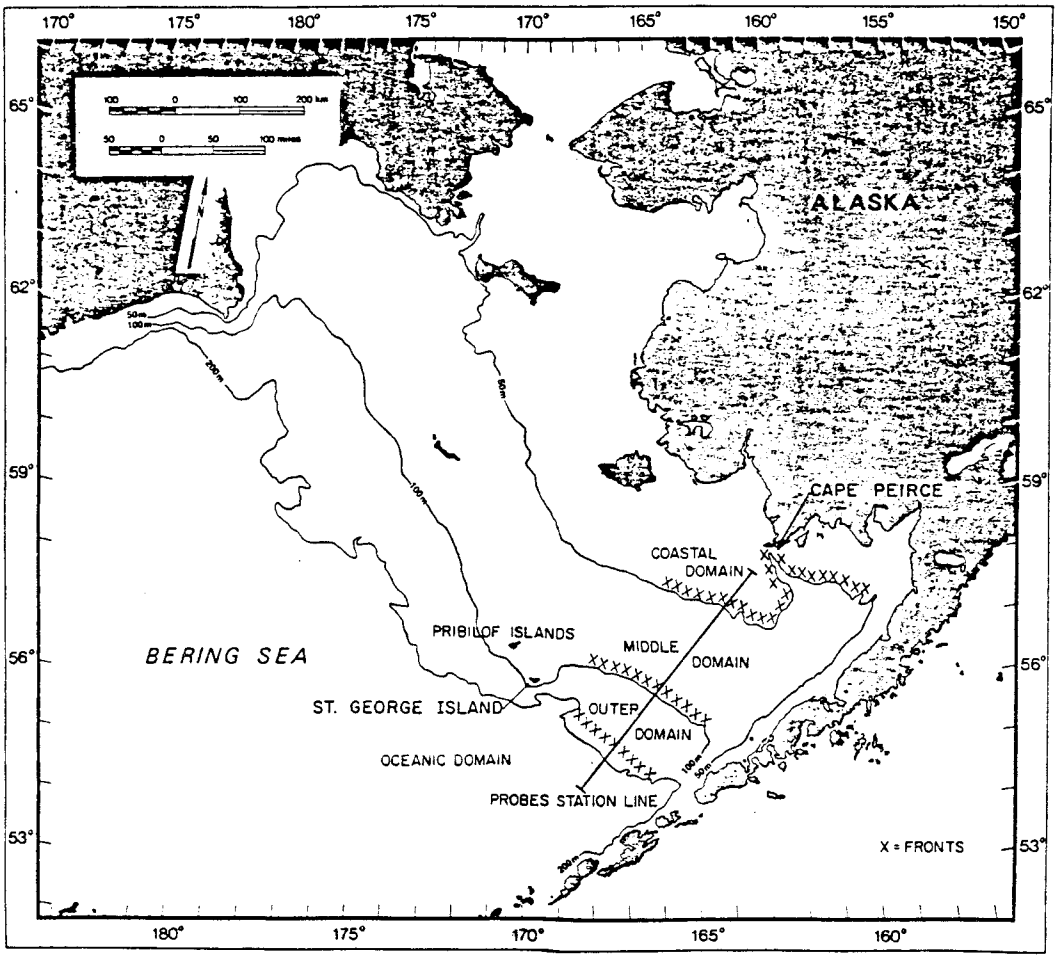

Figure 4a. Approximate boundaries separating the three shelf (coastal, middle, outer) and oceanic hydrographic domains. The boundaries are three fronts which roughly coincide with the 50 m, 100 m, and 200 m isobaths (Kinder and Schumacher, 1981).

Figure 4b. Schematic of hydrographic domains in the Bering Sea (after Iverson *et al.*, 1979).

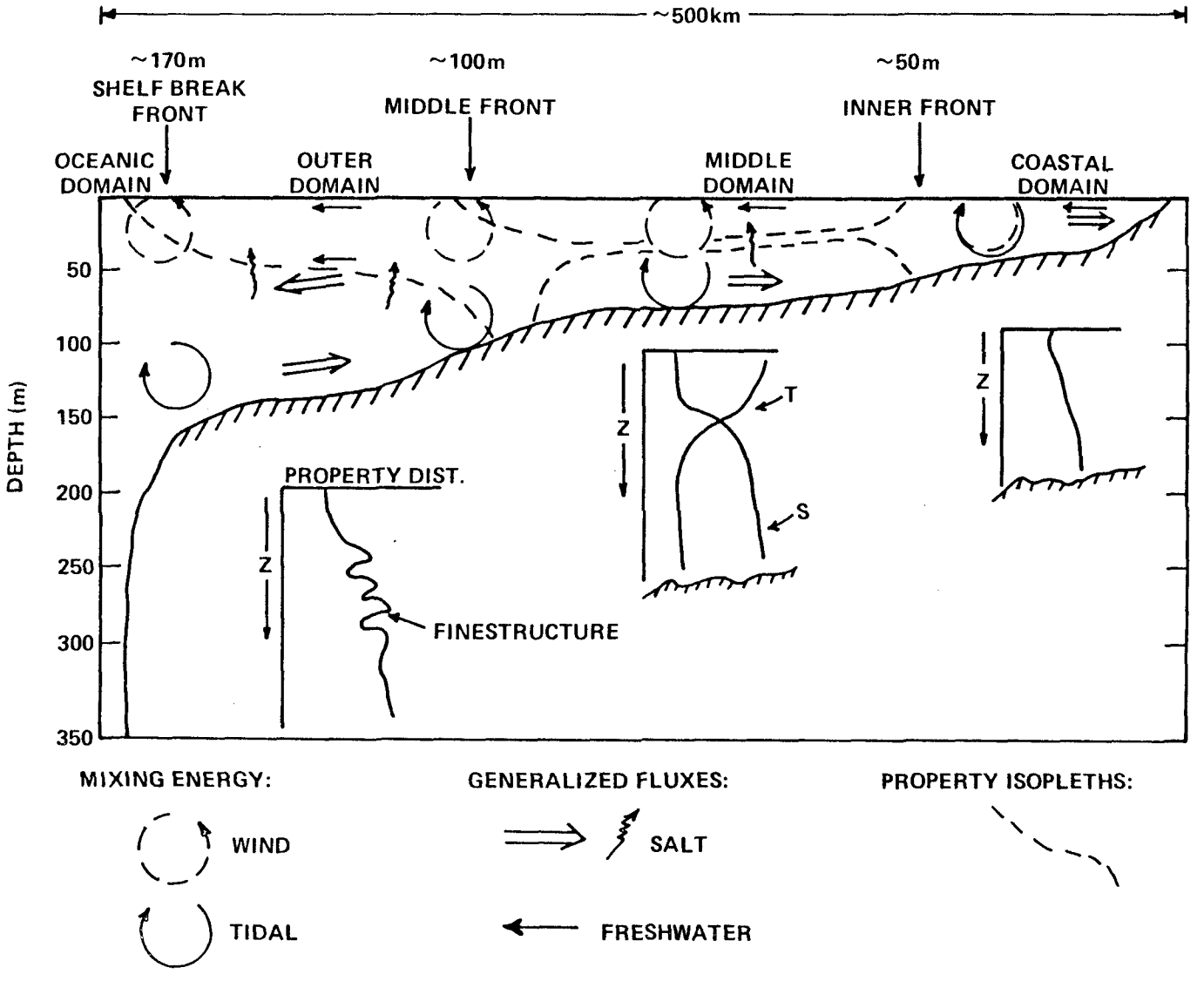
~500km
~170m
SHELF BREAK FRONT
~100m
MIDDLE FRONT
~50m
INNER FRONT
OCEANIC DOMAIN
OUTER DOMAIN
MIDDLE DOMAIN
COASTAL DOMAIN
DEPTH (m)
50
100
150
200
250
300
350
PROPERTY DIST.
Z
FINESTRUCTURE
Z
T
S
Z
MIXING ENERGY:
WIND
TIDAL
GENERALIZED FLUXES:
SALT
FRESHWATER
PROPERTY ISOPLETHS:

and the vertical profile is determined by the interplay of buoyancy and mechanical stirring. In this area tidal mixing reaches from the bottom to the surface and is responsible for the homogeneous vertical structure. The freezing and melting of ice, river input, and radiative transfer are the primary processes which affect the hydrographic structure in the coastal domain. By comparing buoyancy addition (through melting ice, insolation, etc.) to the stirring term (a function of depth and position on the shelf), Schumacher *et al.* (1979) and Kinder and Schumacher (1981) find a ratio between potential energy addition to turbulent energy available equal to a constant times U^3/h where U is the tidal current, and h is the depth. The inner front remains close to its position over the 50-m isobath by the variation of U^3/h.

Seaward of the inner front is the middle domain which extends from the 50-m to the 100-m isobath. The middle domain has been described (Kinder and Coachman, 1978; Schumacher *et al.*, 1979; Coachman and Charnell, 1979; and Kinder and Schumacher, 1981) as a two-layered, strongly stratified region. Within the middle domain the bottom mixed layer is $\sim$ 50 m, and the surface mixed layer is 20-40 m thick. The strongest stratification occurs where these two mixed regions meet. A front, termed "the middle front" (Figure 4a), occurs near the 100-m isobath. This front is described by Kinder and Coachman (1978) as broad and not well defined. Near the 100-m isobath they found the front in temperature, particulate and chlorophyll *a* concentrations with somewhat weak density and salinity gradients.

The water within the middle domain is highly stratified, with low bottom temperatures, even throughout the summer. Bottom temperatures range from -1 to 3°C; vertical heat transfer, and hence warming of the bottom region, is impeded by stratification. The upper layer, $\sim$ 10-30 m deep, warms up to $\sim$ 10°C (the temperature seems to correspond with the severity of the previous winter). This should also be true of the bottom layer. The salinity is generally 31.5 g kg^{-1} and varies < 0.5 g kg^{-1} from top to bottom according to Kinder and Coachman (1979). The cross-shelf gradient is $\sim$ 2.5 x 10^{-3} g kg^{-1} km^{-1} increasing seaward. In spring, melting from ice, vigorous wind mixing, and insolation contribute to the stratification of the region. Melting ice has also been observed in the winter (Kinder and Schumacher, 1981) which again aids stratification, forming a shallow layer near freezing ($\sim$ -1.7°C) overlying a more homogeneous layer. Tidal stirring and wind mixing are the primary turbulent forces in this domain. The outer domain (Kinder, 1976; Kinder and Coachman, 1978; Coachman and Charnell, 1979; and Kinder and Schumacher, 1981) is found seaward of the 100-m isobath (Figure 4) over the shelf break (170-200 m). A weak haline front which separates the outer domain from the oceanic domain occurs over the shelf break. The width of this front is similar to the width of the outer domain itself. A change in the horizontal salinity gradient exists which extends from approximately zero over the deep basin to about 4 x 10^{3} g kg^{-1} km^{-1} over the outer shelf. The outer domain is characterized by finestructure, the layering of vertical profiles on scales from 1 to 25 m. This finestructure occurs

in the mid-water column, between the region mixed at the surface by wind and the bottom tidally-mixed layer. Coachman and Charnell (1979) described the lateral water mass interaction of similar density waters which is believed to be the reason for the finestructure. Warm, salty Bering Sea/Alaska Stream water intrudes shoreward while cooler, fresher shelf water extends seaward. The finestructure is the evidence of this meeting and mixing. Other indications of the outer front are isopycnals which extend from the shelf to intersect the sea surface above the slope as do the other isolines which slant down beneath the front.

Within the outer domain the water column is characteristically stratified with a mixed surface layer, stratified middle layer, and mixed bottom layer. The temperature structure in this region is relatively cold and homogeneous in the winter. In the summer, the surface layer warms and overlies the cold bottom water. The temperature range through the water column is from 3 to 6°C and varies regularly to constant values at depth. The salinity is between 32.0 and 33.2 g kg^{-1}. The shelf water is usually less saline and the adjacent, saltier oceanic water is found below 30 m. The front and hydrography of the region are influenced by the interaction of the oceanic and shelf water masses, and the Bering Slope current has a 2-10 cm/sec flow in the outer domain.

Seaward of the shelf break front at 200 m is the oceanic domain (Figure 4). The oceanic domain can be thought of as including not only the water immediately adjacent to the shelf break but also those water masses found along the Aleutian Chain and in the deep basin. Takenouti and Ohtani (1974) describe the water masses in the Bering Sea basin by

categorizing them according to vertical structures in salinity and temperature. They indicate that the water along the shelf break, yet seaward of the shelf break front, is essentially two-layered with surface and intermediate water temperatures much warmer than other areas in the basin and a salinity gradient which is fairly homogeneous. The authors speculate that the water is formed by mixing of Alaska Stream water and Bering Sea water as it flows over the complex bottom topography of the Aleutian Passes. Takenouti and Ohtani (1974) show water characteristics along the Aleutian Chain that are similar to those along the shelf break. Water characteristics along the Aleutian Chain are also discussed by Reed and Taylor (1965). They describe the Alaska Stream near 175°W (near Atka Island) as having warmer (> 4°C) temperatures and low salinity (< 32.6°/$_{oo}$) at the surface. Favorite (1967) reports the presence of a temperature maximum station (> 4°C) at 150 m and quotes Plakhotnik (1965), who has reported the presence of this warm water in both winter and summer and assumes it is a relatively permanent feature. Favorite (1974) shows a temperature distribution (Figure 1.10, pg. 19, Favorite, 1974) at 100 m which identifies Alaska Stream water in the Aleutian passes.

Circulation

Major reviews of circulation in the Bering Sea are presented in Hood and Kelley (1974) and Hood and Calder (1981). This section covers a brief overview of the circulation on the shelf, over the shelf break, and in the Aleutian basin.

The Shelf Circulation

Kinder and Schumacher (1981) discuss the circulation in the three distinct regimes which correspond to the hydrographic domains presented earlier. Figure 5 shows an overall view of these domains and the proposed circulation. The coastal regime is that area inshore of the 50-m isobath. Eighty percent of the energy in that region is tidal, mostly in the semidiurnal frequency. Tidal speeds are about 20-25 cm/sec. In general, the mean flow parallels the isobaths along the front with speeds from 2-5 cm/sec. According to Kinder and Schumacher (1981) this flow is driven by a pressure gradient. The dynamic method gives good correlation with the currents derived from the current meters and satellite tracked drifters, hence the flow can thus be inferred by the density structure. Additional analysis by Kinder and Schumacher (1981) demonstrate that subtidal energy in this regime is due mostly to meteorological forcing.

In the middle shelf domain (Figure 5), ninety percent of the energy is also tidal. The mean flow is generally less than 1 cm/sec over the middle shelf and is generally parallel to the isobaths. Energy with subtidal frequencies are again related to wind events.

In the outer shelf domain 60-70% of the energy is tidal, 1% is inertial. The mean flow is northwestward, along the shelf break at 5-15 cm/sec and is said to be in geostrophic balance (Kinder and Schumacher, 1981). Subtidal energy in this regime is most probably associated with variations in the Bering Slope Current rather than in local weather.

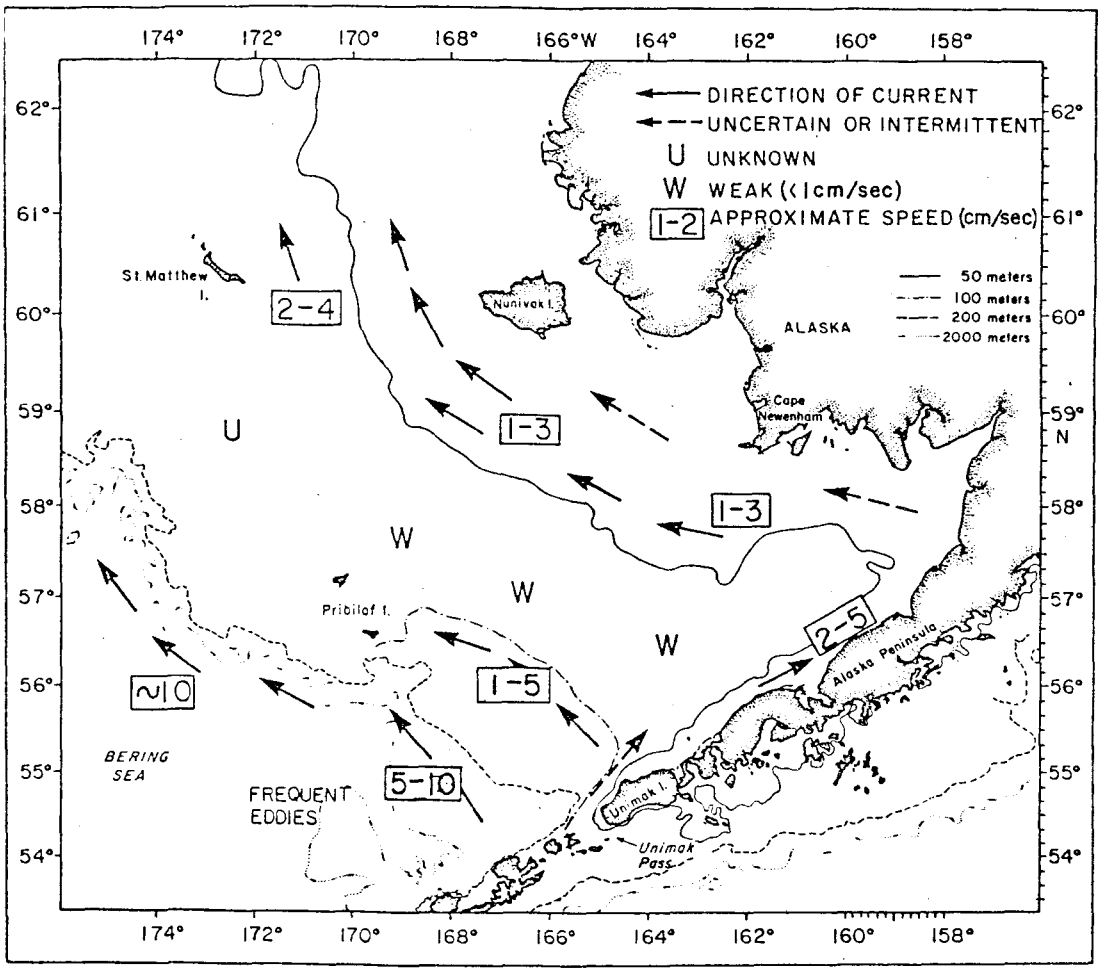

Figure 5. Schematic of currents in the Bering Sea (after Kinder and Schumacher, 1981).

The Bering Slope Current

The Bering Slope Current is described by Kinder and Coachman (1975) and Kinder (1976) as a three-banded current much like an eastern boundary current. The current follows the shelf-break with a band (nearest the shelf) flowing southeast to northwest, a second band flowing toward the southeast, advecting colder, fresher water from the western basin and finally a third band, flowing toward the northwest. Velocities of the current are maximum at 150 m and 750 m depths and are generally 25 cm/sec. Velocities decrease as one moves offshelf. The salinity increases with depth, and the south and southeast region is more saline than the north and northwest. In August, the surface to approximately 30 m is 7-10°C except for one area near 172°-173°W longitude which is 5°C. Subsurface, there is a temperature minimum at 50-200 m of 2-4°C. In October the surface layer to approximately 50 m is approximately 4°C. The horizontal temperature distribution is described by Kinder (1975) as a tongue of higher temperature water from 164-170°W, while colder water in this layer lies on either side, over the continental shelf and well off the shelf. The surface layer (0-50 m), which is between 7-10°C, is believed to be created by summer heating; the subsurface layer (50-200 m) with a temperature minimum of (1-3°C), is formed locally in the winter by convection; and below (250-500 m) there is a uniform layer in temperature and salinity. The deepest layer has small increases in salinity and decreases in temperature with depth, and is believed to be advected through the deepest passes.

The current velocities and directions which were studied through the use of subsurface current drogues and hydrography are in good agreement with geostrophic calculations done by Kinder (1976). The current drogues reveal a westbound current close to the continental slope following isobaths. Some on-off shelf flow is indicated by the drogues with offshelf flow at 150 m and on-shelf flow at 750 m at speeds of about 6 cm sec^{-1}. Kinder (1976) considered this insignificant since estimated velocity errors were about (+5 cm/sec). The banded pattern of the current also revealed at depth with the geostrophic calculations agreeing with the drogue measurements and the water mass properties.

Net transport of the current was found to be 5×10^6 m^3 sec^{-1} to the northwest with a smaller transport by the counter current. Kinder (1976) proposed that the near-shelf band is permanent, and closely associated with the outer frontal domain while the off-shelf band and counter current are neither permanent nor continuous. He maintains that the secondary circulation due to the front helps maintain baroclinic compensation forced by the cyclonic wind stress curl over the basin. Kinder (1976) also proposes that the variation of wind stress causes Rossby waves, which impinge upon the shelf break resulting in variability in the velocity field.

The Basin Circulation

Hughes *et al.* (1974) presents a review of previous work in the western Bering Sea and proposes generally cyclonic surface circulation

with inflow and outflow through the Aleutian Passes (Figure 6). Included in their scheme are arrows indicating the along slope current (Bering Slope Current) and small gyres near the Unmak Plateau. Hughes *et al.* (1974) believes the curl of the wind stress is responsible for establishing flow in the western Bering Sea and Kamchatka Strait and shows that it intensifies in winter. Hughes *et al.* (1974) and Favorite (1974) both speculate that an increase in winter winds intensifies flow into and out of the Bering Sea. Takenouti and Ohtani (1974), Favorite (1974), and Hughes *et al.* (1974) all point to a major inflow to the Bering Sea through the four western passes including the Commander-Near Strait, Amchitka Pass, and the Kamchatka Strait from the Gulf of Alaska. Some flow is indicated in the northern Aleutian Passes by Hughes *et al.* (1974). Takenouti and Ohtani (1974) believe half the volume transport of the Bering Sea enters through the Aleutian Passes and the rest through a pass near Attu. The source of water entering the passes is believed to be the Alaska Stream. Takenouti and Ohtani (1974) show a distribution of various vertical structures found in the western Bering Sea which implies this inflow.

Eddies

Eddies and gyres of dimensions on the order of 100 km have been inferred by the dynamic topographics of Arsen'ev (1967), Ohtani (1973), Hughes *et al.* (1974), and Favorite and Ingrahan (1972) for the deep Bering Sea. Kinder *et al.* (1980) provide a summary of the recent

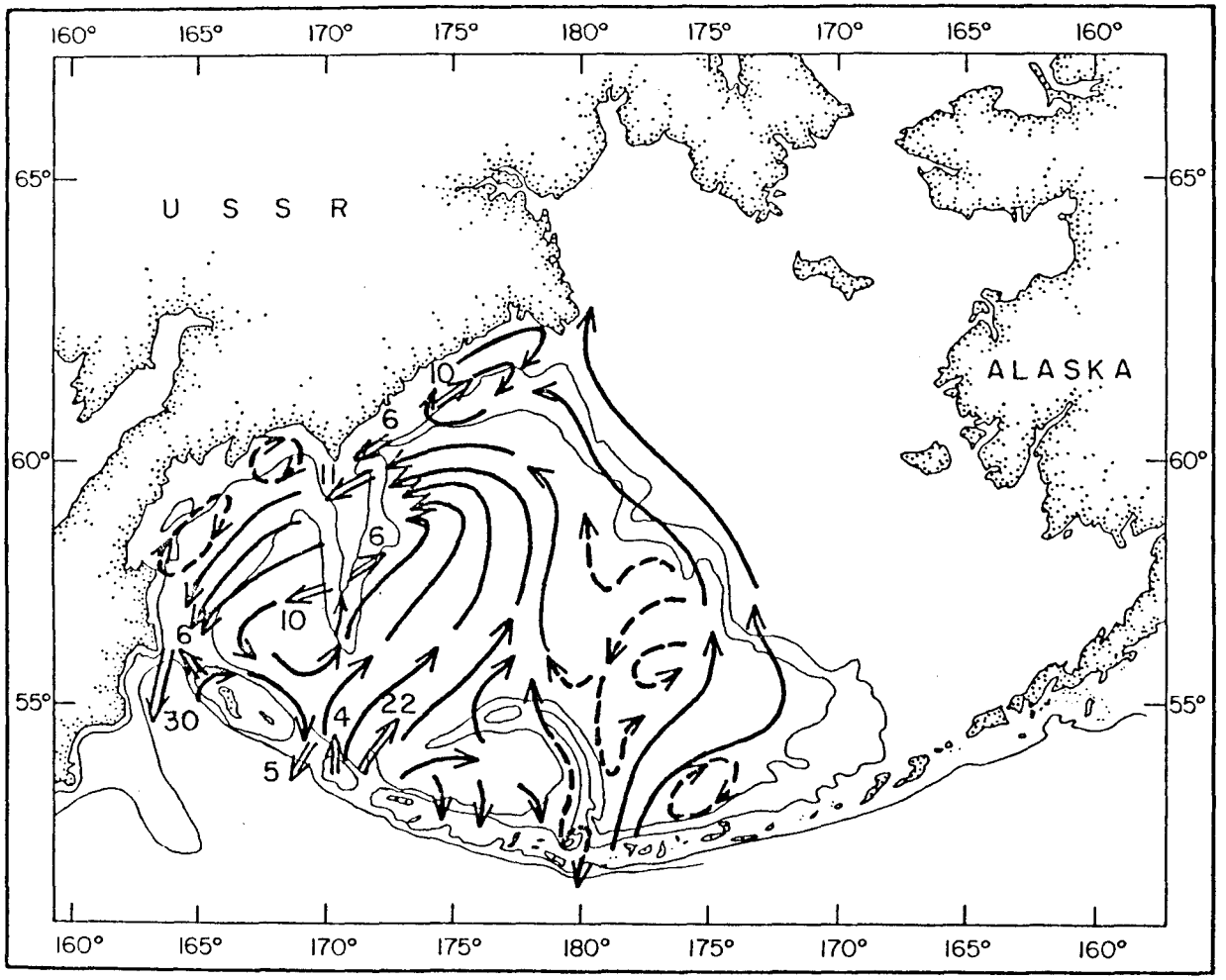

Figure 6. Proposed surface circulation in the Aleutian Basin; ——> certain, ----> less certain, ⟹ measured flow (cm/sec) (after Hughes *et al.*, 1974).

evidence of eddies in the Bering Sea, which includes eddies along the continental slope in August 1972 described by Kinder *et al.* (1975), a cyclonic current ring near the Pribilof Canyon in July 1974 described by Kinder and Coachman (1977), vortices east of Kamchatka in January 1976 and June 1977 described by Solomon and Ahlnäs (1978), and a cyclonic eddy in the eastern Aleutian Basin in July 1977, May-October 1977, as described by Kinder *et al.* (1980).

Kinder (1976) and Kinder *et al.* (1975) describe a system of high and low pressure cells in August 1972 along the continental slope, revealed by dynamic topographies. This system of pressure cells is revealed by a STD survey and drogue study of the Bering Slope. Kinder (1976) interprets the cells as the result of a combination of barotropic Rossby waves incident upon and reflected from the continental slope. The hydrographic data indicates an anticyclonic eddy located near the Unmak Plateau, a cyclonic eddy in Zhemchung Canyon, and another anticyclonic eddy further west of Zhemchung Canyon.

In July 1974, hydrographic data shows a large elliptical cyclonic cell (100 km in diameter) over the Pribilof Canyon which Kinder and Coachman (1977) believe was formed in a manner similar to current rings observed elsewhere. The cell is revealed by salinity distributions which become more pronounced as the water depth increases and shows typical basin water in the core and slope water in the outer portion. Dynamic topographies show the cell located in the outer Pribilof Canyon, seaward of the inner branch of the Bering Slope Current. The vertical extent of the cell is 1000 m, and the maximum geostrophic

speeds are about 30 cm sec^{-1}, average speeds are less than 20 cm sec^{-1}. The geostrophic speeds are calculated relative to 1100 db, and current meter data supports the geostrophic balance calculated from the density field.

Kinder and Coachman (1977) compare this cell to those rings formed when a meander is pinched off. They find the characteristics very similar. The cell retains the sense of rotation of the meander, and trapped water in its core from the opposite side of the current. The authors discuss how the northwest band of the Bering Slope Current closely parallels the bathymetry and curves cyclonically into the Pribilof Canyon. They suggest this forces the current to meander and restrains the ring once it separates. They proposed this same mechanism for Zhemchung Canyon, yet found no ring, only a meander with a high salinity core. Kinder and Coachman (1977) propose that the internal radius of deformation, calculated from the fastest growing baroclinic instability, would cause a meander of dimensions which closely matched the width of the Pribilof Canyon, but not the Zhemchung Canyon. It is also proposed that the ring was not a permanent feature but might re-occur.

Another eddy was found in July 1977 in the Bering Sea (Kinder *et al.*, 1980), which was defined by satellite tracked drifter buoys with drogues at 17 m. Hydrographic data shows evidence of the eddy at 200-1500 m in salinity and temperature measurements. The authors note that no surface signature of the eddy was found. The drifters indicated the eddy was located near 55°00'N and 169°30'W. The hydrography confirms

the location showing the cell centered near 54°54.7'N and 169°24.8'W, a location off the continental slope, slightly southeast of the Pribilof Canyon. Hydrographic data reveals the eddy had a cooler, saltier core and that the different salinities and temperatures correspond to isotherms and isohalines vertically displaced approximately 100 m. The T-S correlation for this cell compares favorably with the cells seen in 1972 and discussed by Kinder *et al.* (1975) and Kinder (1976), but is different from the eddy seen in 1974 that was believed to be formed by entrapment.

The dynamic topographies and drift tracks indicate a cyclonic flow of a smaller feature. Maximum speeds were 16 cm sec^{-1} at the 10/1500 db level computed by the geostrophic method. These speeds were compared with speeds computed from drifter tracks, which were consistently higher, with the mean speed 14 cm sec^{-1}. The authors attribute speed difference to the choice of reference level and method of choosing drifter trajectories. Kinder *et al.* (1980) suggest that likely eddy-generating mechanisms include current instability, direct wind forcing, and topographic interaction but were unable to arrive at a definite generation scheme.

METHODS

The major data set used in this study are visible, infrared, and enhanced infrared satellite images. Surface temperatures, hydrographic information, and meteorological data are also used to aid in interpretation of the satellite images and to be used as "surface truth" information. The method of analysis of the satellite imagery was visual inspection of the satellite imagery for features apparent through film density differences which represent temperature differences. Negatives were analyzed with a densitometer to confirm the existence of the density differences, hence temperature differences. In this section, a description of the methods of data acquisition, interpretation, and analysis are given along with the accuracy, precision, and representativeness of satellite imagery.

Infrared Satellite Imagery

The satellite data used here are from the visible and thermal infrared region of the electromagnetic spectrum. The visible region is 0.55-0.90 μm, the near infrared is 0.725-1.10 μm, and the thermal infrared region between 2.5 and 14 μm. Infrared sensing utilizes the properties of matter above absolute zero, which causes it to emit radiation in the infrared band of the electromagnetic spectrum. The quantity and wavelength of radiation depends largely on the nature of the surface emitting radiation or emissivity. The bands from 10.5-12.5 are most useful for sensing sea surface temperature. Emittance from surface objects varies with time of day and season due to

differential heating. Water, which has a high thermal inertia, warms and cools slowly and consequently has a small diurnal range but a large seasonal range. Land has a low thermal inertia and hence a large diurnal range. The time at which an area is sensed also contributes to the quality of imagery; night and early morning images provide the best thermal contrast because the surface material is responsible for the temperature reradiated, and interference from incoming radiation is minimal. Interferences due to the gases, particulate matter, and water vapor content of the atmosphere are also factors to be considered but will be discussed later in this section. Additional details about infrared radiative properties can be found in Reeves *et al.* (1975).

The images used in this project are from the TIROS-N and NOAA-6 satellites. Both satellites are in near polar, sun synchronous orbits. TIROS-N became operational in January 1978 but was no longer used in 1980 because of operational problems; NOAA-6 became operational in June 1979 and is still operational. The TIROS-N satellite occupied an orbit of 854 km, NOAA-6 orbited at 833 km; both complete 14.2 orbits a day. NOAA-6 was the primary source of imagery, and since TIROS-N carried the same radiometer, the two sensor systems will be discussed as one. The morning orbit (descending; that is, going north to south) passes overhead the equator at about 7:30 local Alaska Central time, the afternoon orbit (ascending) is at 1500 (NOAA, 1979). Thermal infrared imagery is taken on all passes; the visible imagery is collected on the afternoon passes. The data from these satellites

is received at NOAA's Command and Data Acquisition station (CDA) at Gilmore Creek, Alaska.

The satellites cover the areas from north of the Bering Strait to south of the Aleutians, Hudson Bay to the East Siberian Sea, continental Alaska south to the Gulf of Alaska and to Seattle. The angle at which the pass is taken is determined by the equator crossing. Each pass covers 2200-6600 km at a scale of 1:7.5 million (Ahlnäs, 1981).

The AVHRR (Advanced Very High Resolution Radiometer) is the sensor which is responsible for acquiring the data. The satellite sends an analog signal to the processing station where a sectorizer unit digitizes and transfers the radiative temperatures to a photographic negative. The photographic image appears with 16 steps of gray with the gray tone inversely proportional to the radiative temperature of the emitting surface. An onboard calibration technique, described later, allows corrections and calibrations to be made so that the determination of the temperature from the gray scale is accurate except for limitations imposed by atmospheric effects on the transmission (Jayaweera, 1976).

The radiometer on board TIROS-N/NOAA-6 has five channels (Table 1) covering the visible, near infrared, and thermal infrared regions of the spectrum. Channel 1 (0.55-0.90 μm) and channel 2 (0.725-1.10) are used to discern clouds, land/water boundaries, and snow and ice extent. These channels constitute the visible and near-infrared end of the spectrum. Channel 3 is generally used in conjunction

Table 1. Sensor characteristics for the Advanced Very High Resolution Radiometer (AVHRR) onboard the TIROS-N and NOAA-6 satellites. Retyped after NOAA Tech. Memo. No. 107, 1979.

Channel	Resolution at Subpoint	Wavelength (μm)	Primary Use
1	1 km	0.55 - 0.90	Daytime cloud and surface mapping
2	1 km	0.725 - 1.10	Surface water delineation
3	1 km	3.55 - 3.93	SST, nighttime cloud mapping
4	1 km	10.5 - 11.5	SST, day/night cloud mapping
5	1 km	11.5 - 12.5	SST

with channel 4 to determine sea surface temperature. By using channel 3 with channel 4, it is possible to remove ambiguities introduced by clouds in the field of view. This method is generally used in warmer regions where one channel is dedicated to sensing cloud tops and the other is used to discern SST. This method is used generally in the Indian Ocean but is not regularly used in the arctic because sea surface temperatures are so cold (Don Sundren, personal communication). An attempt was made to use Channels 3 and 4 to derive a vapor correction and is discussed later. Channels 4 and 5 are used to determine SST in the North Pacific and Bering Sea.

Accuracy and Precision of Satellite Imagery

Accuracy and precision of satellite imagery are largely due to two factors: sensor operation and capabilities, and quality of surface truth methods and data. The radiometers are extensively tested and calibrated prelaunch, against a precision blackbody source which is registered at the National Bureau of Standards. This calibration is performed in a thermal vacuum to simulate space. A second test measures a series of temperatures to determine the instruments response as a function of temperature and to determine any deviations. This data serves as a baseline and is used in conjunction with periodic in-flight calibrations to calibrate the sensors and tables used with the images (NOAA, 1979). An in-orbit calibration of IR channels is possible because output is linear with input energy. During each scan the sensor unit views space, the cold point (0

radiance), and then the warm point, four platinum resistance thermometers embedded in the housing of the spacecraft. The output values are included in the data stream along with "housekeeping" information (i.e., how the thermistors and sensor electronics are behaving). The instrument response curve is generated, and if corrections are needed, they can be incorporated into the tables used to convert gray scale to temperature (NOAA, 1979; and Don Sundgren, personal communication). Because the instrument is constantly being calibrated, the imagery is very precise.

The accuracy of the satellite needs to be discussed in terms of spatial and thermal resolution. The spatial resolution is given in Table 1 as 1 km for high resolution picture transmission (HRPT) which is the system used at the Gilmore CDA station. Although the sensor can resolve temperatures spaced at 1 km, the actual location of features, such as thermal fronts, temperature contours, and currents, has been noted as ± 5 km (NOAA, 1980). A new processing technique used at the Gilmore Creek CDA station rectifies geographical distortion previously seen on some imagery. The distortion occurs because the radiometers scan horizontally as the craft passes vertically through the center of the images. The improvement of this new process on spatial resolution has not yet been documented, but some geometric distortion still exists (K. Ahlnäs, personal communication).

NOAA (1980) notes the absolute thermal accuracy is ± 1.5°C. Information from Dalu *et al.* (1979) and Reeves *et al.* (1975) indicates absolute accuracy can be improved to as great as 0.3°C if water vapor

corrections are applied. The maximum obtainable accuracy is also highly dependent on the quality of data used as surface truth information. Relative temperatures--that is, gradients--can be determined accurately at ± 0.5°C (NOAA, 1980). Jayaweera (1976) also notes that relative temperatures can be read to within ± 0.5°C. Tabata and Gower (1980) demonstrated that field corrected satellite data is capable of measuring SST with an accuracy of ± 0.5°C. It was not clear whether this was relative or absolute. The data used in this has an accuracy of ± 0.5°C for relative temperatures.

Data Collection and Methods of Interpretation

The Gilmore CDA station processes approximately six passes of the NOAA-6 satellite a day; when TIROS-N was still operational, additional transmissions were received and processed. The satellite passes generally cover the areas described previously. The passes which are over the Bering Sea generally occur in the morning (approx. 9:00 local Alaska time) and late evening. When possible, visible, infrared and enhancements of any clear days over the Bering Sea are collected. Visible imagery is available from April-November, depending on available light, and for day passes only. The visible imagery is used to define cloud, fog, and ice areas, although these are also discernible on the regular and enhanced infrared. Usually all three types of imagery were used in interpretation.

Each pass collected from each day since December 1979 through August 1981 was inspected. Of the 3810 satellite passes inspected,

only 84 were cloud-free or partly cloud-free and covering the area of interest, and they provide the data set for this thesis. The regular infrared image uses different tones of gray to represent temperature; white represents the coldest point, black the warmest, and shades of gray represent temperatures in between. The sensitivity of the NOAA-6/TIROS-N sensor allows for 256 digital steps or eight bits to cover the temperatures between -60 to 40°C (Ahlnäs, 1981). Because the human eye is not very efficient in distinguishing gray tones which are close in density range, enhancements are used. In an infrared enhancement, a temperature range is preselected, fed into the minicomputer, and the gray steps are assigned to cover the new range (Ahlnäs, 1979). Usually the temperature range is chosen so that two gray steps correspond to a 1°C temperature step. In this way the enhancement does not exceed the relative accuracy of the system (± 0.5°C). Often a double gray scale is used when the temperature distribution of an area falls in two ranges, i.e., open water and pack ice. In this case two consecutive temperature ranges are chosen, and a gray scale which goes from white to black is assigned to each range. See Ahlnäs (1979, 1981) and Jayaweera (1976) for a more detailed description and applied use of the technique.

As the range of sea surface temperatures varies throughout the year, the temperature range chosen for the enhancement must change also. Clear day passes were enhanced with an appropriate table or series of tables to achieve the maximum amount of contrast and detail in the images. The enhancements were then inspected for patterns

which were recognizable as some oceanographic feature. Often visible, infrared, and enhancement were compared and used together to establish clouds, ice extent, and sea surface tempeature features. The visible imagery was valuable for delineating clouds and land and ice/water boundaries. Once sea surface temperature features were established, that is, temperature distributions, eddies, temperature gradients, a measure of the temperatures represented in the image was undertaken. It should be noted that the intent in this study was to identify features and relative temperatures. Determination of absolute temperatures requires much more rigorous ground truth support, and that was beyond the scope of this study.

In establishing temperature gradients and relative temperature measurements, a densitometer was used in conjunction with the data used to make the enhancements. This data consists of the sensor calibration table and the enhancement table. The sensor calibration table gives the temperatures which correspond to density counts sent down from the satellite. The enhancement table gives the density shade, the tonal value which appears on the image which corresponds to the density count. On each enhancement negative, the image is made up of gray tones; the complete range seen on the image is represented by a strip of 16 or 17 gray tones printed on the top of the enhancement negative. These tones span the temperature range chosen for that enhancement. Using the densitometer, the density of the gray tones on the image are measured and contoured. These density contours provide a check against the human eye; they also reveal the features detected

by the initial visual examination. The densities of the 16 or 17 gray tones printed on top of the negative are also measured. Using the enhancement table from which that negative was made, the density count which corresponds with the gray tone can be identified. From this density count and the sensor calibration table, the temperature or temperature range of the contour can be identified. Comparing the densities from the 16 boxes to the densities on the image, then comparing this to the sensor counts, eliminates differences due to variations in negatives and densitometers. Figure 7 shows the information used to derive the temperatures from the satellite images. Often the temperature range of the enhancement is not easily broken into 16 steps, or gray tones; when this occurs, distinct temperatures are not easily identified. The gray tone can fall within a range of densities; hence these cases are identified as the range, e.g., 1.0 to 1.5°C, not as a single temperature. The contour maps made from the densitometric analysis not only serve as a check against "imagined" features, but they also provide the information used to compare the satellite-derived temperature to the surface temperatures collected by other means. An overlay showing bathymetric contours and land masses was used to give a geographic location of the features on the images.

Surface Truth Measurements

Surface truth measurements are needed to verify results and provide some measure of the quality of the satellite measurements.

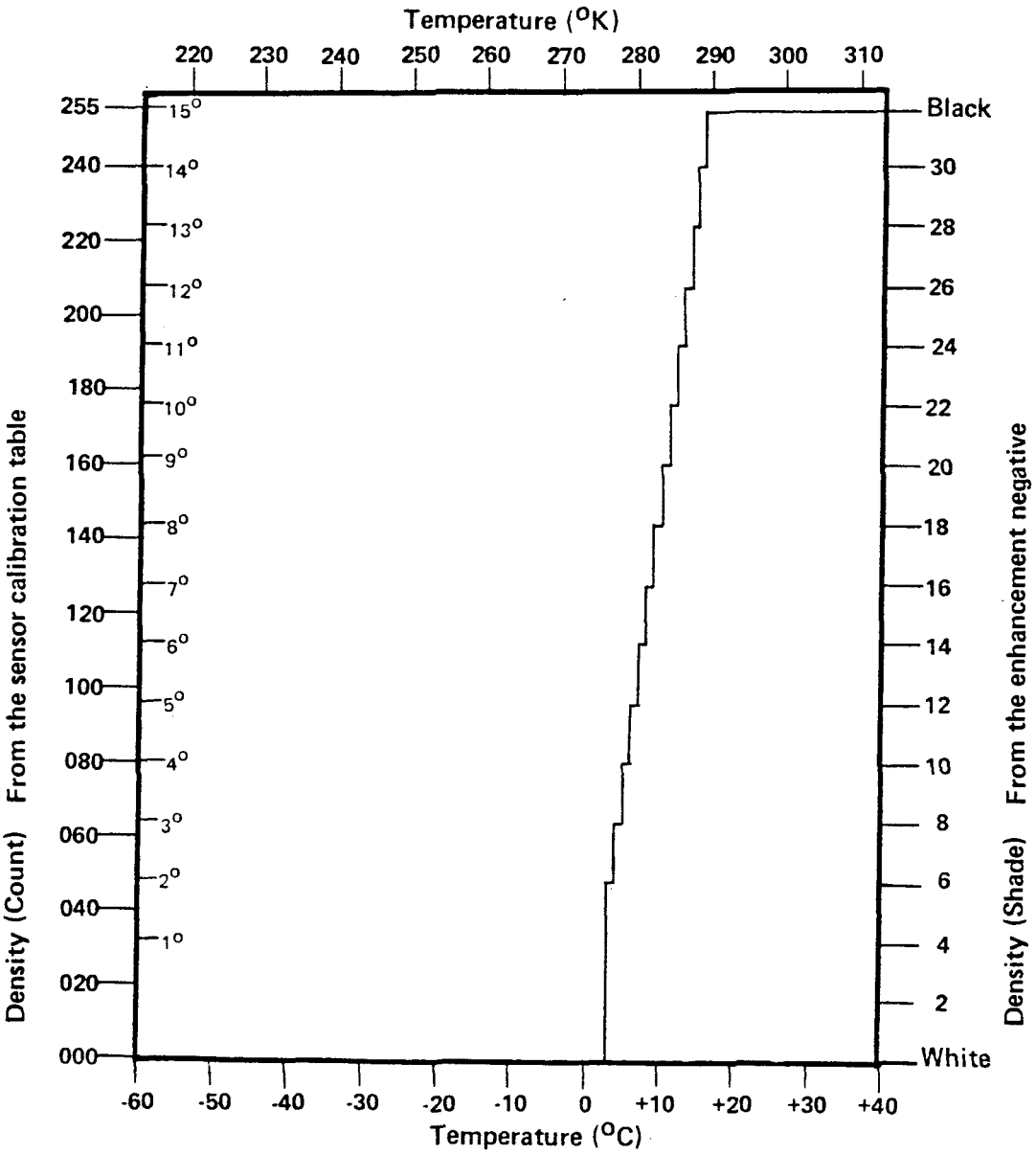

Figure 7. Sample infrared enhancement curve; 64X.

Surface truth sampling techniques, and the number and quality of the measurements are largely determined by the accuracy desired. Since the satellite measures the "skin temperature", measurements should be as close to the surface as possible. An assumption is generally made that the "skin" (approx. 1 mm) which the satellite senses is generally the same temperature as the upper meter; however, it is possible that this may not be the case. Samples should, ideally, be taken at the time of overflight in the area of interest. Where a large overall view is desired, this is virtually impossible, and it should be kept in mind that possible errors may arise due to small-scale variations of temperature in space and time. In a dynamic system this error could be quite large, but in a region where processes are slower, it may be acceptable.

A major problem to consider in satellite remote sensing is attenuation of energy by the atmosphere. Atmospheric absorption by water vapor is the primary cause of attenuation in the infrared band. To avoid this problem, sensors generally are programmed to operate in atmospheric spectral windows. These "windows" allow the propogation of infrared radiation with the least interference; however, even then, certain spectral lines on the wings of the window are sensitive to water vapor. The two major windows in the infrared region are found between 3-4 μm and 8-14 μm, and the satellite sensors are set to collect data within these bands.

Consideration of the water vapor question falls into two categories: calculating the effect to improve the absolute accuracy,

and disregarding the effect and accepting measurements at the reported accuracy. There is a method available to correct for attenuation by water vapor, and it is most commonly used when digital data are available. Reeves *et al.* (1975) provides a discussion of the theory involved, and Smith *et al.* (1970) presents a method for correction. More recently, Dalu (1979) and Tabata and Gower (1980) discuss several methods for correcting for water vapor and transmission effects and improving the accuracy (absolute) to ± 0.5°C. All methods generally involve computation of a calibration/correction line.

For considering relative temperatures over a large area, these methods are probably not feasible without immense logistic support. Water vapor tends to be highly variable in the atmosphere both vertically and horizontally. The distribution is assumed to decrease exponentially in height, and horizontally it tends to "roughly" follow pressure systems. Different air masses have characteristic water vapor contents; generally the sea level water vapor density varies from 10^{-2} g m^{-3} in cold, dry air to 30 g m^{-3} in hot, humid regions (Reeves *et al.*, 1975). The clearest views of sea surface temperature are associated with atmospheric fronts which are followed by cold, dry air. This tends to be the case with the Bering Sea; clear views generally occur when the arctic air mass is present over the Bering Sea.

In investigating the possibility of water vapor error in this study, an attempt was made to obtain vertical sounding covering the area in order to determine general water vapor patterns during the

periods of clear images. This was not feasible because (1) radiosonde soundings are only available at weather stations, and they constitute only three points: St. Paul, Cape Newenham, and Unimak Island; (2) although the satellite is equipped with a vertical sounding sensor, this data is not processed, and, furthermore, if it were, it would require surface truth information to verify its results. The fact that the arctic air mass is generally a very dry air mass, and using the vapor content from Reeves *et al.* (1975), a comparison was made with a table found in Dalu (1979) giving the sensor response in the 11 μm and 13 μm channels, the wavelength at which NOAA-6/TIROS-N also sample. It was found that transmittance was still 100-80% for up to 1 g/cm^2. The problem of the horizontal variation of water vapor interferring and causing the features detected in the sea surface temperature was addressed by examining images taken in the water vapor band from a European satellite. They revealed that generally in clear, cloud-free areas in the visible and infrared, it was generally clear in the vapor band. Most important, atmospheric features are several orders of magnitude larger than the oceanic features, that is, eddies in the atmosphere had sizes on the order of large circulation gyres, not 100-km eddies.

A last attempt was made to make a vapor correction using a method described by McClain (1980). According to McClain (1980), corresponding data from a second and third spectral band can be used in conjunction with the primary spectral band in a regression equation to give a corrected sea surface temperature. Data was collected from band 3

(3.8 μm) in addition to the band 4 (11 μm) data and enhanced in the same manner as the band 4 data. The resulting band 3 image showed a large amount of noise (Figure 8a,b,c) so that contours of density could not be measured. This problem was also noted by McClain (1980). Daytime passes and nighttime passes were inspected to test whether reflected incoming radiation (common in day passes in band 3) was the problem. Day and night images showed an equal amount of noise. Although temperatures could not be measured to be used in the regression equation, the band 3 images showed excellent delineation of cloud and vapor features.

Thus, it is not feasible to correct for water vapor attenuation for this data set. The uncorrected data is acceptable because the goal is to look at large-scale features evidenced by temperature gradients. Relative temperatures will suffice to establish these gradients. Because of the low vapor content in cold arctic air (Reeves *et al.*, 1975) and close examination of the imagery to distinguish clouds, the relative temperatures are representative of the sea surface and not of atmospheric features. Sea surface temperatures measured by hydrographic methods are compared to temperatures derived from the imagery by the densitometer method to verify the existence of sea surface temperature gradients and indicate how representative the satellite temperatures were at that time.

The sea surface temperatures used for the surface truth data set are from cruises of the oceanographic research vessels *Miller Freeman*, *T. G. Thompson*, and *Alpha Helix* (Table 2). The temperatures

Figure 8a. Visible imagery of an area in the Aleutian Basin, 27 July 1981.

b. Band 3 imagery, enhanced with Table 63X, 27 July 1981.

c. Band 4 imagery, enhanced with Table 64X, 27 July 1981.

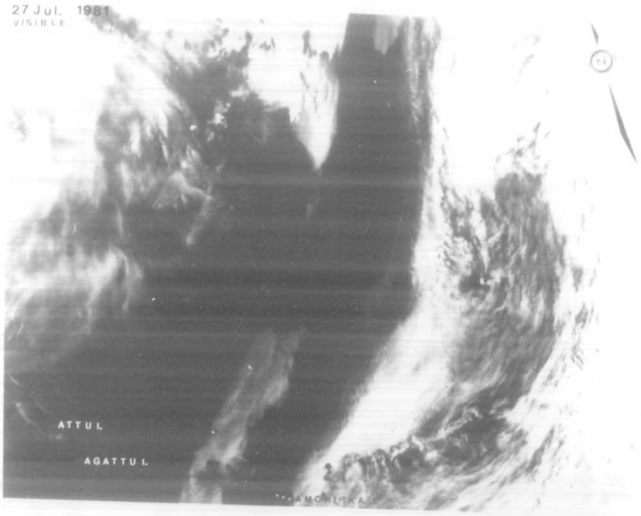
27 Jul. 1981
VISIBLE
ATTU I.
AGATTU I.
AMCHITKA I.

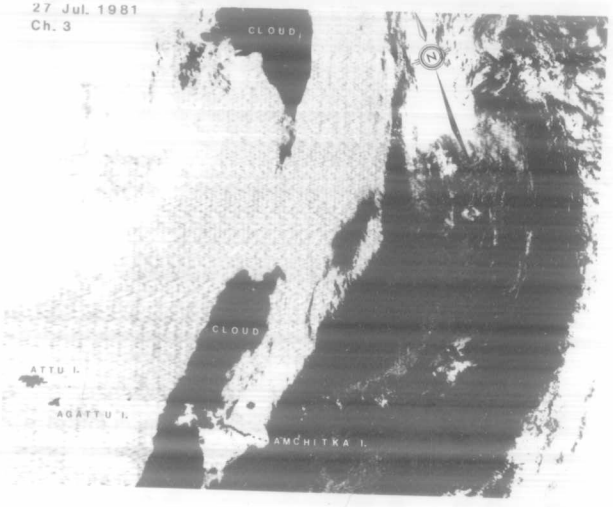
27 Jul. 1981
Ch. 3
CLOUD
CLOUD
ATTU I.
AGATTU I.
AMCHITKA I.

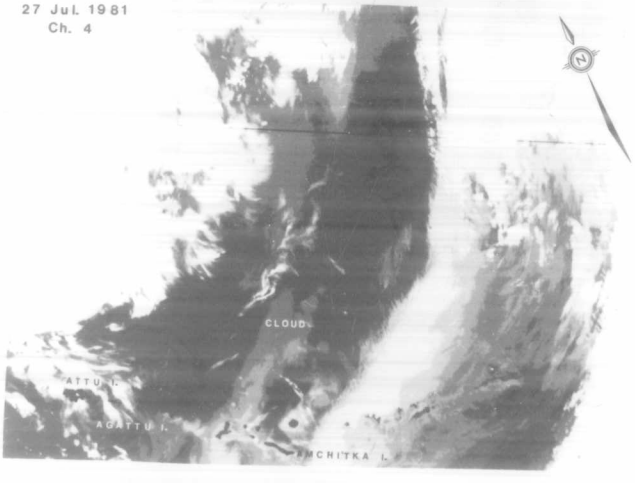
27 Jul. 1981
Ch. 4
CLOUD
ATTU I.
AGATTU I.
AMCHITKA I.

Table 2. Sea surface temperatures used as surface truth data.

DATE	AREA COVERED	SOURCE	METHOD OF COLLECTION
January 23-31, 1980	Along the Bering Sea Shelf	G. Hufford, Anchorage Nat'l Envir. Satellite Service. From R/V *Miller Freeman*.	By thermograph with bow sensor probe at 3 m. Avg. correction due to heating: -0.2°C.
February 1-12, 1980	Along the Bering Sea Shelf	G. Hufford, Anchorage Nat'l Envir. Satellite Service. From R/V *Miller Freeman*.	By thermograph with bow sensor probe at 3 m. Avg. correction due to heating: -0.2°C.
September 1980	Gulf of Alaska near Unimak Pass, Bering Sea near Unimak Pass	Schumacher *et al.*, 1981	CTD
October 4-24, 1980	Along the Bering Sea Shelf	R/V *Alpha Helix*, Cruise 9	CTD
April 11-20, 1981	PROBES line	R/V *T.G. Thompson*, Cruise 159, Leg 1	CTD
May 1981	PROBES line	R/V *T.G. Thompson*, Cruise 159, Leg 2	CTD
June 1981	PROBES line	R/V *T.G. Thompson*, Leg 3	CTD
July 1981	Along Bering Sea Shelf	R/V *T.G. Thompson*, Leg 4	CTD

were measured with a CTD except on the *Miller Freeman* where they were measured with the bow sensor probe of a thermograph at 3 m. It has been noted that surface temperatures measured in this way tend to be somewhat warmer than actual temperatures; however, a correction factor was recommended by the supplier of the data (G. Hufford) and was used (Table 2). The CTD measurements generally measure and record temperature at 0.2-second intervals and are averaged every meter with an accuracy estimated to be within ± .02°C. Though the temperature does not always coincide with the dates and areas of the images, they give a general idea of the sea surface temperatures at the time of sampling. They are used generally to verify relative measurements and not absolute temperatures.

January 1980 surface truth showed that temperatures agreed very closely. The ship temperature showed that water off the shelf was between 2°C to 4°C; the satellite imagery revealed this same temperature range and close spatial agreement. Later, January images showed cooler water on the shelf, which was beyond the extent of the surface truth data but again still within expected temperatures for that time of year. The February images from TIROS-N were also in close agreement with the surface truth data. The NOAA-6 images were slightly cooler but did match well in the area near the Pribilof canyon. The variation between the images from the satellites arises because TIROS-N was slightly off calibration at this time. Although a general correction was applied, the image may still appear warmer than actual conditions and hence match more closely with the ship data which also

would tend to be warmer than "skin" conditions. The April and May imagery match well with the on shelf temperatures. It is noted that in areas near clouds, temperatures on the images are cooler than ship's temperatures. This would be expected because of vapor interferences. October's images showed good agreement with measured sea surface temperatures. Two tables were used to reveal the maximum temperature structure; both showed the same general temperature structure; however, Table 64V showed more detail. These images are presented later in the Results section. In general, April and May 1981 showed somewhat cooler temperatures than the surface truth data; however, temperature gradients were still clearly established. Wind shear, waves, and vapor could cause the temperature differences seen.

Overall temperature agreement between the images and the surface truth data was very good in the winter, much better than expected, e.g. within ± .5°C. In spring and summer agreement was not as close; on the average the images showed temperatures cooler by 1 to 1.5°C. This difference was probably due to wind, wave action, or vapor interference.

Meteorological Data

The meteorological conditions, especially the wind speed and direction, were analyzed for the dates in which physical features were revealed by the satellite imagery. Twelve hour surface pressure maps obtained from the Anchorage branch of the National Weather Service were used to determine the type and strength of the pressure

systems governing the weather, to determine wind speeds, and to give some idea of which air mass (arctic or continental) was affecting the region.

Wind speeds were obtained from the Local Climatological Data Bulletin (NOAA Environmental Data Service) from the surface level weather maps. Values from the St. Paul Island and Unimak Island stations were used. Stick plots were used to demonstrate wind speed and direction.

RESULTS

Visible, infrared, and enhanced infrared images have been collected from December 1979 to August 1981. Physical features have been implied from the sea surface temperature structure revealed in the satellite images. Information in the literature gives support for the existence of these features. As some features might occur seasonally and some might be related to other physical features detected synoptically, the information from the images will be presented first as a time series, with temporal and spatial relationships in mind. A summary of the features, and their time and space relationships, will be presented later in the section. A complete listing of all the images and related information is given in the appendix.

December 1979 - January 1980

During this period 7 clear images were found which gave a good view of the Bering Sea from the Bering Strait to the basin area. Figures 9, 10, and 11 are representative of the conditions present in the Bering Sea during this period. Because of the large number of images and the repetition of the features which they show, not all the images will be presented. Those images which show the more interesting features and that are representative are presented.

Ice and sea surface temperature patterns were noticeable in all the images during this time period. The visual correlation of the ice

edge and sea surface temperature patterns with bathymetric contours is very clear in these images. A transparent overlay, produced from Figure 2a, was used to make these visual correlations.

For January 1980, five images were found, three of which constituted an abbreviated time series spanning January 10-11. This time series revealed the surface signature of a cyclonic eddy with a cooler core located off the shelf break over the Pribilof Canyon (Figures 9, 10, and 11). Figures 9a, 10a, and 11a are the satellite images; 9b, 10b, and 11b are the densitometric analysis maps showing the relative temperatures. A second eddy-like feature was noted further to the west approximately near the Zhemchung Canyon. The third image (Figure 11), late on January 11, showed some traces of water with a similar temperature, but the eddy was no longer a discernible feature. The eddy (Figures 9, 10) was detected as a warmer signature within another warm band located roughly between the 100 and 3000 m isobaths; water on either side of this band was cooler. Warm water was seen along the Aleutian chain and through Unimak Pass, continuing on across the shelf. In these images the ice edge follows the 50-m contour closely, as do the other temperature gradients. Note that the ice had filled the western portion of the Bering Sea to St. Matthew Island.

On January 28 the ice edge had progressed to between 58 and 57°N at its southern-most extent, with warmer water over the shelf. The most distinct feature was the warmer signature of what is assumed to be the Alaska Stream seen on the seaward side of Kodiak, approximately paralleling the Aleutian Chain, and then slanting in toward Unimak

Figure 9a. Infrared image for 10 January 1980; enhanced with Table N4P.

Features of interest are: cyclonic eddy south of the Pribilof Islands, ice edge which follows the 50-m bathymetric contour, warm surface water (darker shades of gray) along the Aleutian Chain and in Unimak Pass.

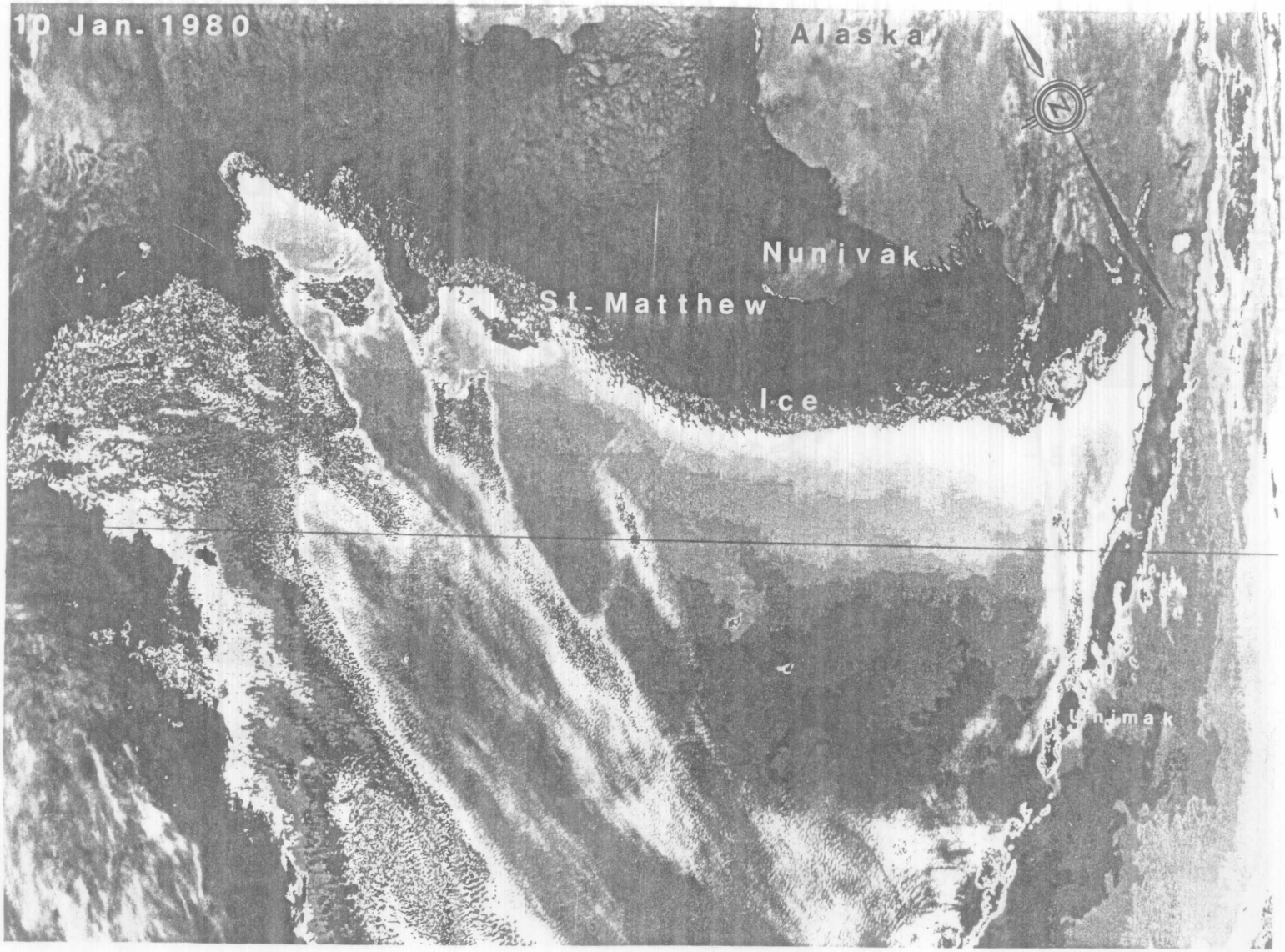
10 Jan. 1980
Alaska
N
Nunivak
St. Matthew
Ice

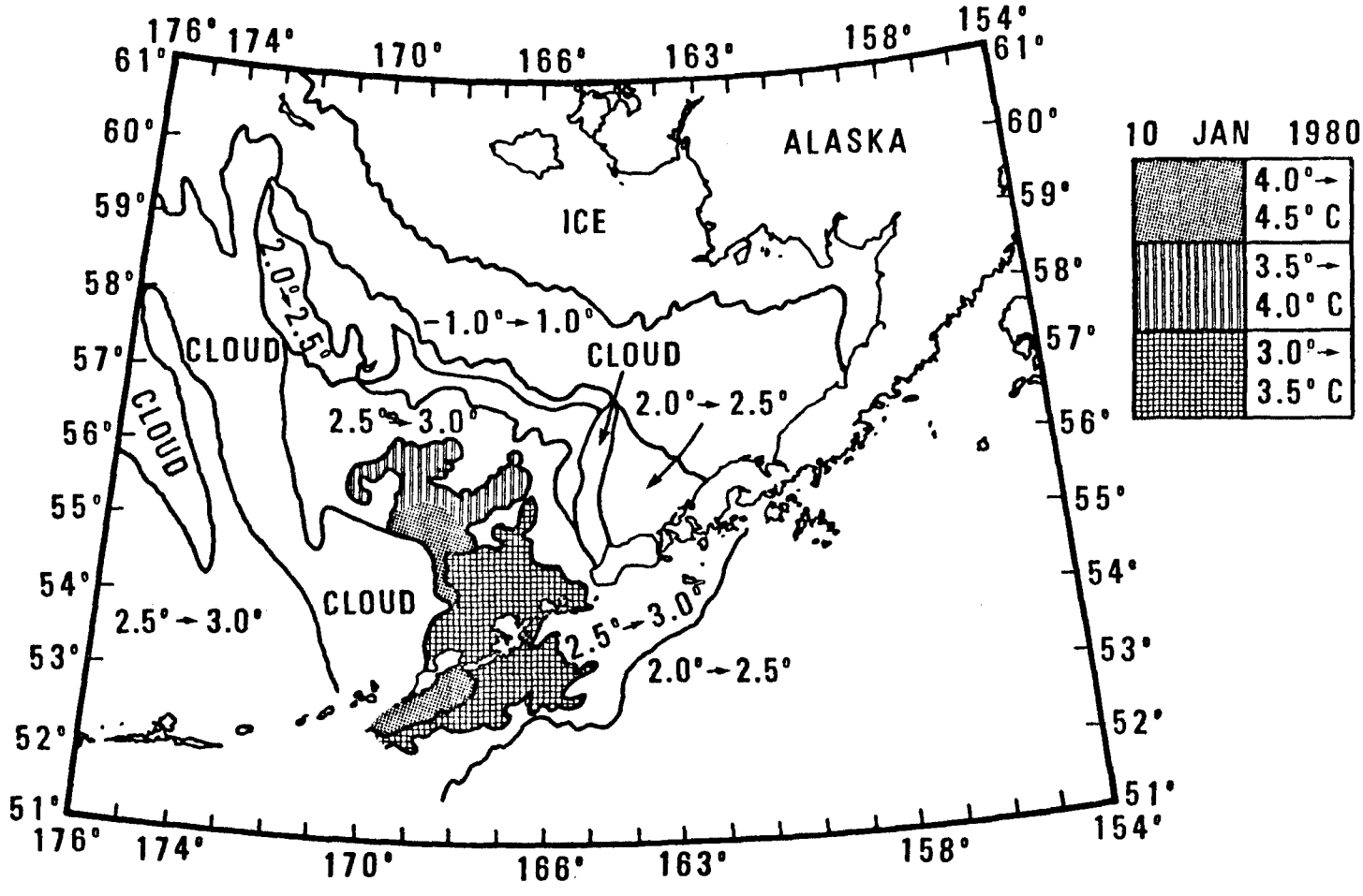

Figure 9b. Temperature contours produced from densitometric analysis, 10 January 1980.

Figure 10a. Infrared image for 11 January 1980, GMT 01:42:21; enhanced with Table N4P.

Features of interest are: cyclonic eddy south of the Pribilof Islands and similar warm feature to the northwest, along the shelf break, warm surface water along the Aleutian Chain, in Aleutian passes, and along the Bering Sea side of the Aleutian Chain, temperature contour which follows the 100 m bathymetric contour on the north and then extends into the basin.

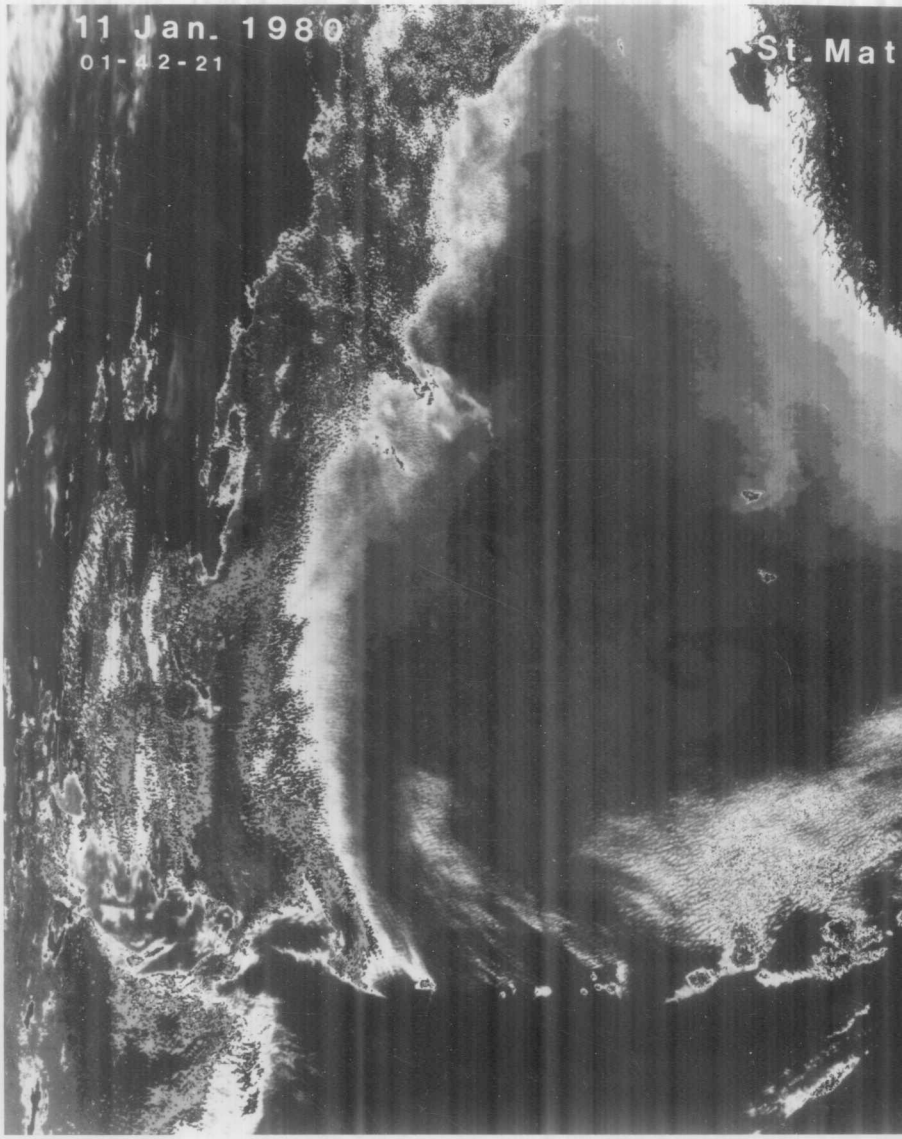
11 Jan. 1980
01-42-21
St. Mat

t h e w
Alaska
Nunivak
N
Ice
Cloud
Unimak

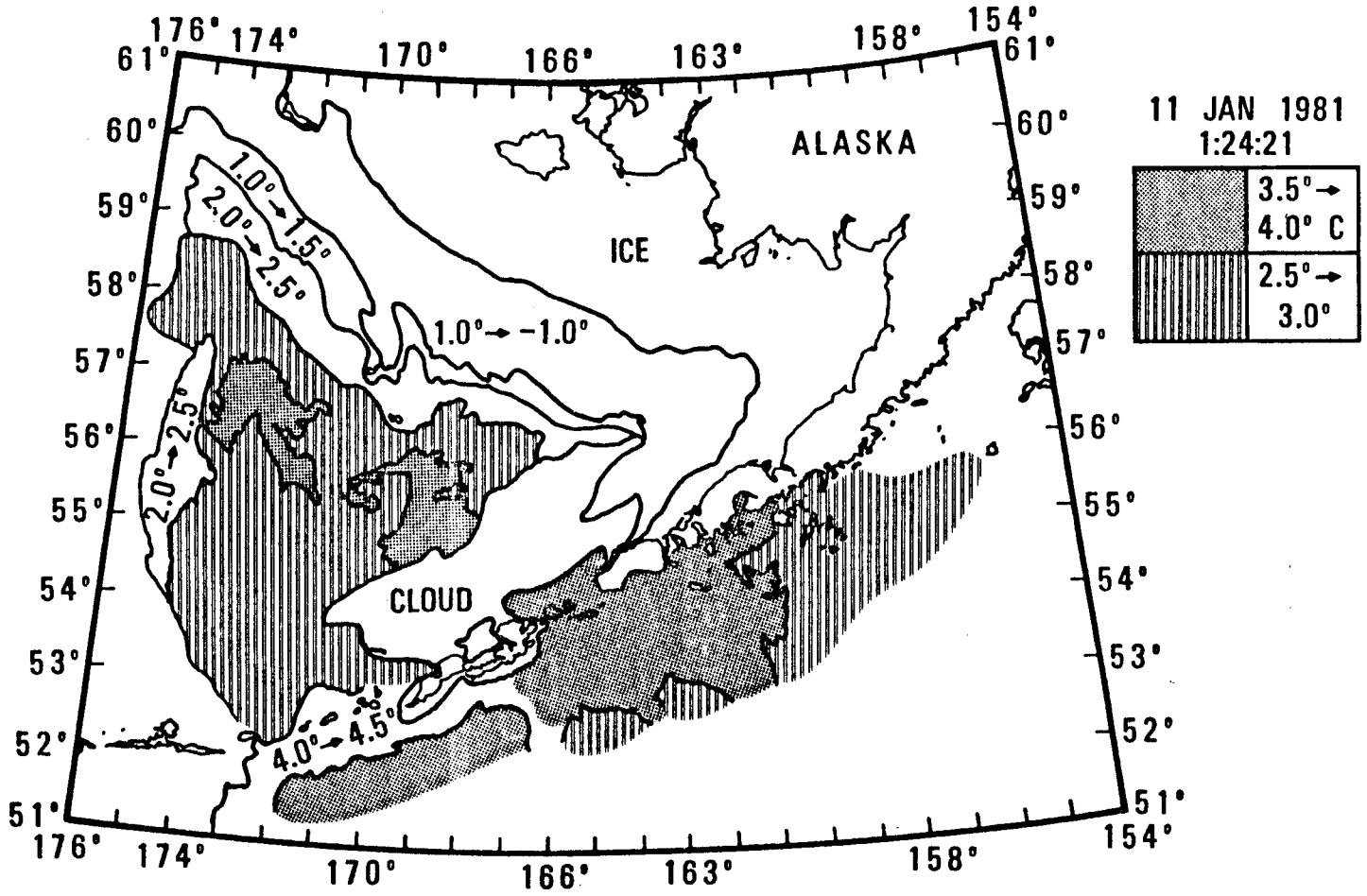

Figure 10b. Temperature contours produced from densitometric analysis, 11 January 1980; GMT 01:42:21.

Figure 11a. Infrared image for 11 January 1980, GMT 15:36:21; enhanced with Table N4P.

Features of interest are: patches of warm water over the 200-m contour where the eddy was previously, warm surface water along the Aleutian Chain and in the passes, temperature contour following the 100-m bathymetric contour and extending out into the basin.

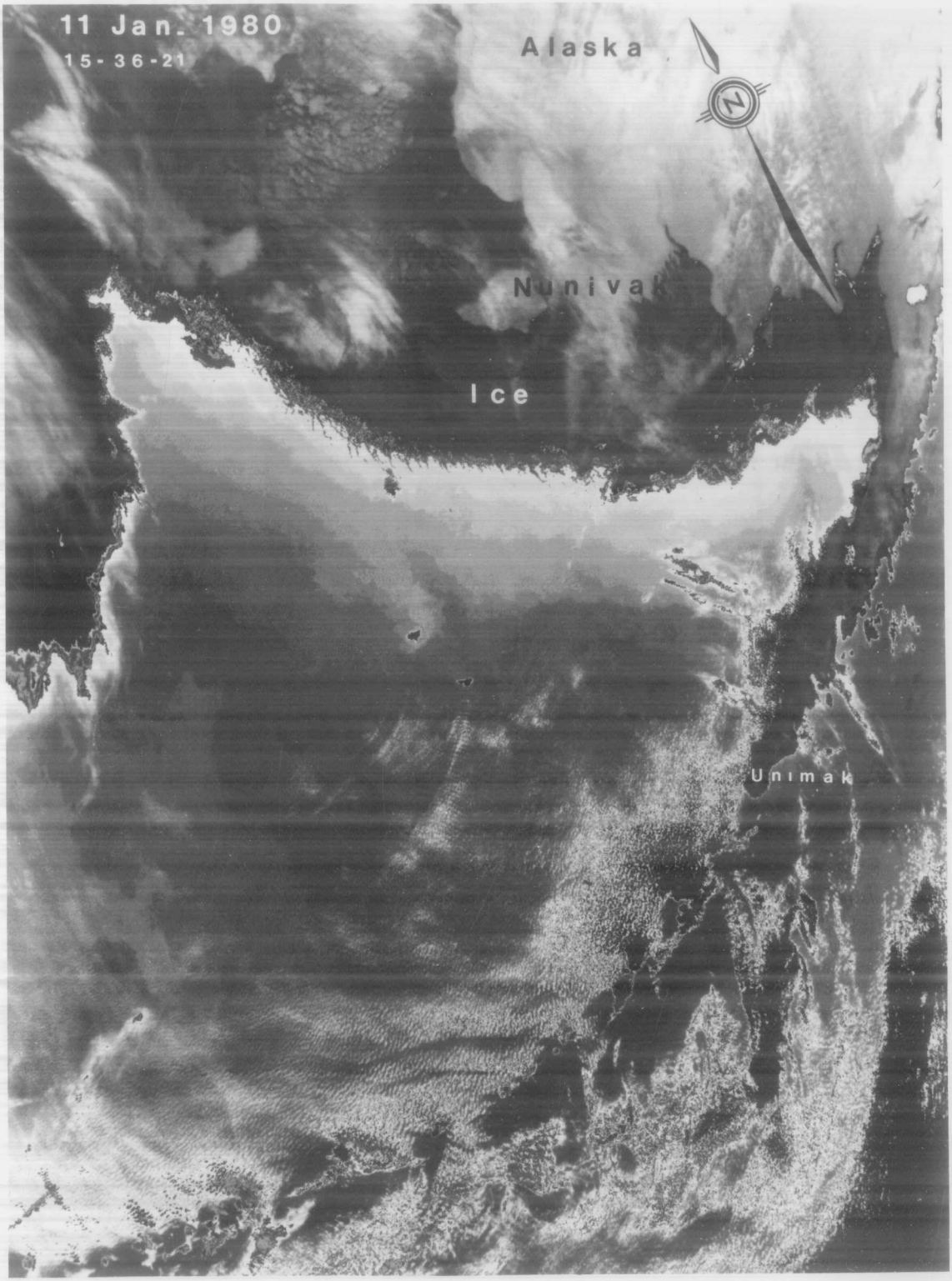
11 Jan. 1980
15-36-21
Alaska
N
Nunivak
Ice
Unimak

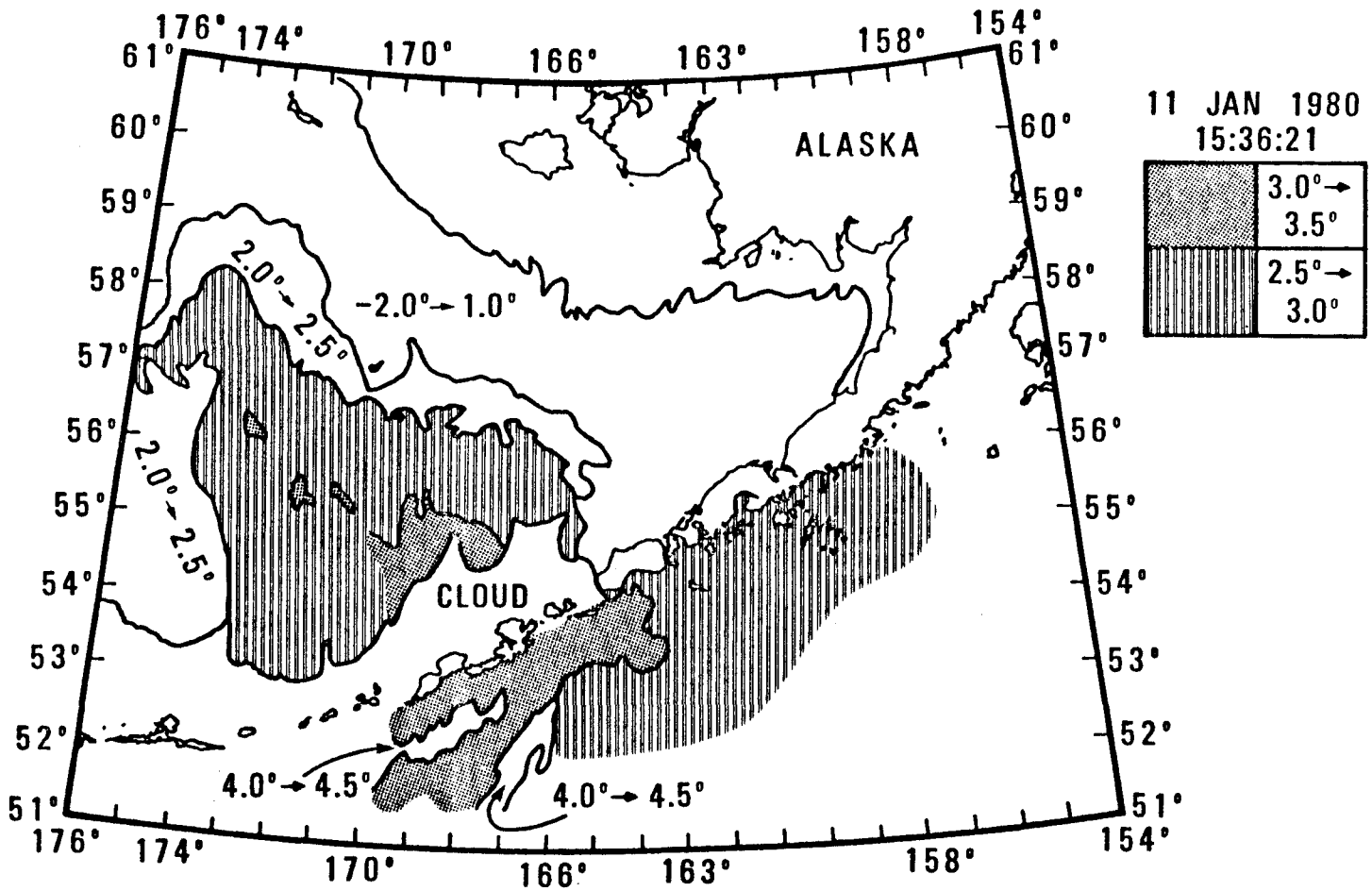

Figure 11b. Temperature contours produced from densitometric analysis, 11 January 1980; GMT 15:36:21.

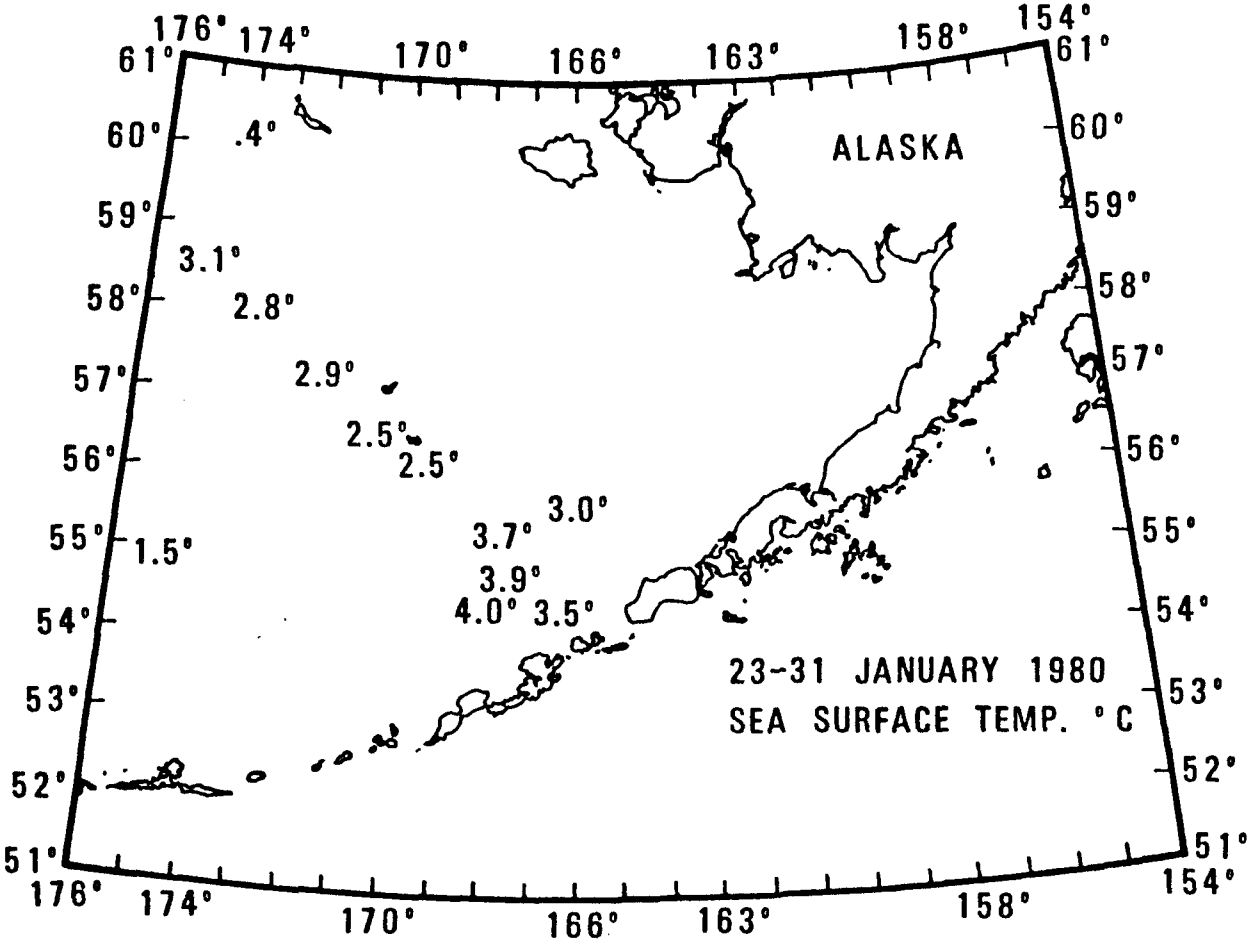

Figure 12. Sea surface temperatures for 23-31 January 1980 used for surface truth data.

Pass, narrowing as it progressed south. Swirling, eddy-like features were seen within this warm band and also between Kodiak Island and the coast of Alaska. On January 31 (Figure 13) some of this warm band was again seen near Unimak Pass and near the Alaska Peninsula. The ice edge had advanced so that it had filled in almost all of Bristol Bay and was approximately 120 km from the northern-most Pribilof Island, St. Paul. In this image (Figure 13), a warm band can be seen between the 100- and 3000-m isobaths, generally following the shelf break. Within this, directly over the 200-m isobath, was still warmer water which had an undulating pattern.

February 1980 - April 1980

Coverage was obtainable in February, March, and April resulting in 11 images showing the shelf break region and Bristol Bay. The February images show the most interesting features which are presented in Figures 14-20 while features in the March-April imagery are pointed out but not discussed. The image on February 20 (Figure 14) shows that the ice edge had nearly reached St. Paul Island and that all of Bristol Bay was ice-covered except for a narrow strip along the Alaska Peninsula. In the open water, SST gradients were seen paralleling the 100-m isobath and another warmer band along the 200-m isobath. On February 26 (Figure 15), the position of the ice edge appeared to have retreated. Previously, it was approximately 40 km from St. Paul on the 20th, and appeared to be approximately 50 km from St. Paul on the 26th. In the open water a very definite

Figure 13a. Infrared image for 31 January 1980; enhanced with Table 64P.

Features of interest are: warm water patches over 200-m bathymetric contour, in Unimak Pass, and along the Aleutian Chain (darkest shade of gray in the open water), ice edge.

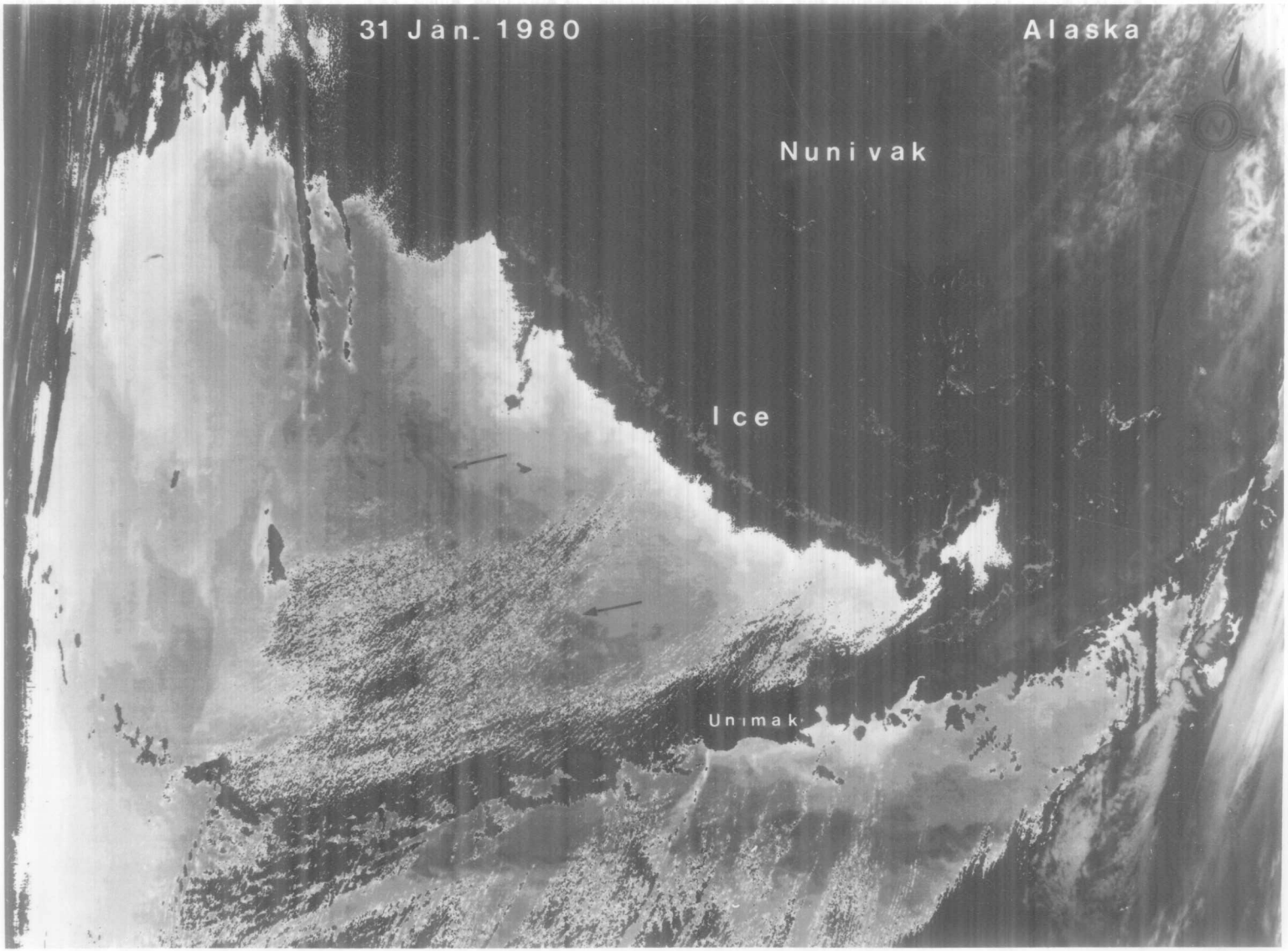
31 Jan. 1980
Alaska
Nunivak
Ice
Unimak

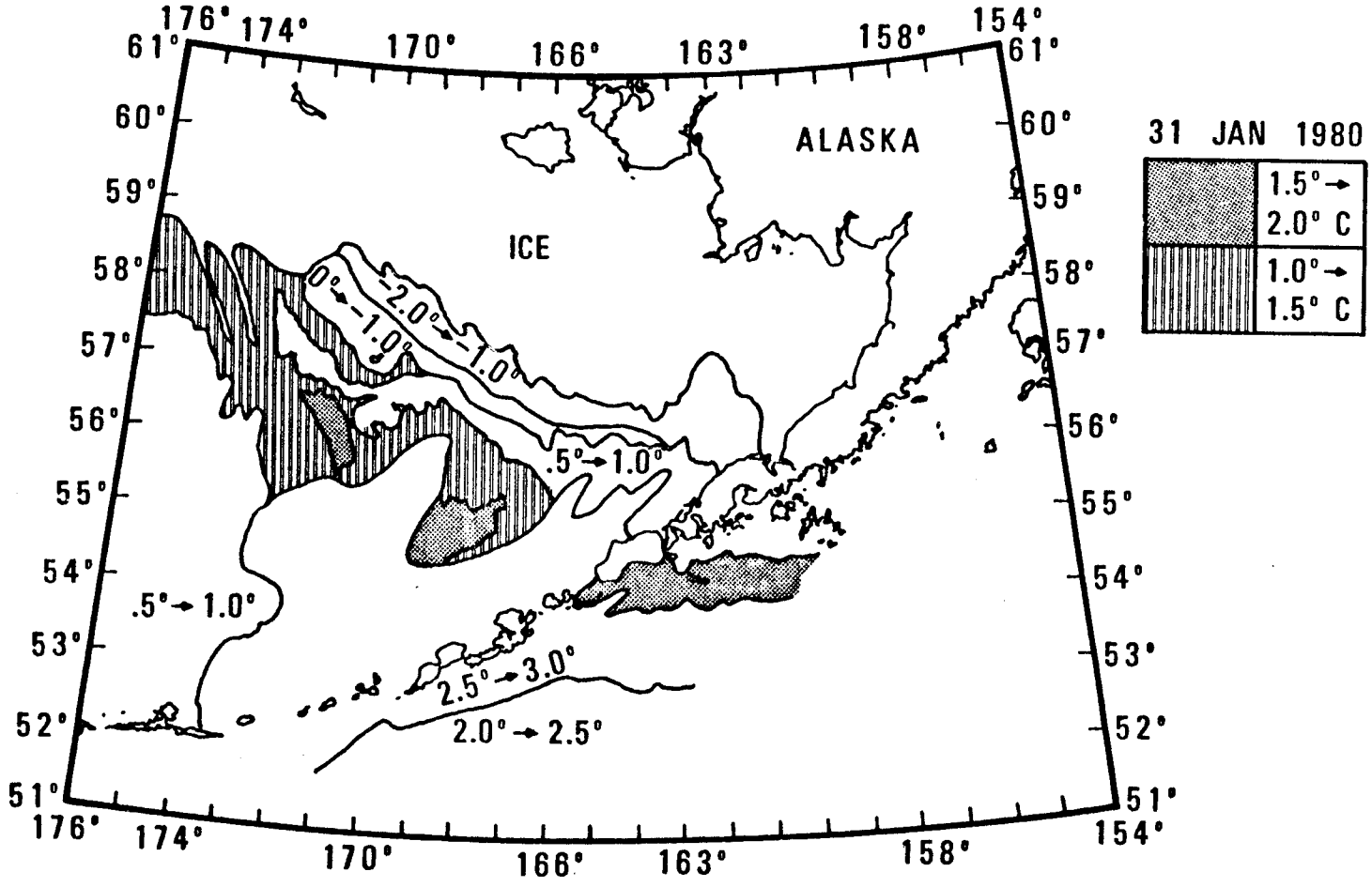

Figure 13b. Temperature contours produced from densitometric analysis, 31 January 1980.

Figure 14a. Infrared image for 20 February 1980; enhanced with Table N4P-7.

Features of interest are: warm surface water band over the 200-m bathymetric contour, ice edge follows isobaths which run southeast to northwest.

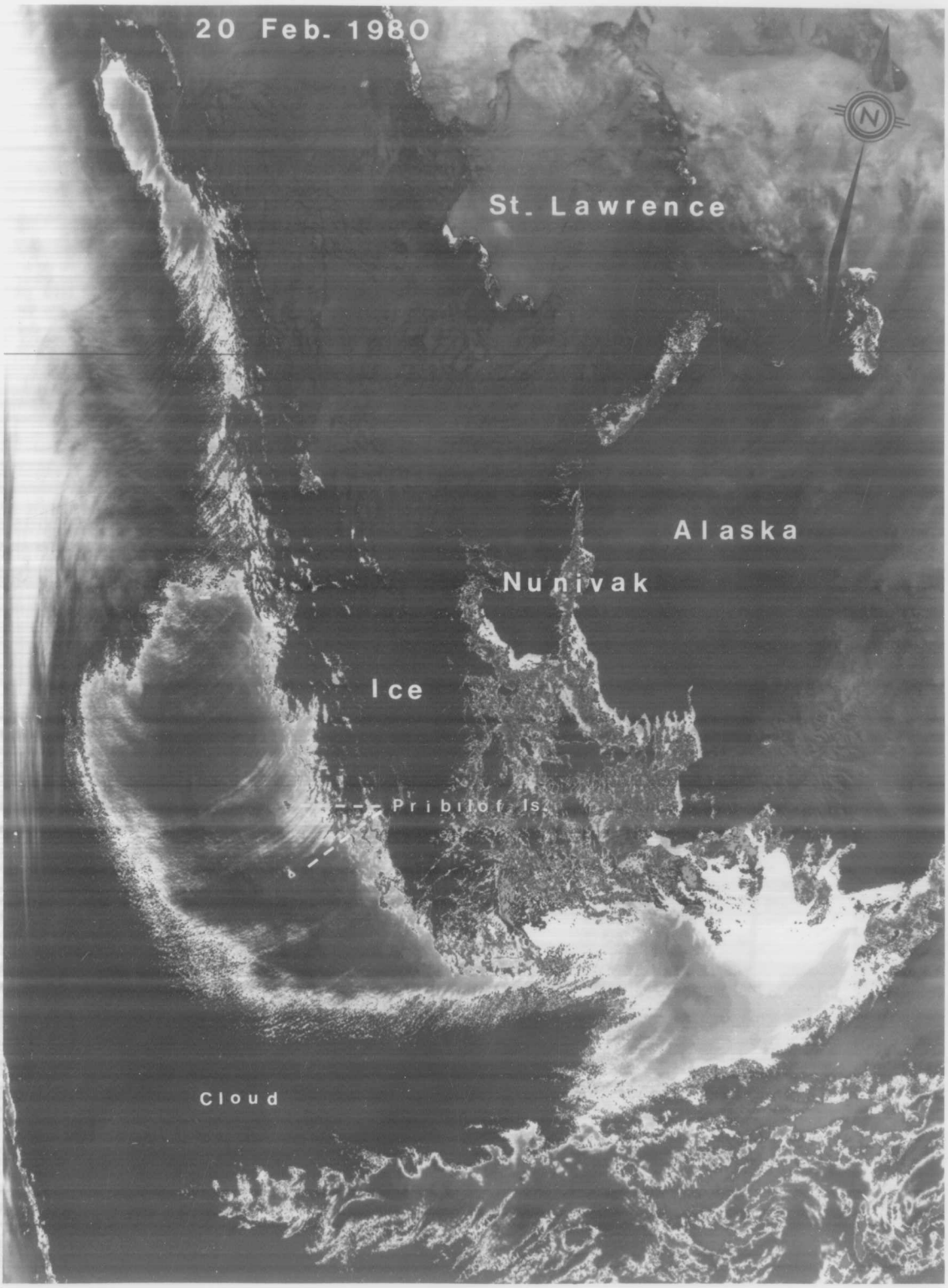
20 Feb. 1980
N
St. Lawrence
Alaska
Nunivak
Ice
Pribilof Is.
Cloud

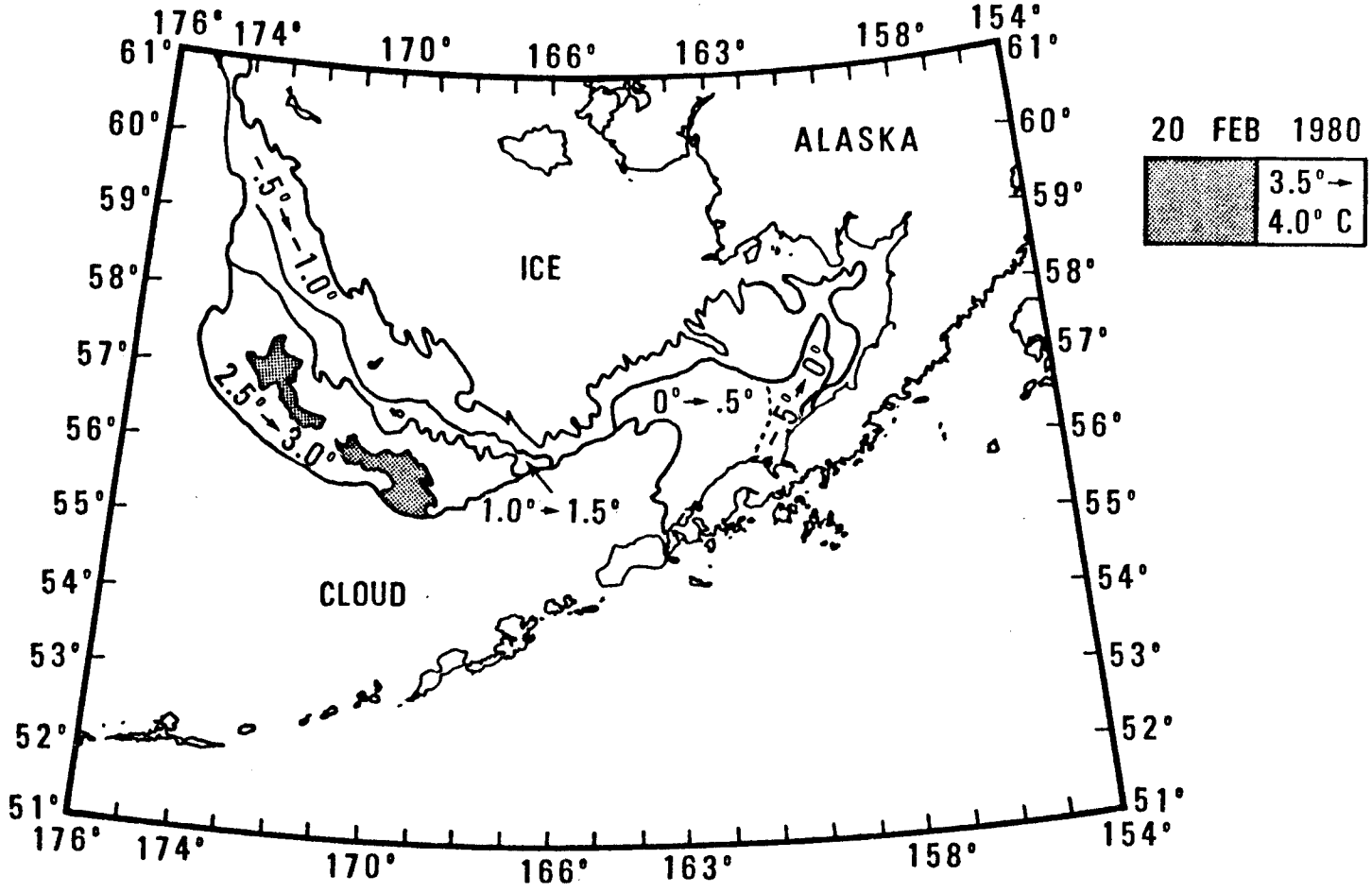

Figure 14b. Temperature contours produced from densitometric analysis, 20 February 1980.

Figure 15a. Infrared image for 26 February 1980, GMT 15:31:01; enhanced with Table N4P-7.

Features of interest are: the three eddies aligned along the shelf break (south of the Pribilof Islands) – from right to left there is a cyclonic cold core eddy, an anticyclonic warm core eddy, and an anticyclonic cold core eddy; note the wave-like pattern the cooler water forms between the 3 eddies; warm surface water along the Alaska Peninsula and within Unimak Pass; the ice edge ∿ 50 km from St. Paul Island.

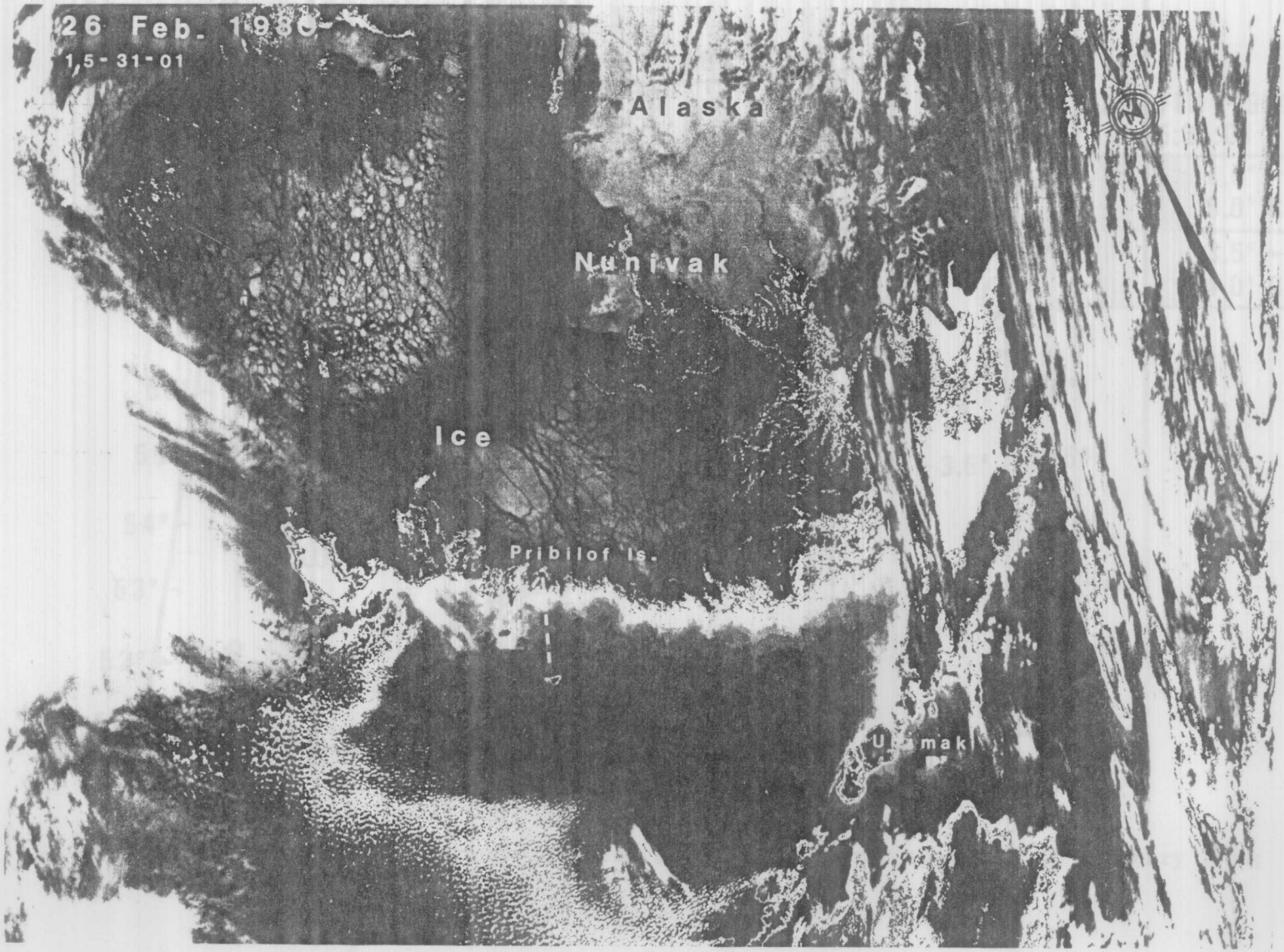
26 Feb. 1930
1,5-31-01
Alaska
Nunivak
Ice
Pribilof Is.
Umak

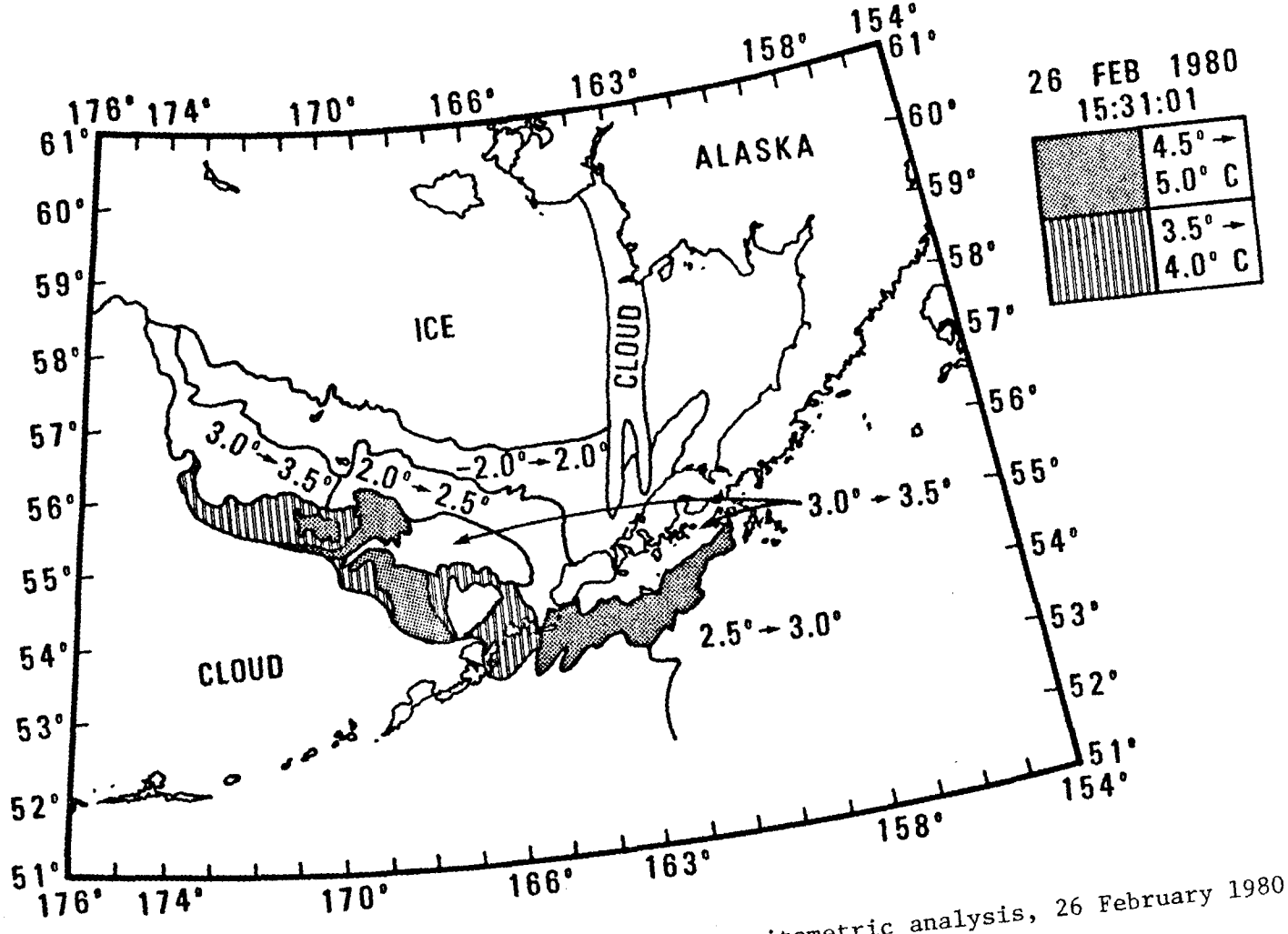

Figure 15b. Temperature contours produced from densitometric analysis, 26 February 1980; GMT 15:31:01.

SST gradient could be seen paralleling the 200-m bathymetric contour. Three eddies could be seen seaward of this gradient. From right to left the first was a cyclonic, cold core eddy; then over the Pribilof Canyon the eddy was anticyclonic with a warm core; the third was anticyclonic with a cooler core and appeared to be just east of Zhemchung Canyon (Figure 15a). Overall, there appeared to be an undulating band of cooler water within the warm band which extended from the 100-m contour out into the basin. The warm band of water which paralleled the Aleutian Chain on the North Pacific side was also visible and well defined in Figures 15-18. The second image on the 26th of February was received five hours later than the first by the NOAA-6 satellite; all the previously described features were still visible (Figure 16a). On the 27th of February, the eddies were still visible, and the undulating pattern of the cooler water was more pronounced (Figure 17a). The ice edge had advanced so that the water around St. Paul was between -1.5 to -2.0°C (more probably -1.5 to -1.7), and in places the ice edge had nearly reached 56°N. The second image on February 27 (Figure 18a) also shows these features, but the eddy near Zhemchung Canyon is no longer visible.

The remaining images in this time period showed that the ice edge had retreated to a position 70 km from St. Paul during March, while in April, visible and unchanged infrared indicated that Bristol Bay was clear of ice and cloud cover. The enhancement revealed that the open water was between -1.5 and -2.0°C, possibly indicating that the ice had just melted. Some SST gradients could be seen in the deeper

Figure 16a. Infrared image for 26 February 1980, GMT 20:03:21; enhanced with Table 64P-7.

Features of interest are: the three eddies described previously, located by the arrows; the warm surface water along the Alaska Peninsula and in Unimak Pass, the ice edge; very cold water (-1° to -2°C) which now surrounds St. Paul Island.

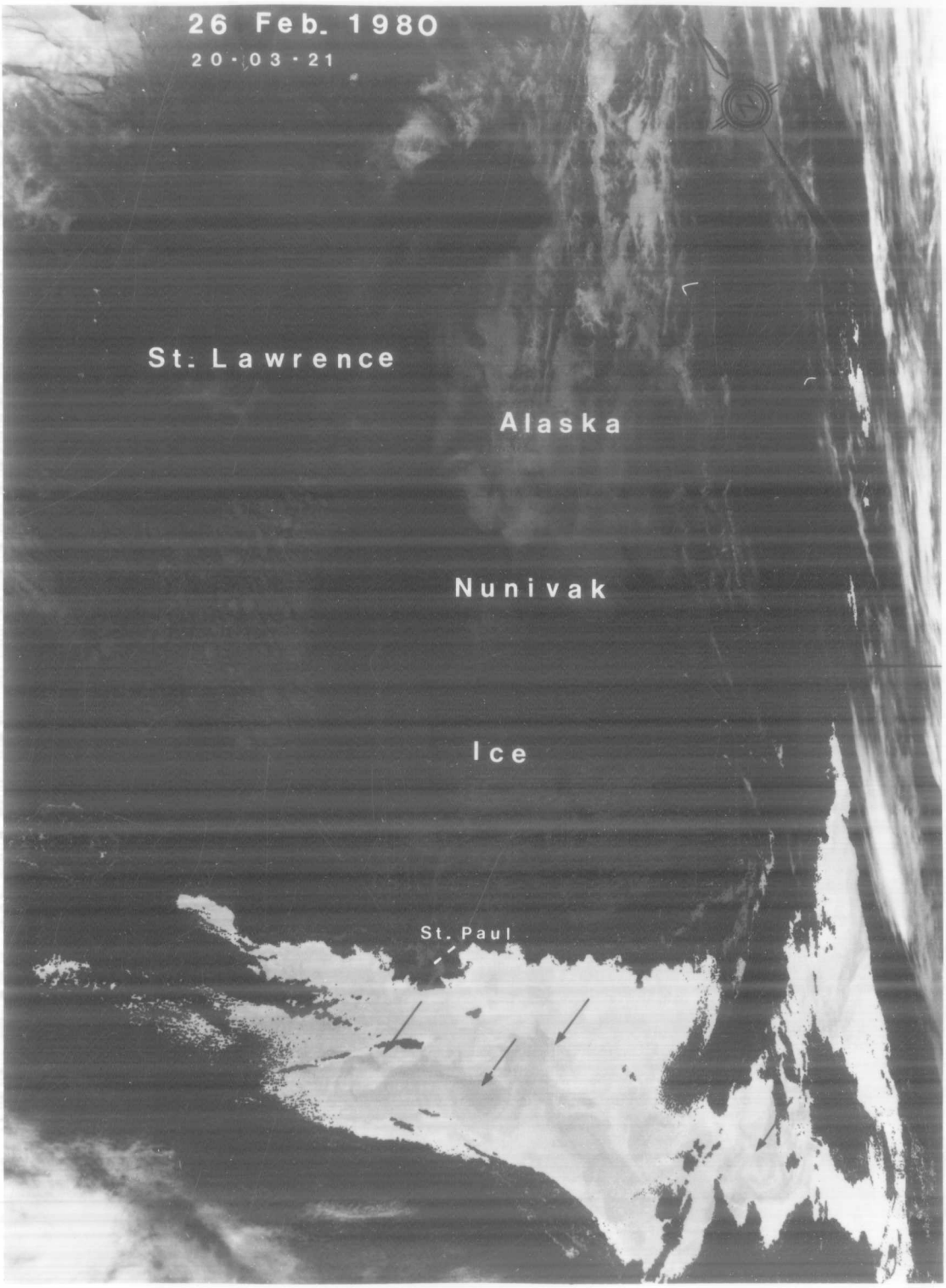
26 Feb. 1980
20·03·21
St. Lawrence
Alaska
Nunivak
Ice
St. Paul

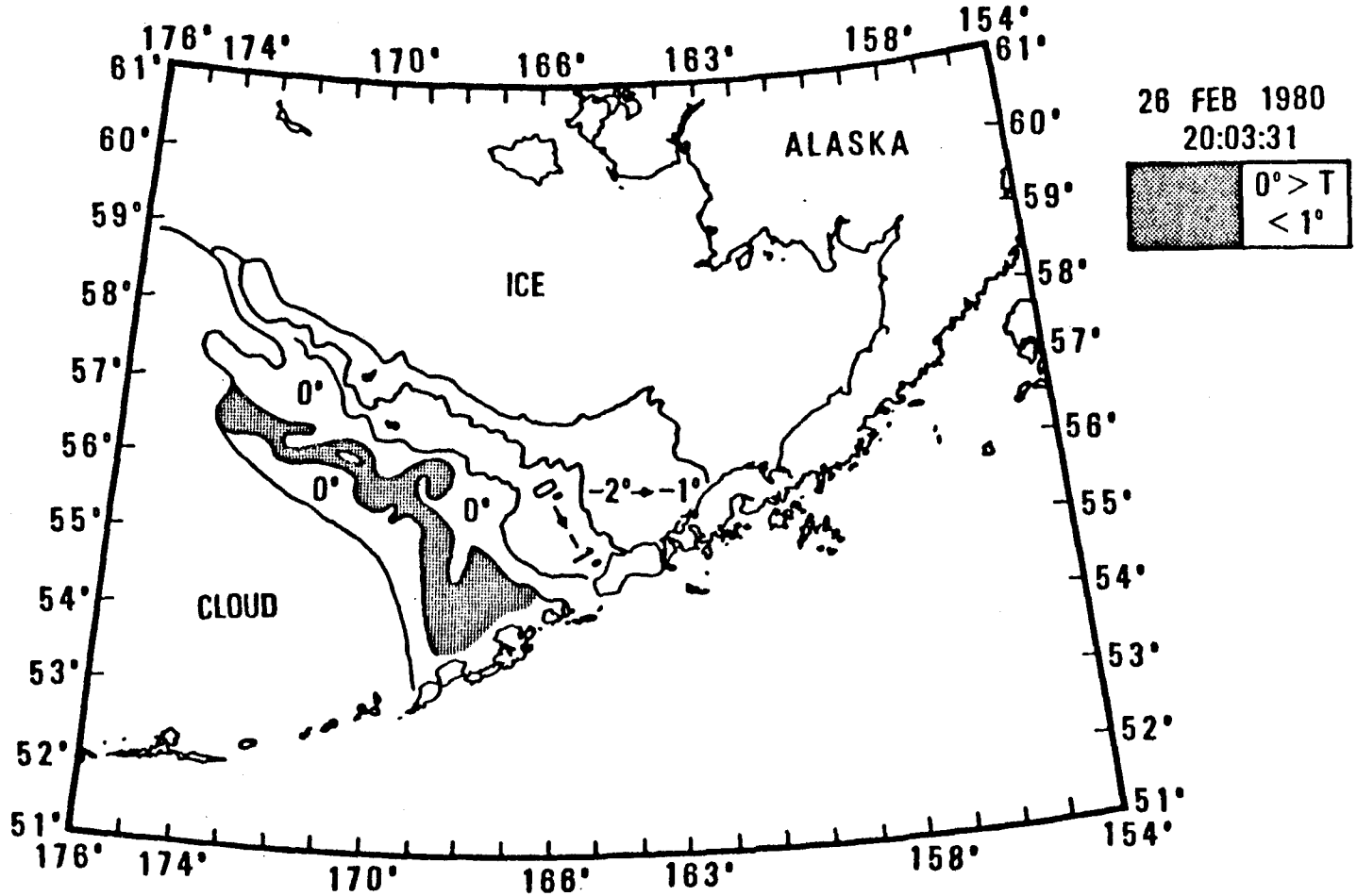

Figure 16b. Temperature contours produced from densitometric analysis, 26 February 1980; GMT 20:03:21.

Figure 17a. Infrared image for 27 February 1980, GMT 05:55:11; enhanced with Table 64P-7.

Features of interest are: the first and second eddy which are still visible, aligned along the shelf break, the warm surface water along the Alaska Peninsula and in Unimak Pass, the ice edge, and very cold water (-1° to -2°C) around St. Paul Island.

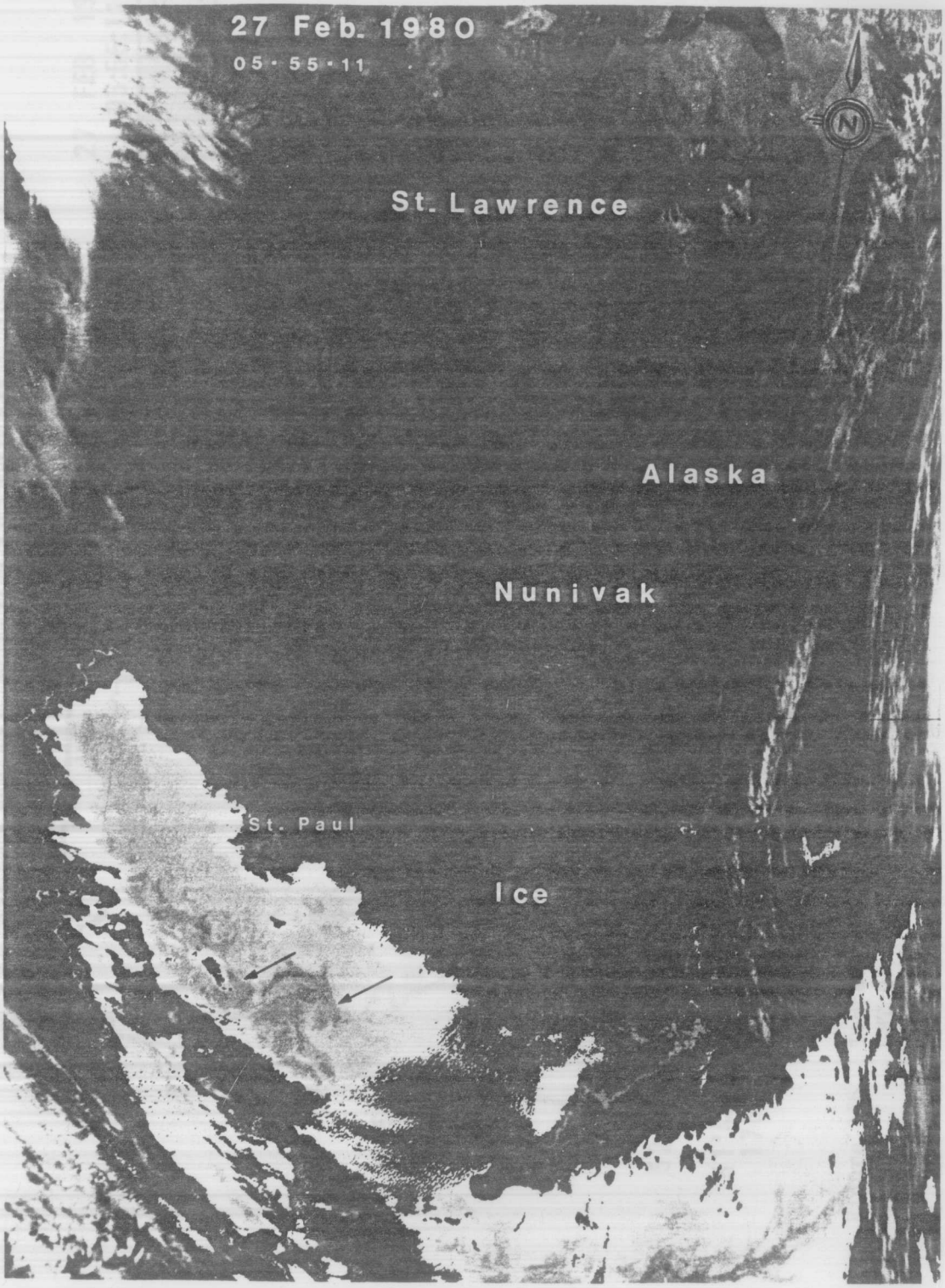
27 Feb. 1980
05·55·11
N
St. Lawrence
Alaska
Nunivak
St. Paul
Ice

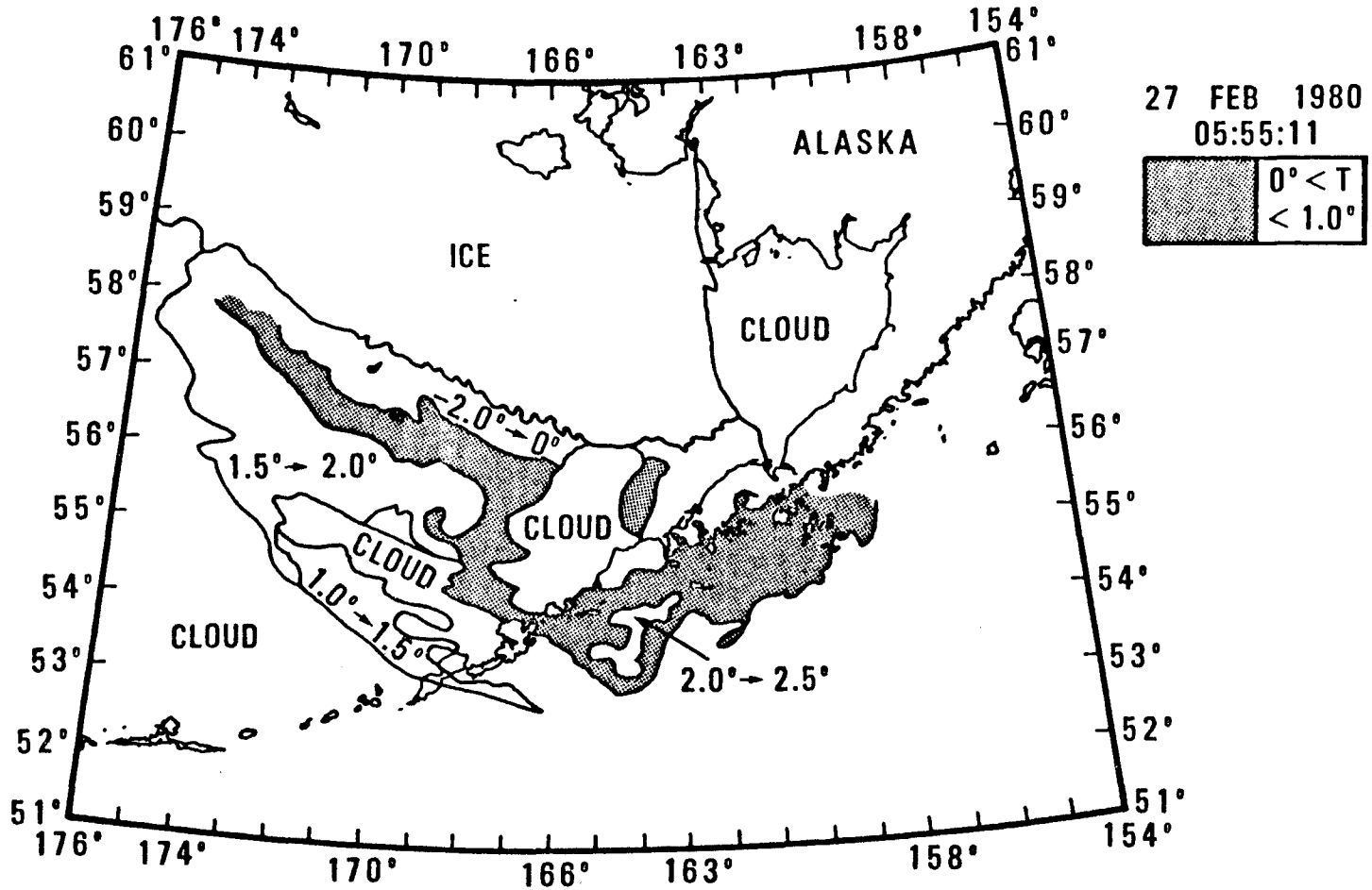

Figure 17b. Temperature contours produced from densitometric analysis, 27 February 1980; GMT 05:55:11.

Figure 18a. Infrared image for 27 February 1980, GMT 19:41:31; enhanced with Table 64P.

Features of interest are: the remaining two eddies along the shelf break, the wave-like nature of the sea surface temperature patterns along the shelf break, the ice edge, and the very cold (-1° to -2°C) water around St. Paul Island.

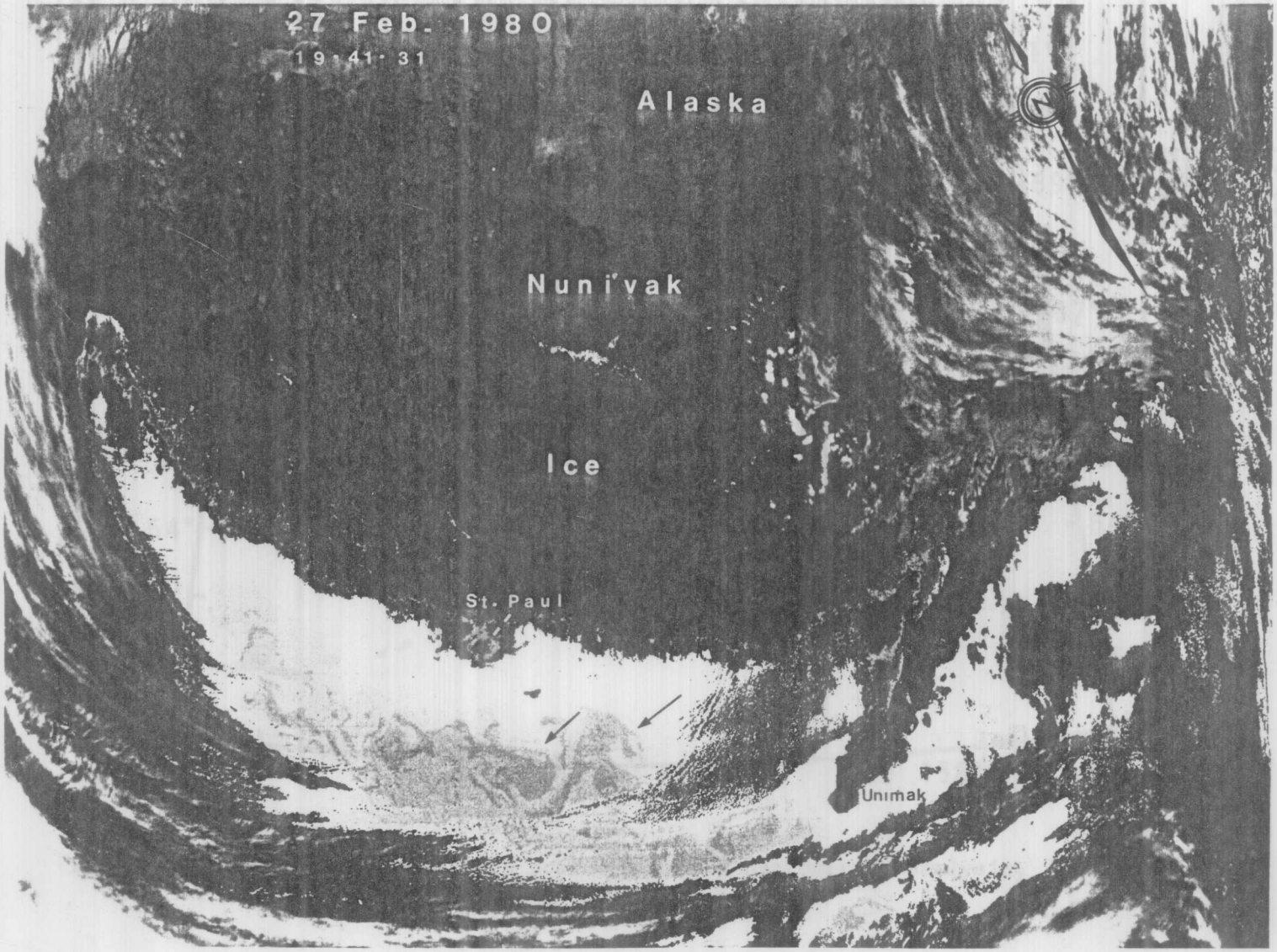
27 Feb. 1980
19:41:31
Alaska
Nunivak
Ice
St. Paul
Unimak

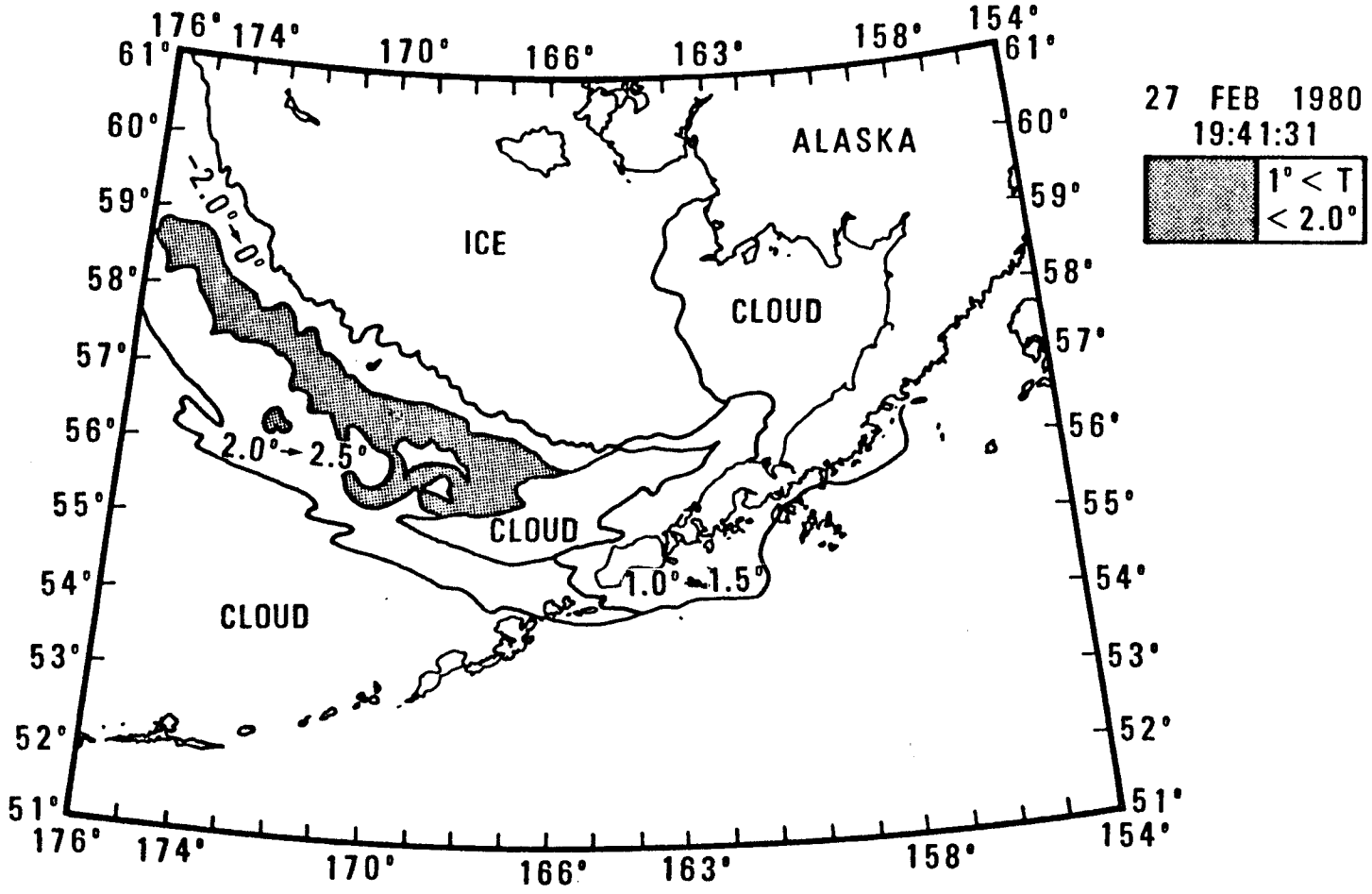

Figure 18b. Temperature contours produced from densitometric analysis, 27 February 1980; GMT 19:41:31.

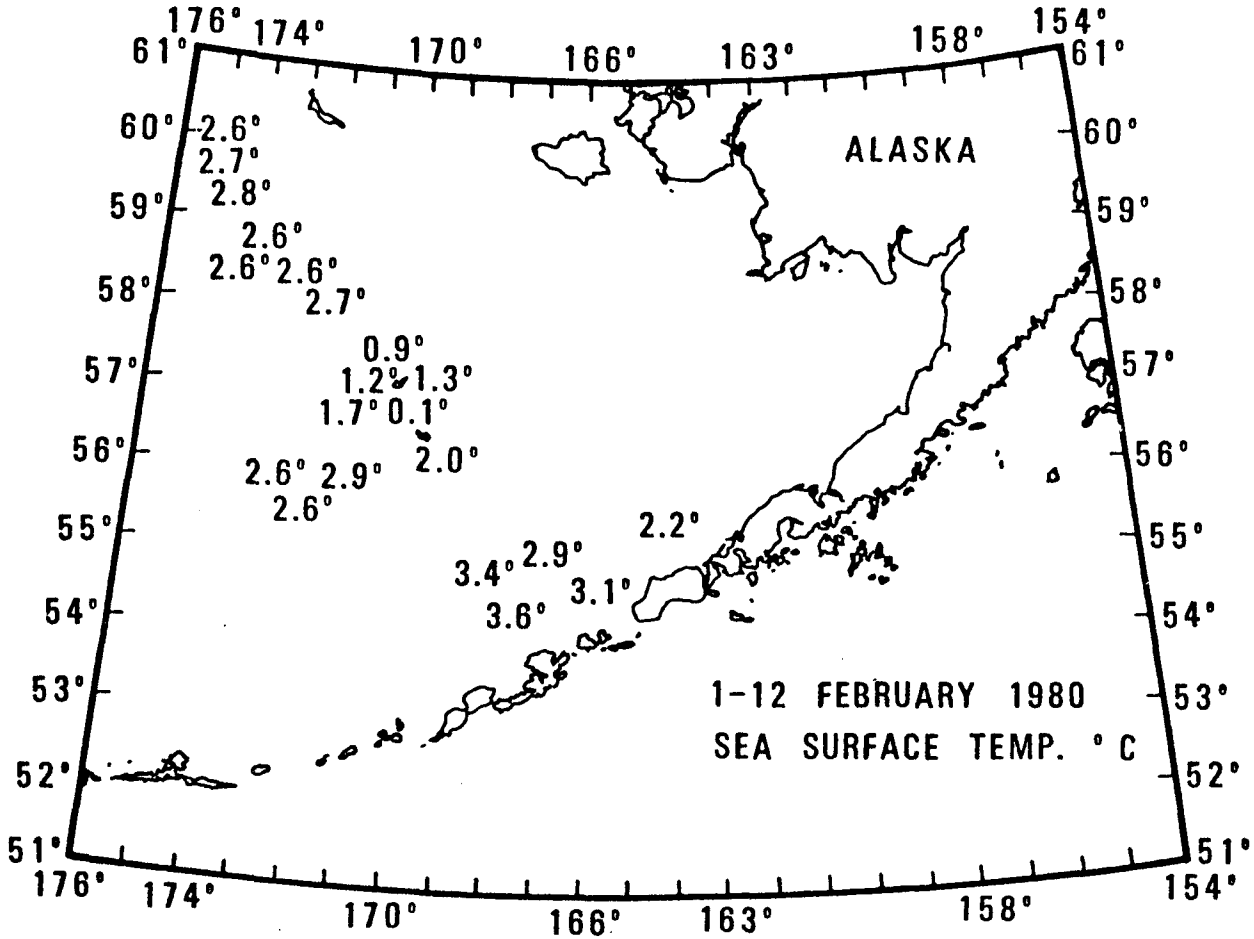

Figure 19. Sea surface temperatures for 1-12 February 1980 used for surface truth data.

water near the 100-m isobath, and the warm band of water could also be seen, again paralleling the Alaska Peninsula and nearing Unimak Pass.

May 1980 - August 1980

A total of 22 images were found during this period with coverage of Bristol Bay during May-July and coverage of the shelf break in August. The information derived from visual inspection of these images is presented in order to establish the temporal trends of features in the Bering Sea. August imagery was analyzed, and the most interesting features are presented in Figure 20.

Four images were found on 5, 8, 19, and 20 May, which covered Bristol Bay. In all of these images, SST gradients could be seen following the 20- and 30-m isobaths. The water was warm near the shore, with cooler water seaward. The water near the mouth of the Kuskokwim was cooler; however, a small patch beyond the 50-m isobath was warmer than the surrounding water.

On 8 and 23 June, there were clear images of Bristol Bay again. These images showed the same structure as was seen earlier in May. These images revealed a gradient paralleling the 50-m isobath and patches of cooler water seaward of the 50-m contour. On the 23rd, the warm band, possibly the Alaska Stream or the Alaska Coastal current, could be seen following the same path as was previously described. Note that in summer there tends to be more clouds and less thermal contrast due to insolation, so the imagery is less frequent and well defined.

In July, eleven images were found giving clear views of Bristol Bay. An image on 9 July was then followed by a six-day time series spanning 19 through 25 July. The major feature seen in all of the images was the temperature gradient which followed the 50-m isobath. Seaward of the 50-m isobath was cooler water with an even cooler, localized area just south of the tip of Cape Newenham. The temperature structure remained relatively constant, spatially, throughout the six-day time series. The term "relatively" is used because not all the scenes are over the exact same area, and also some scenes are more contaminated by clouds and fog than others. Another feature seen was the finger-like temperature structures at the mouth of the Kuskokwim and SST gradients along the 70-, 100-, and 200-m isobaths.

A time series of images was found in August, spanning the 21st to the 25th. The image on the 21st revealed SST gradients which paralleled the 40-, 50-, and 60-m isobaths from Bristol Bay out to St. Matthew Island and up near St. Lawrence. An area of cooler water could be seen curled around St. George, and some also around St. Paul Island. This water appeared to be part of a band of water coinciding with the 100-m isobath. On the 22nd the cool water patch around the Pribilof Islands was more pronounced and extensive. The patch completely surrounds both islands and curled around the Pribilof Canyon. The following day, August 23 (Figure 20), an eddy was seen slightly southeast of the Pribilof Canyon. The eddy was anticyclonic with a warm core that seemed to match water temperatures in the shelf

Figure 20a. Infrared image for 23 August 1980; enhanced with Table 64X.

Features of interest are: an anticyclonic, warm core eddy southeast of St. George Island, cool water (lighter shade of gray) along the Aleutian Chain on both Pacific and Bering sides and within the passes, a small anticyclonic cold core eddy just north of Amutka Island, an isolated patch of warm surface water in the Gulf of Alaska near the Aleutian Chain.

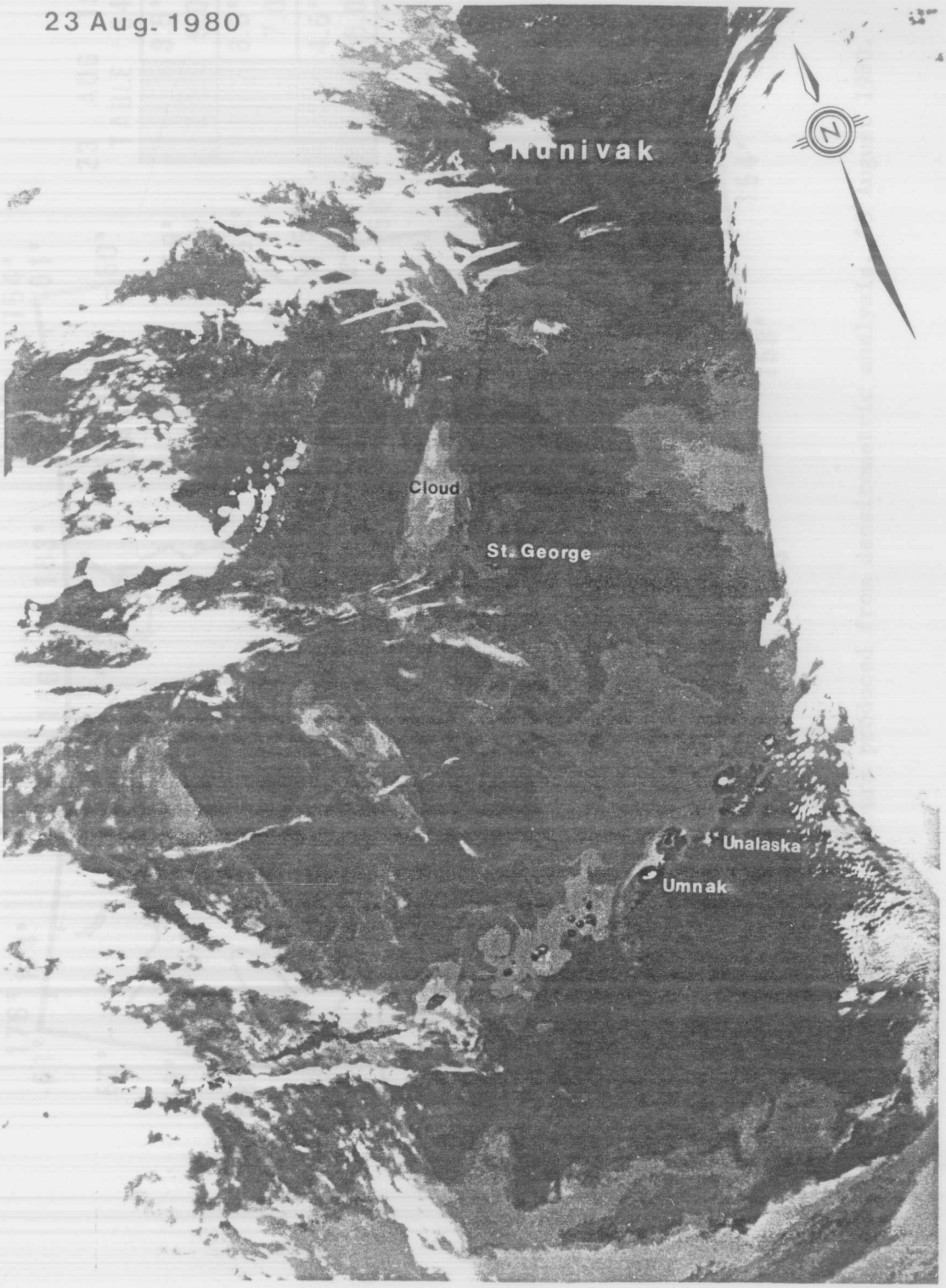
23 Aug. 1980
Nunivak
N
Cloud
St. George
Unalaska
Umnak

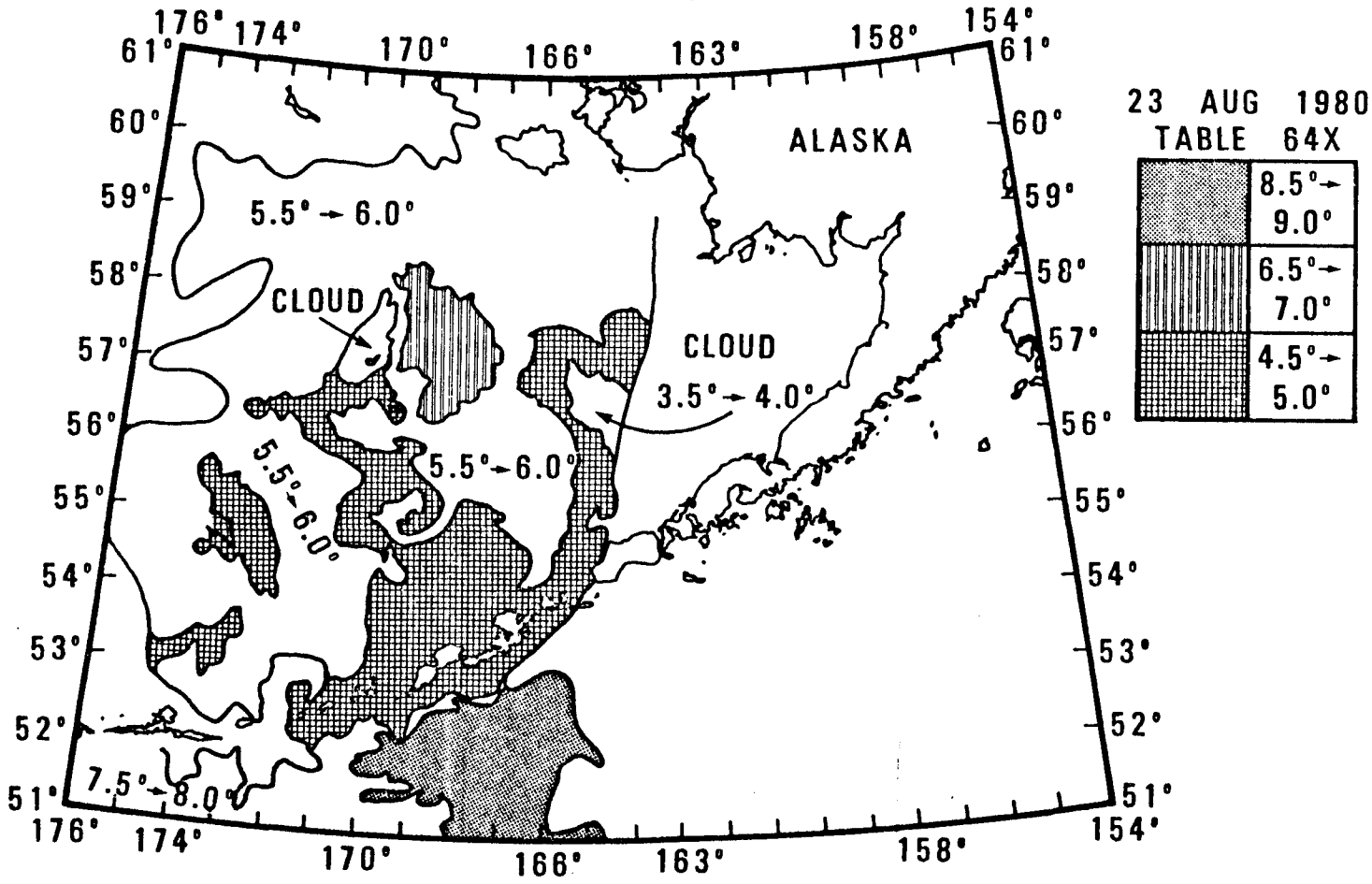

Figure 20b. Temperature contours produced from densitometric analysis, 23 August 1980.

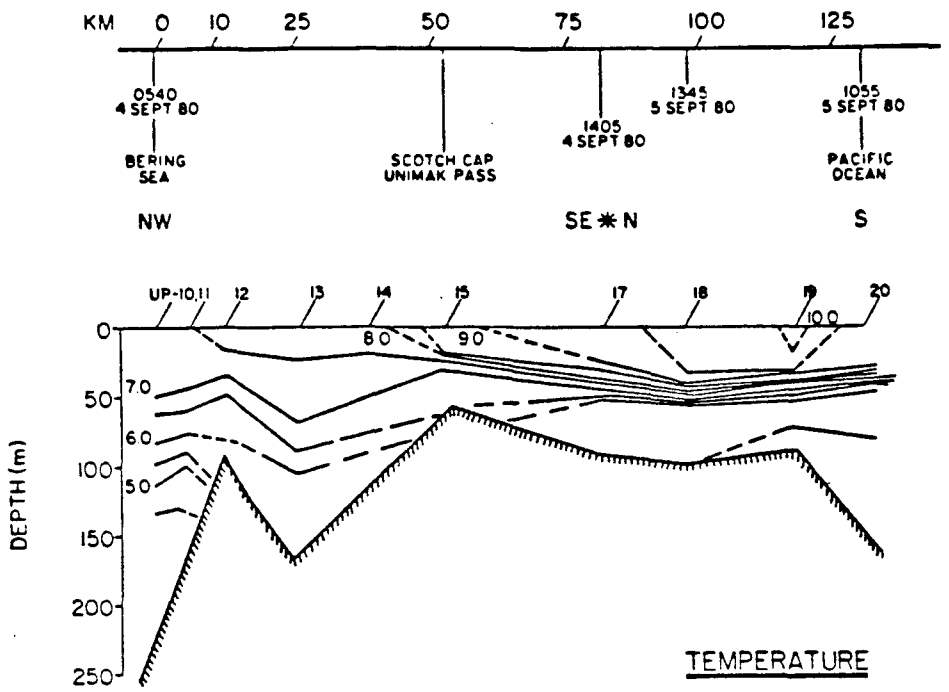

Figure 21. Hydrographic sections for Gulf of Alaska to the Bering Sea through Unimak Pass, September 1980 (after Schumacher *et al.*, 1981).

region. The temperature of the outer ring of the eddy appeared to match the temperature of water along and within the Aleutian Island passes in that area. Smaller, swirling, eddy-like structures could be seen within those passes. Much warmer water was seen on the south side of the Aleutian Islands. On the 24th and 25th of August the temperature structure of the water along the Aleutian Islands and on the shelf in Bristol Bay was the same as described on the 23rd; however, clouds obscured the area where the eddy was previously seen.

September 1980 - November 1980

Satellite imagery during this period was sparse; storms are very frequent during this time of the year, and it is not usual to find imagery over the Bering Sea for this time. An image in September was found which showed that the features on the shelf, described previously, could be seen. Several images for October are presented; however, no clear images were found in November.

In October clear images were found on the 8th, 9th, 10th, and 27th. The image on the 8th showed SST gradients coinciding with the 10-, 20-, 30-, and 40-m isobaths. On the 9th (Figure 22) a band of warm water is seen extending onto the shelf and curling cyclonically around the Pribilof Canyon. Table 64X was used originally for Figure 22a; however, Table 64Z (Figure 22b) (-3 to 12°C) was also used to reveal as much temperature structure as possible. The second table, 64Z, uses a different gray tone every half degree of temperature whereas the first table uses less steps, hence less gray tones to

Figure 22a. Infrared image for 9 October 1980; enhanced with Table 64X.

b. Infrared image for 9 October 1980; enhanced with Table 64Z.

Features of interest are: the region of warm surface water extending from the Alaska Peninsula to near the Pribilof Islands where it curls cyclonically; in the second image (b) there is a region of still warmer water within the larger region, the warm band in the Gulf of Alaska paralleling the Alaska Peninsula.

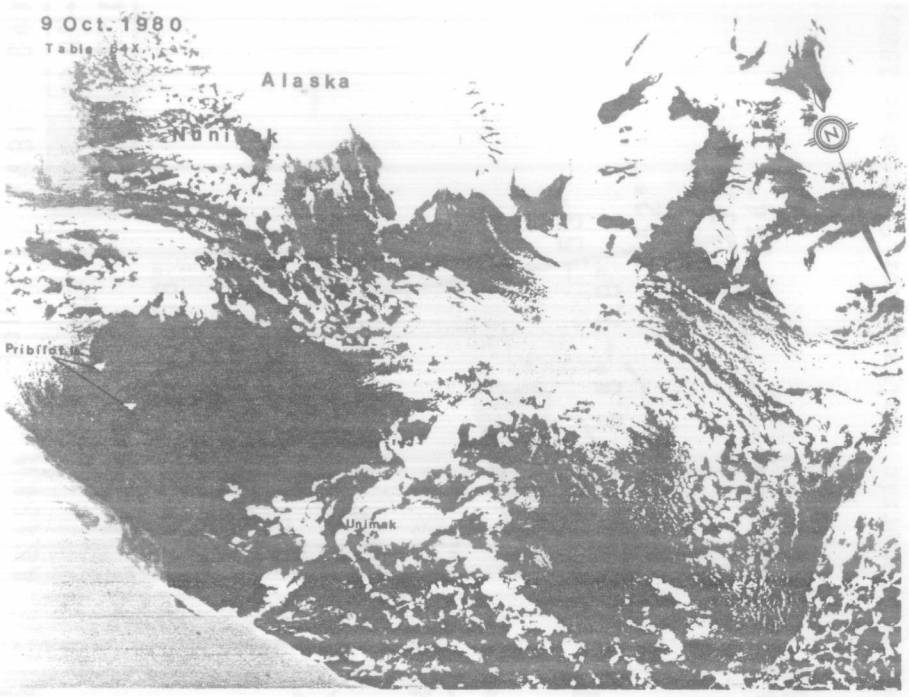
9 Oct. 1980
Alaska
Unimak

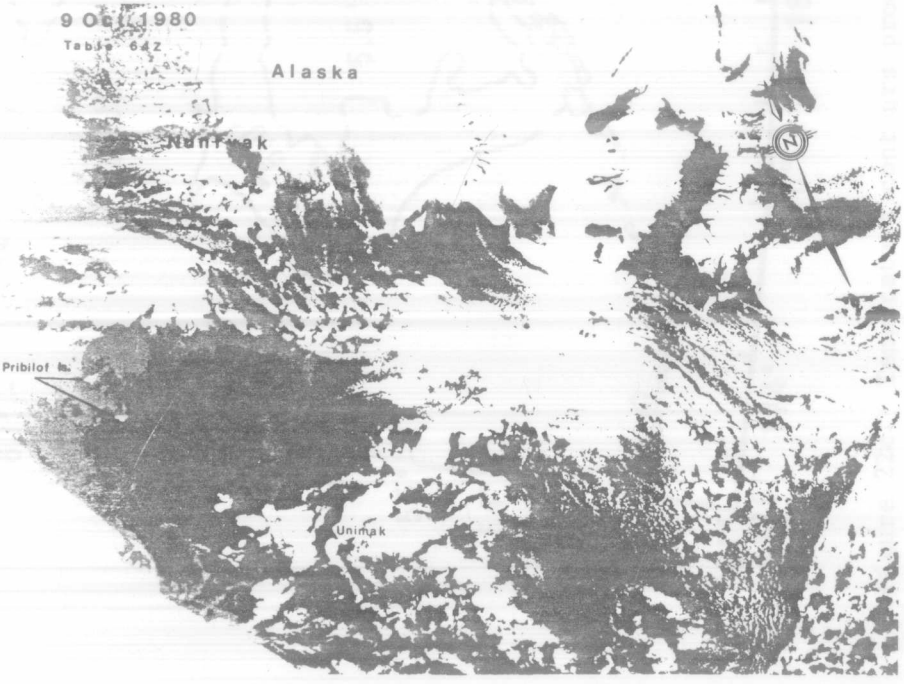
9 Oct. 1980
Alaska
Unimak

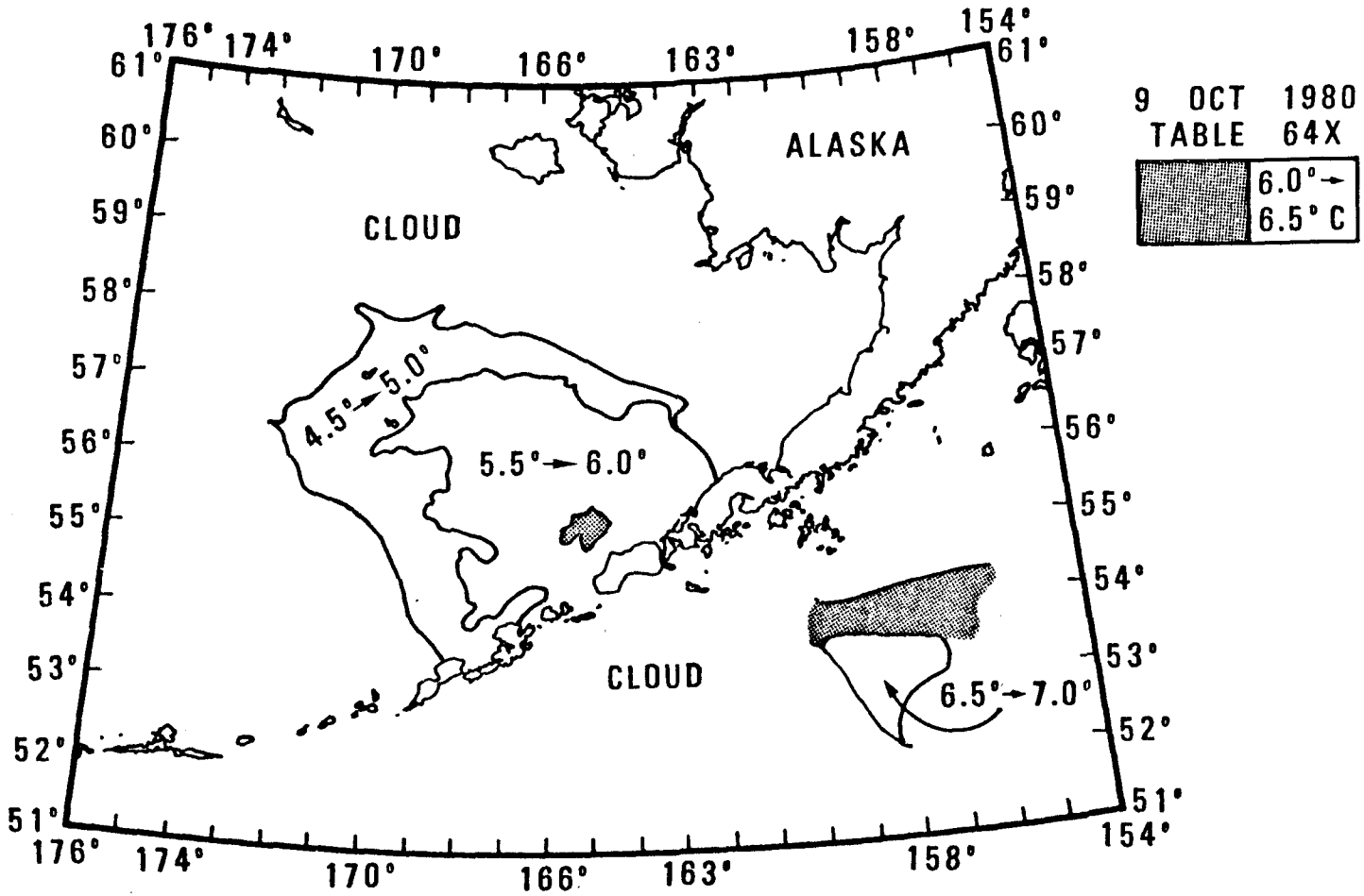

Figure 22c. Temperature contours produced from densitometric analysis for 9 October 1980; with enhancement Table 64X.

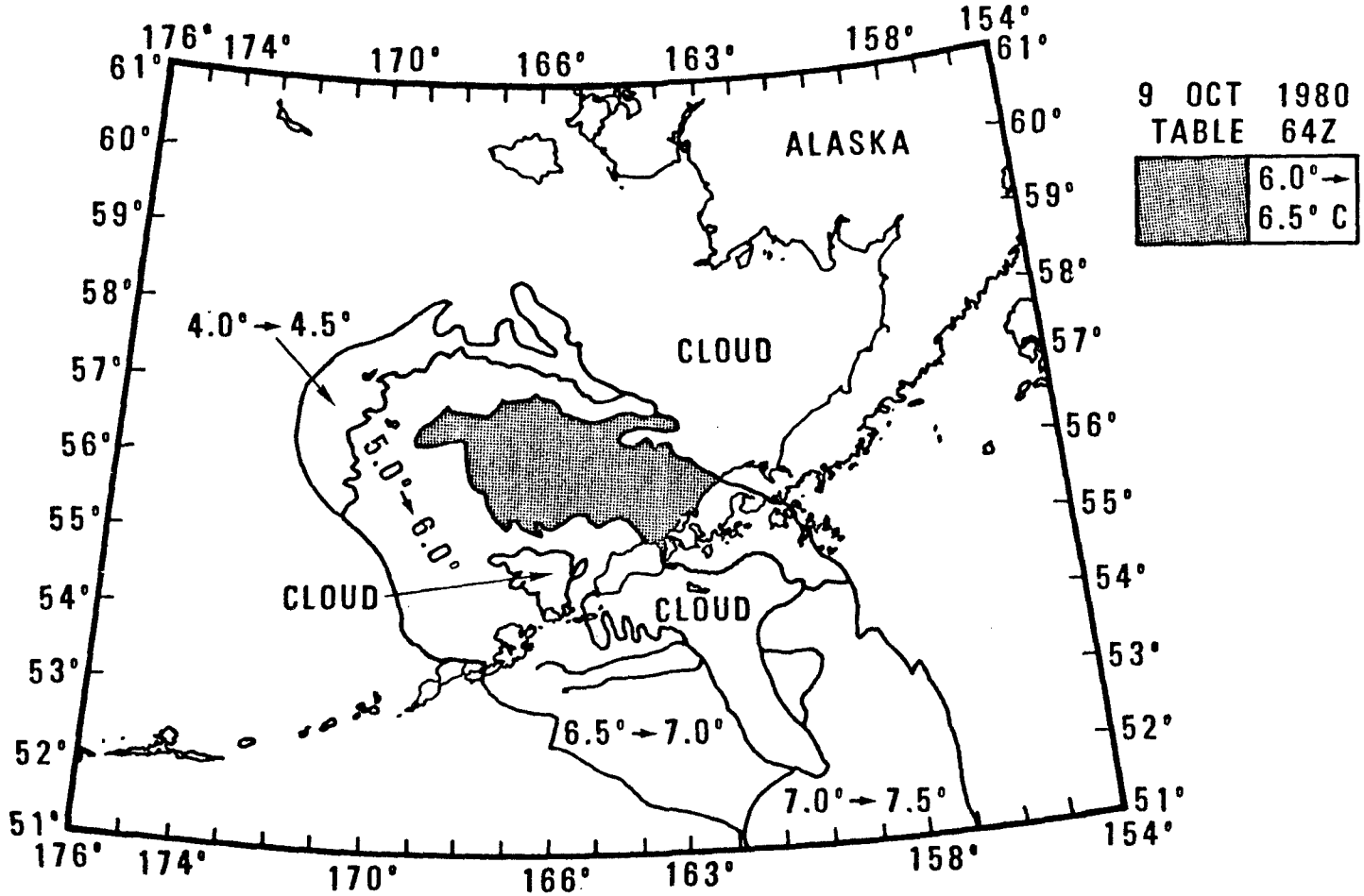

Figure 22d. Temperature contours produced from densitometric analysis for 9 October 1980; with enhancement Table 64Z.

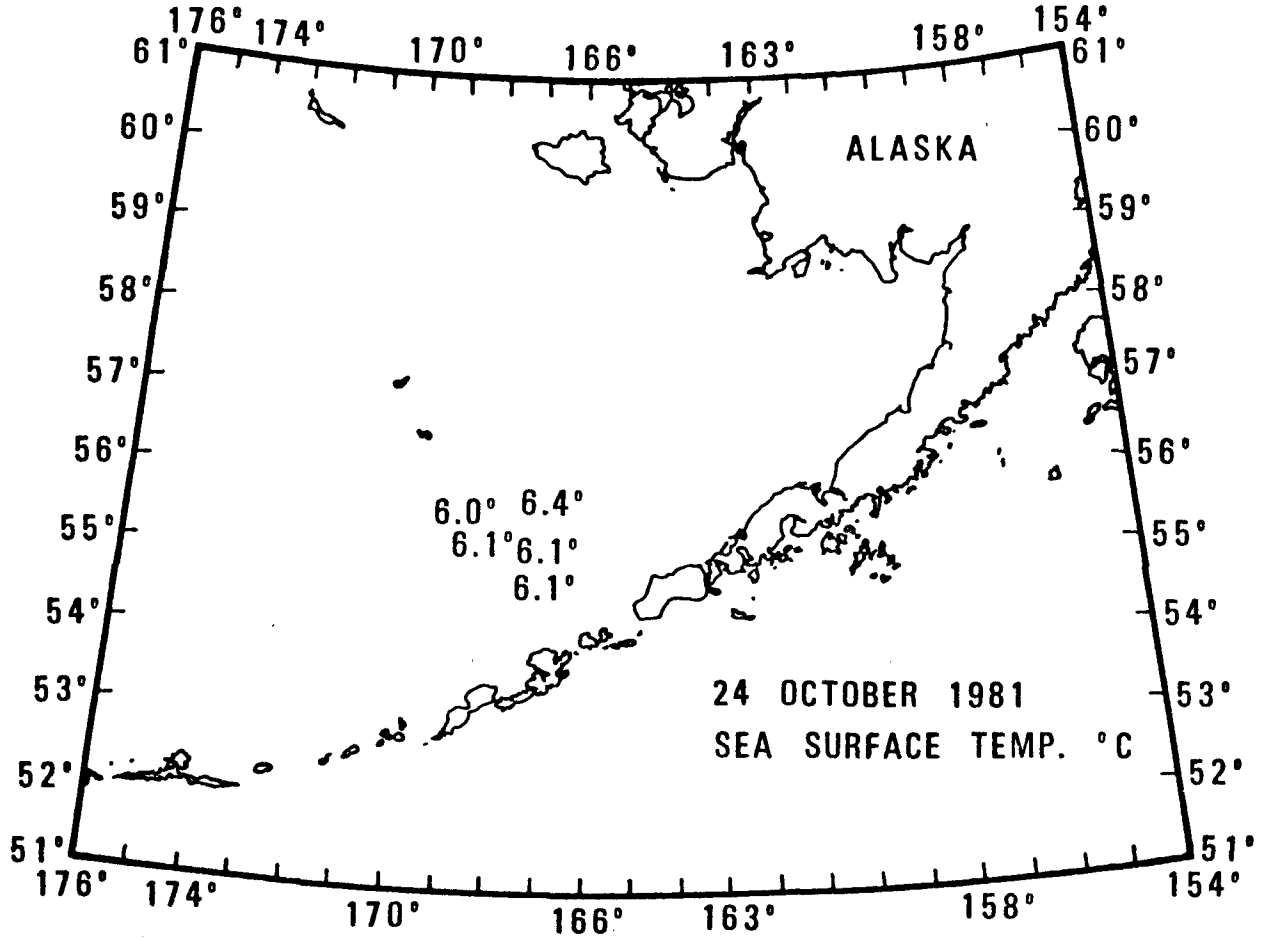

Figure 23. Sea surface temperatures for 24 October 1980 to be used as surface truth data.

cover the temperature range. The additional enhancements revealed a warmer area within the band originally seen. The same curling structure was seen, and within the warmer band of water other cyclonic curls could be seen. Since these features did not separate from the water of similar temperature surrounding them, they were not referred to as eddies. On the 10th and 27th the shelf break area was cloud-covered; however, the SST gradients coinciding with the 50-m isobath in Bristol Bay could be seen.

December 1980 - February 1981

In December 1980, ten images were available: two on the 10th and 11th, one on the 24th, three on the 25th, one on the 26th and 27th. The images on the 10th showed the ice had reached Nunivak Island and had formed along the coastline in Bristol Bay. The SST gradients were very well defined and follow the bathymetric contours. On the 11th clouds obscured all but the area around the Pribilof Islands. In this area SST gradients were seen which followed the 100-m and 70-m isobaths. By the 24th of December the ice edge had completely surrounded Nunivak Island and was between 59 and 58°N latitude. The SST gradients were seen, and they closely followed bathymetric contours, especially the 100-m contour. A warmer region was noted southeast of the Pribilof Islands, between 100 and 130 m of water. In the image taken on the 25th of December (Figure 24a), the ice edge appeared to follow the 50-m contour very closely. The SST contours again were seen following the 100- and 70-m isobaths. A very

Figure 24a. Infrared image for 25 December 1980, GMT 06:40:25; enhanced with Table 64P.

Features of interest are: the band of warm surface water following the shelf break, a warmer band of water within the previously mentioned band — this feature located roughly over the 200-m bathymetric contour, warm surface water paralleling the Aleutian Chain in the Gulf of Alaska and within the Aleutian passes, the ice edge paralleling the 50-m bathymetric contour.

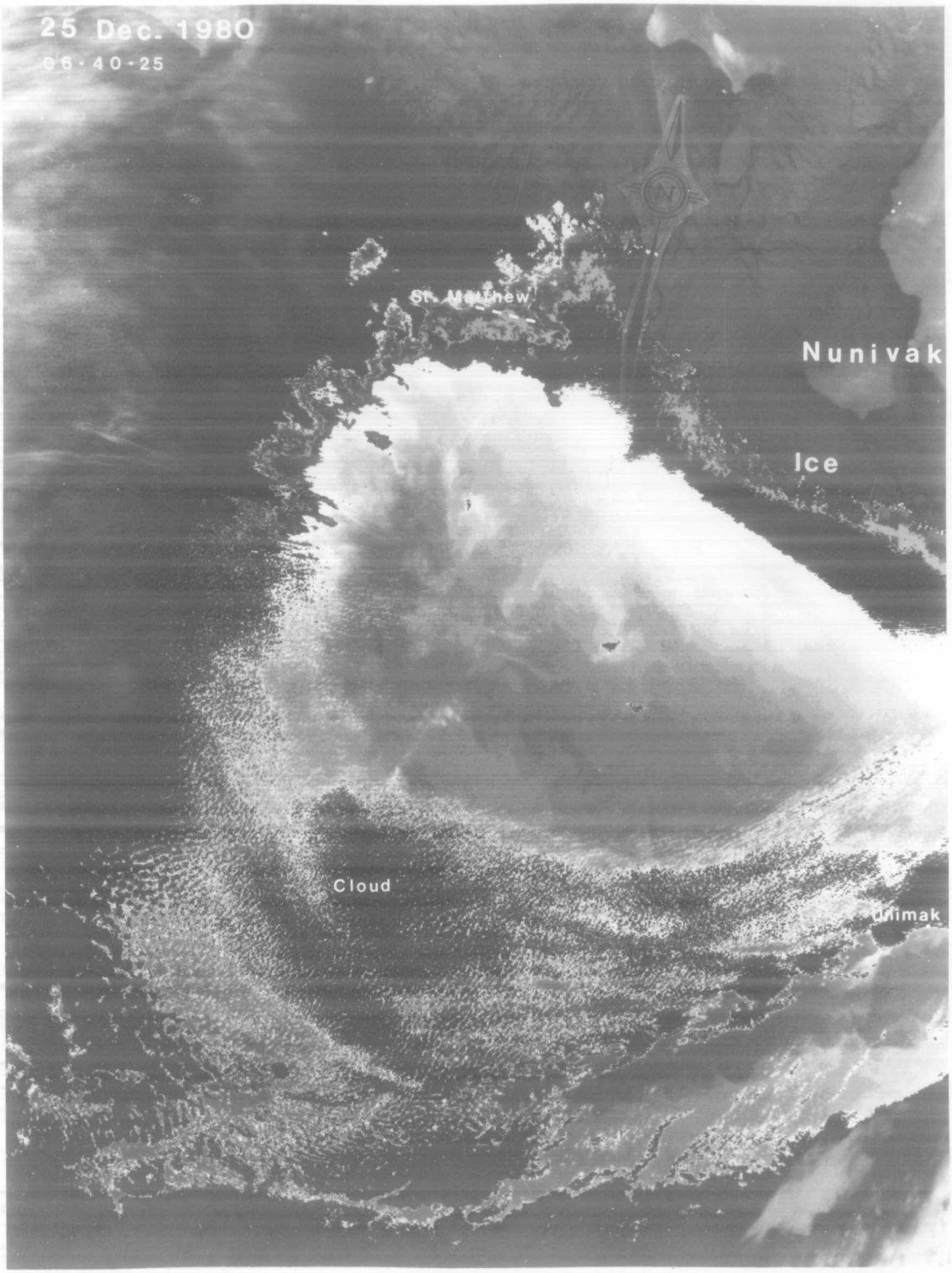
25 Dec. 1980
06·40·25
N
St. Matthew
Nunivak
Ice
Cloud
Unimak

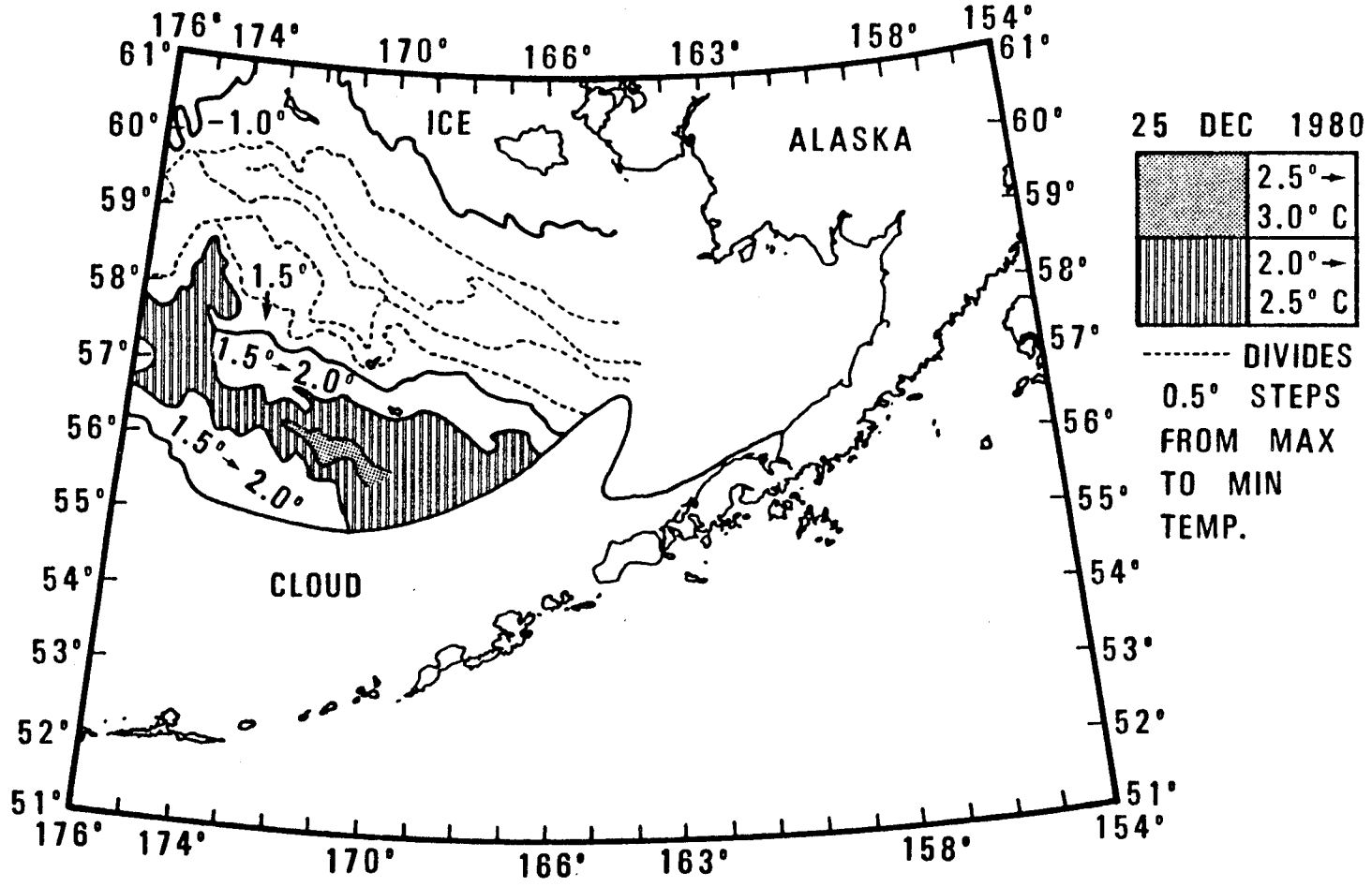

Figure 24b. Temperature contours produced from densitometric analysis for 25 December 1980; GMT 06:40:25.

prominent feature was the band of warm water following the 200-m bathymetric contour (Figure 24a). The limits of the band were the approximately 100- and 3000-m isobaths; this band is broadest at the southeast corner, narrowest in the northwest corner. Also, there was cooler water surrounding St. Paul, but not St. George Island. Later images on 25, 26, and 27 (Figures 25a, 26a) revealed an even warmer band located over the 200-m contour, within the previously described broad, warm band of water. This warmer band had an undulating nature and was seen in the northwest portion. On either side of the 100-m and 3000-m bathymetric contours, surface water was cooler. Over the Bering Sea basin, SST structure was noted (Figure 25a) which appeared to run from the southeast corner of the basin to the northwest corner. No clear images were available in January.

An image on February 23 showed that the ice edge had advanced to the 60-m isobath in the western Bering Sea but was still no further south than the 50-m isobath in Bristol Bay; the southernmost point was approximately 57°N. Clouds obscured much of the sea surface; however, the warm band in the Gulf of Alaska, paralleling the Alaska Peninsula (assumed to be the Alaska Stream), could be seen in the same place as it was seen previously (Figures 9, 10, 11).

March 1981 - May 1981

For March, four clear images were found. The images on the 21st and 22nd (Figure 27) showed large leads had formed in the ice in the western Bering Sea. Nunivak Island, Bristol Bay, and Norton Sound

Figure 25a. Infrared image for 25 December 1980, GMT 20:27:40; enhanced with Table 64P.

Features of interest are: the band of warm surface water paralleling the shelf break, between the position of the 100-3000 m bathymetric contours, the undulating band of even warmer water within the previously mentioned band, the sea surface temperature pattern which runs from the Aleutian Chain across the basin to the shelf break, and the ice edge extent.

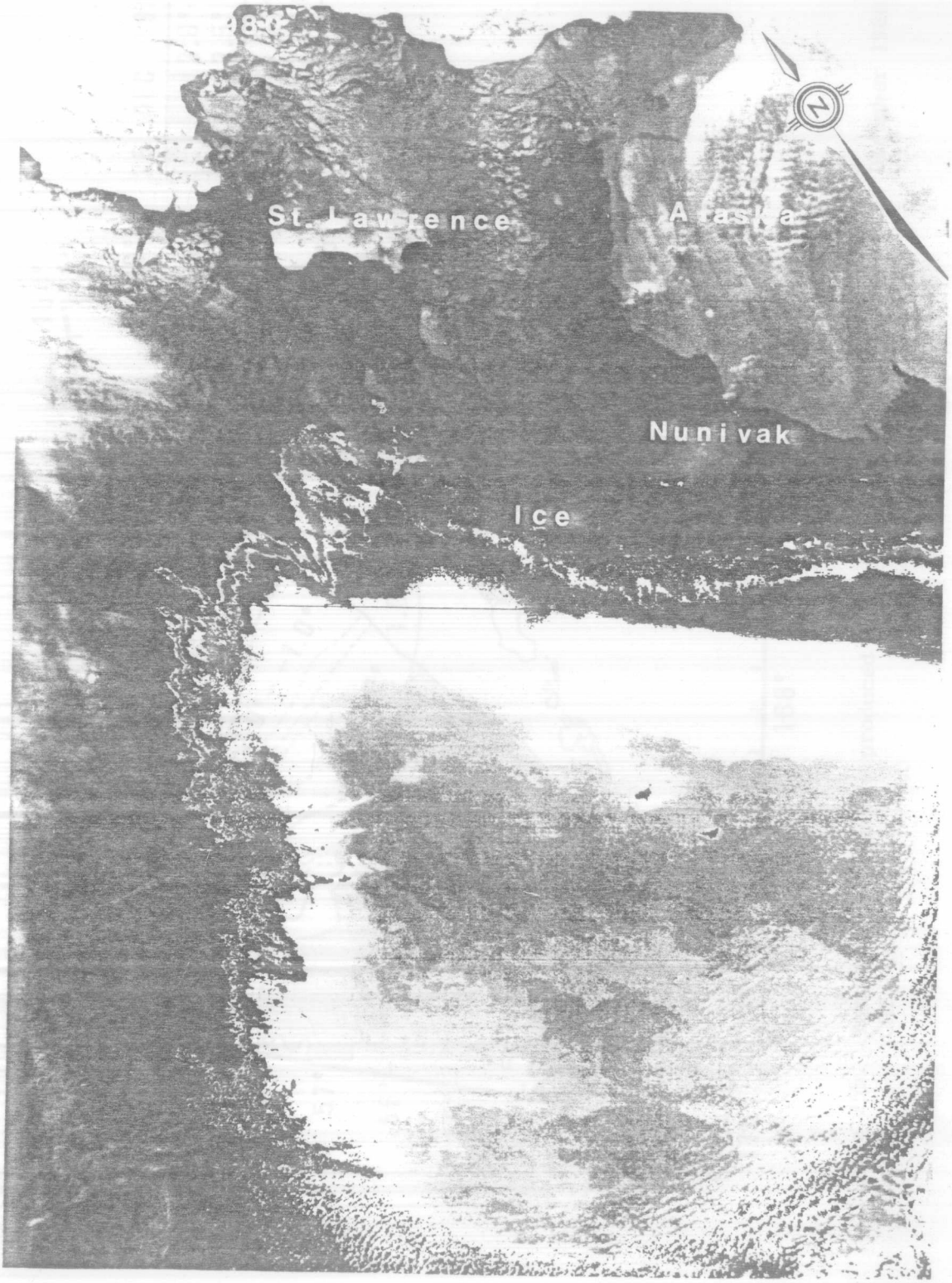
St. Lawrence
Alaska
Nunivak
Ice

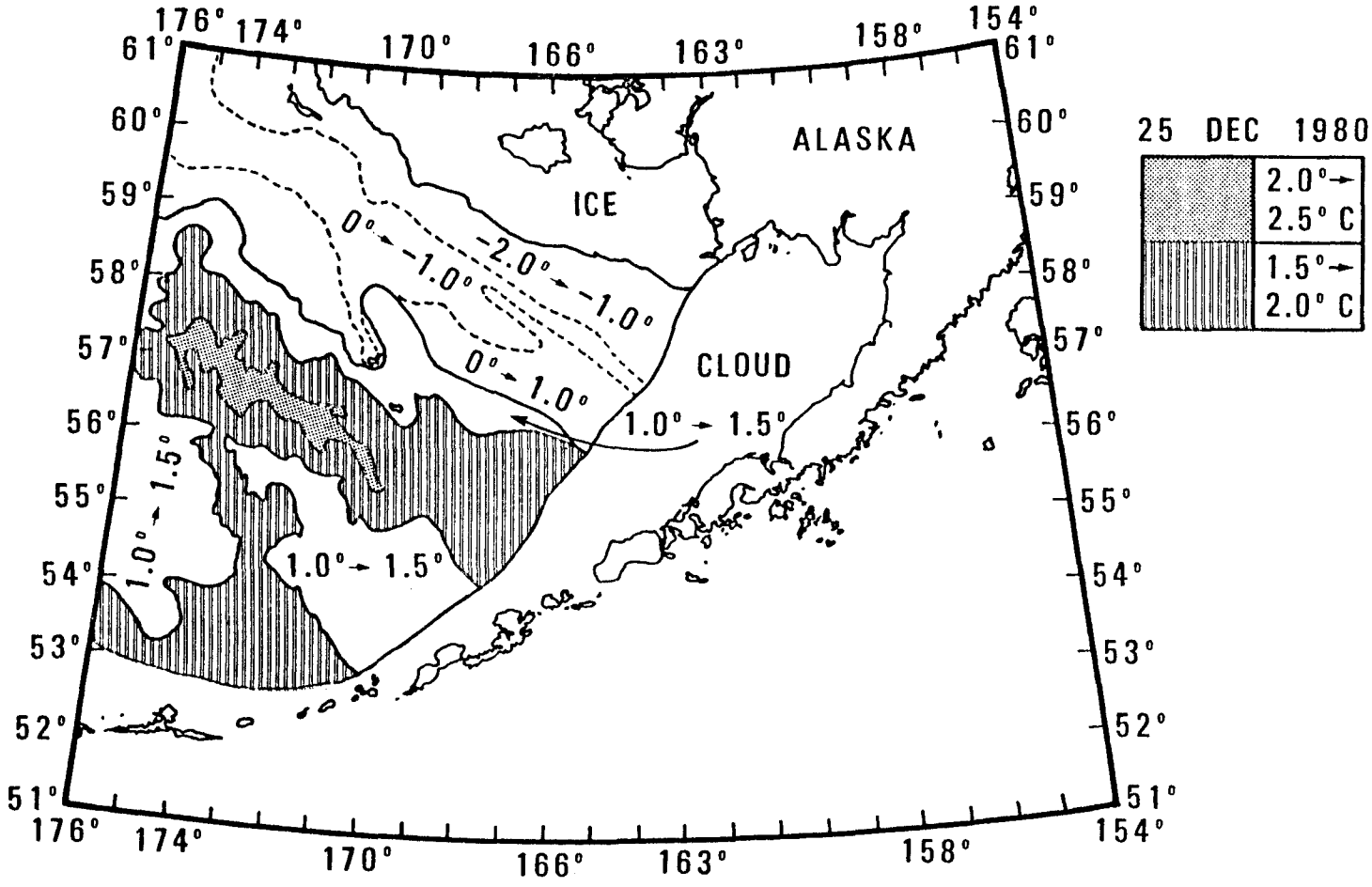

Figure 25b. Temperature contours produced from densitometric analysis for 25 December 1980; GMT 20:27:40.

Figure 26. Infrared image for 26 December 1980; enhanced with Table 64P.

Features of interest are: the northwest end of the warm shelf break band (seen in the two previous images), the region of warm surface water along the Gulf of Alaska and Bering Sea sides of the Aleutian Chain and within the passes, the ice edge extent.

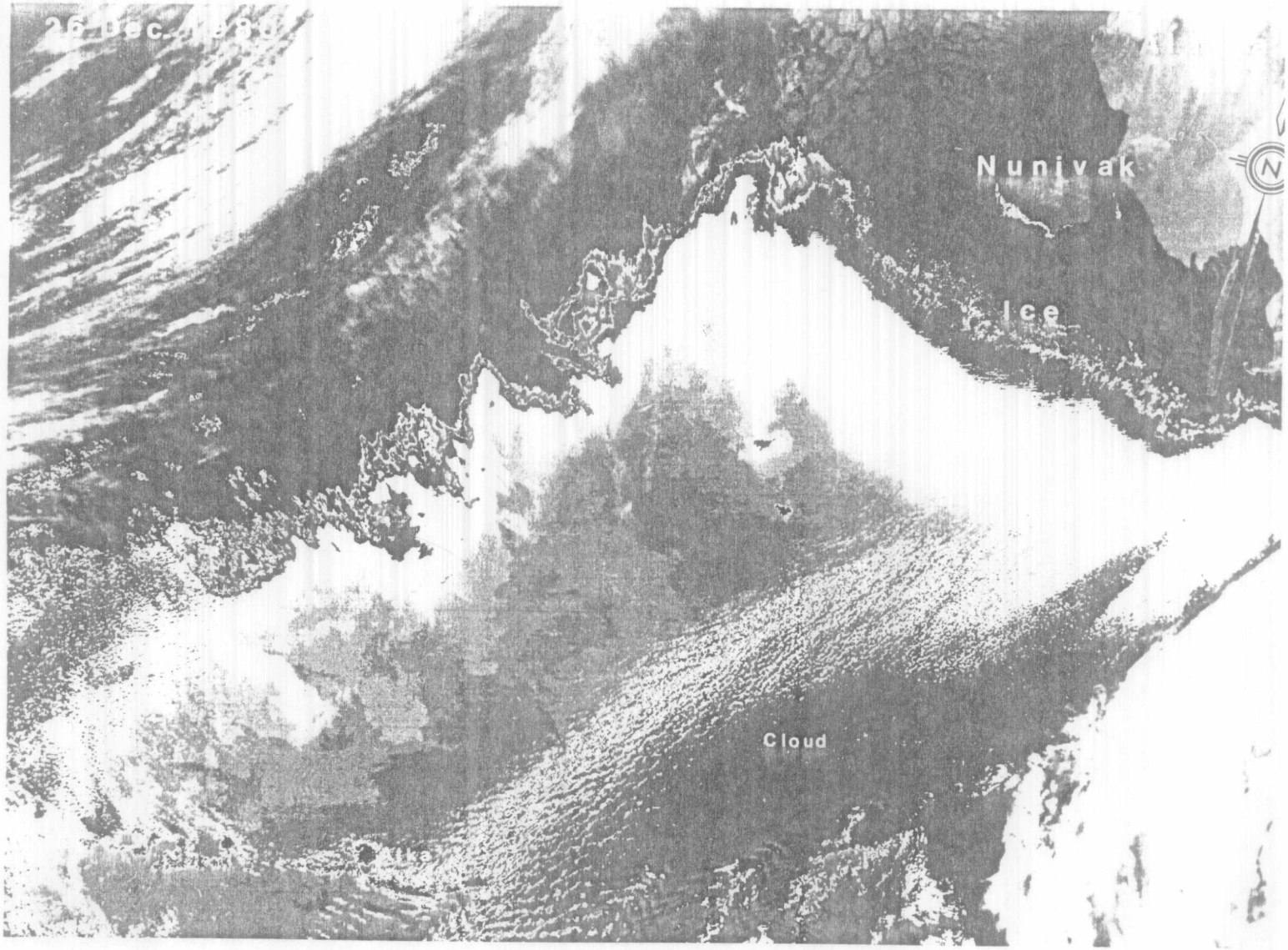
Nunivak
Ice
Cloud

Figure 27a. Infrared image for 22 March 1981; enhanced with Table 64P.

Features of interest are: the broad Christmas tree-like sea surface temperature pattern which is along the shelf break, the large leads (-1° to -2°C water) in the ice pack.

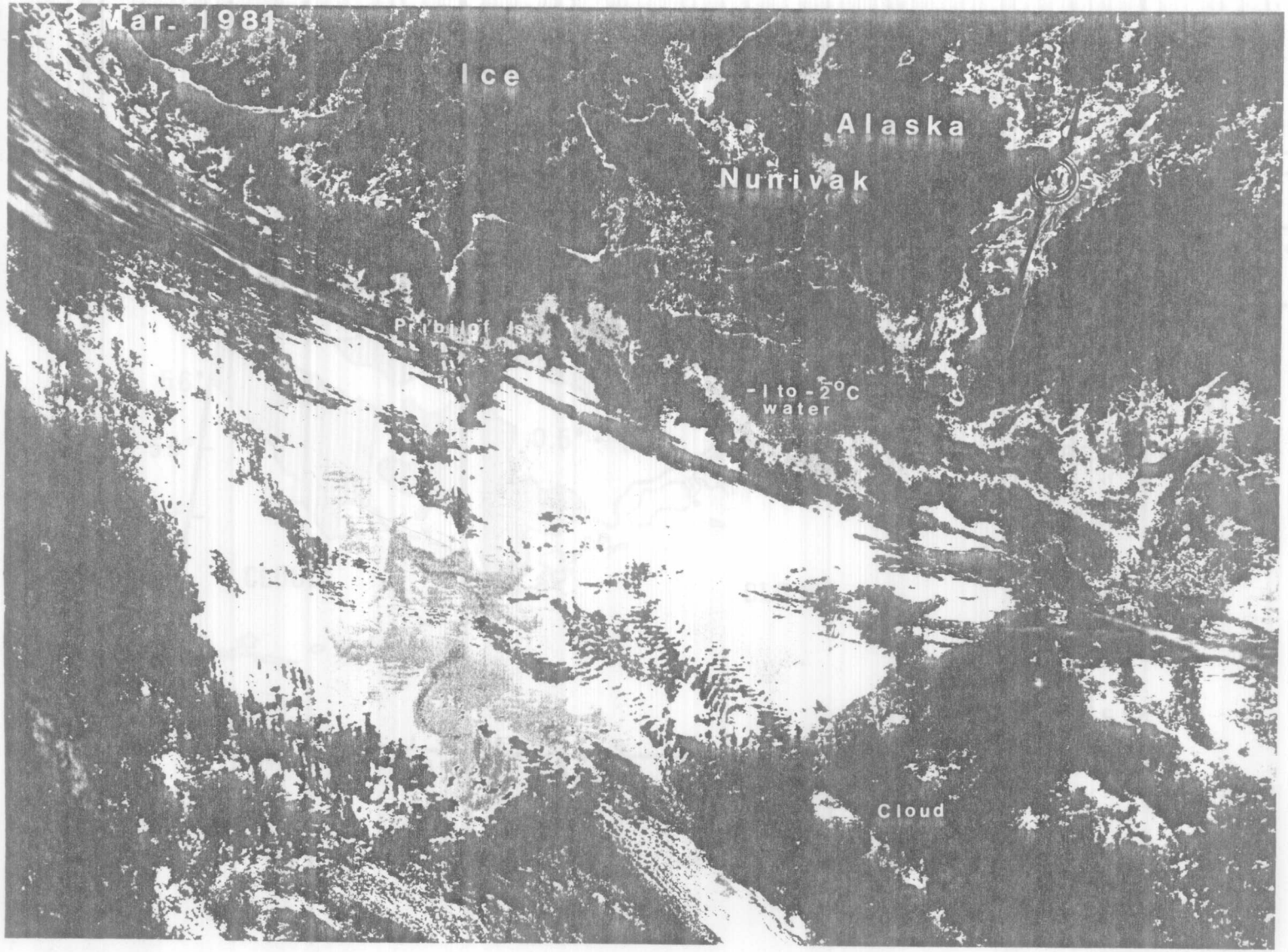
22 Mar 1981
Ice
Alaska
Nunivak
Pribilof Is.
-1 to -2°C
water
Cloud

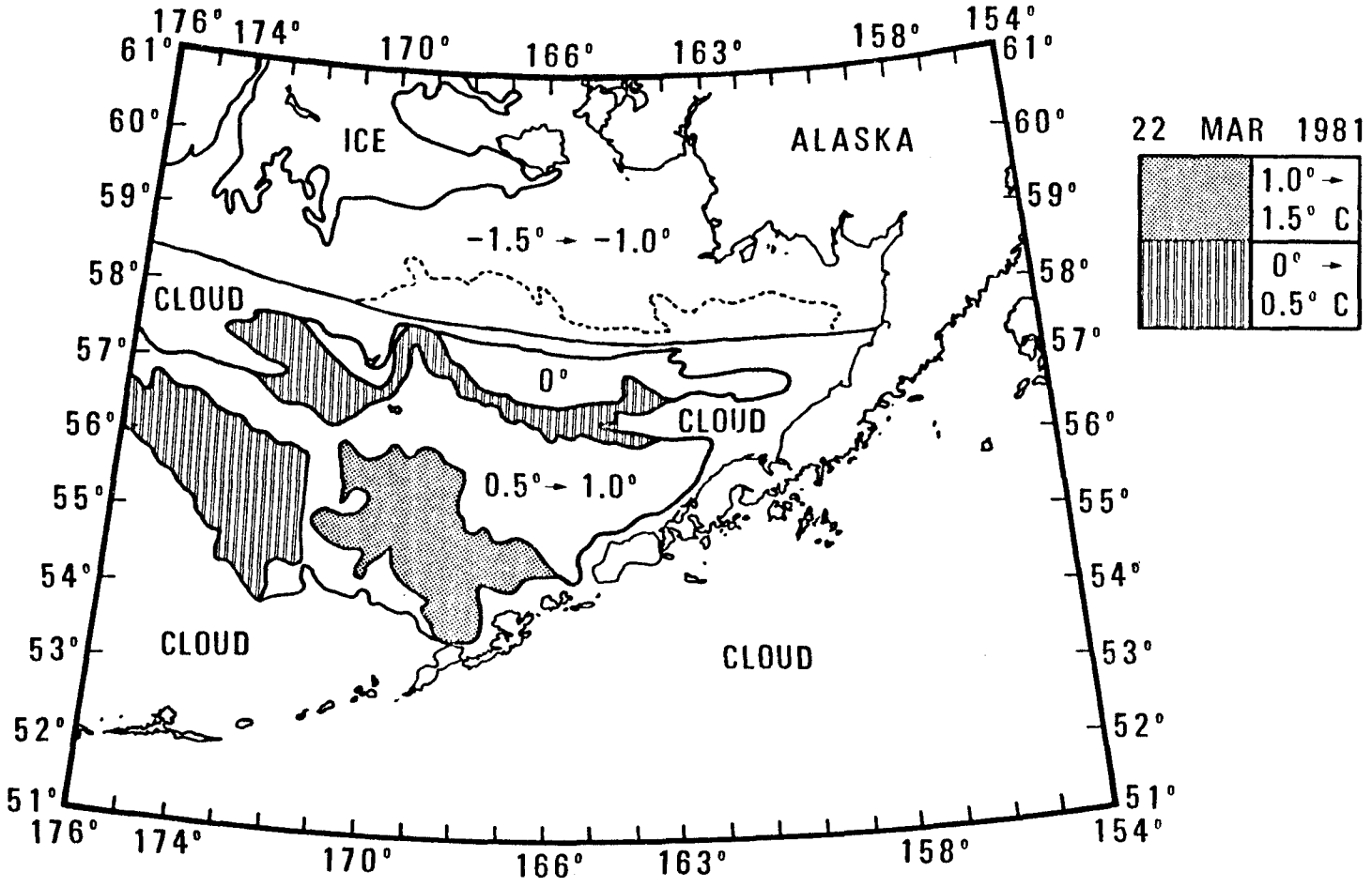

Figure 27b. Temperature contours produced from densitometric analysis for 22 March 1981.

were also ice-free. The water in these areas was between -1.0 to -2.0°C, indicating it had recently melted. Over the 200-m contour a very warm undulating band of water could be seen (Figure 27a). Images on 25 and 31 March showed large areas of ice-free but cold (-1.0 to -2.0°C) water and warmer water over the 50-m to 200-m shelf area. No distinct SST gradients were seen.

A time series is available for April 1981, spanning April 12-15, with an additional image on April 10. The image on the 10th covered the area in Bristol Bay showing SST gradients which were well defined but did not correspond to isobaths and temperatures which increased seaward. The image on the 12th (Figure 28a) revealed an eddy-like feature near the Pribilof Canyon. The eddy was cyclonic with a cold core. A band of warm water, similar to the temperature of the eddy, was seen along the Gulf and Bering side of the Aleutian Islands. Swirling, eddy-like features could be seen on the Bering Side and in and among the passes. Another interesting feature could be seen in the area of the 70-m isobath where the bathymetric contour forms a finger-like extension onto the shallower portion of the shelf. Within this finger-like extension was warmer water with a fringed pattern along the boundaries. On April 13 the eddy was no longer a distinct separate feature but seemed to have been incorporated into a large, indistinct curl of warmer water (Figure 29a). The feature at the 70-m finger was still present and more distinct, as was the warm band along the Aleutian Islands. Images provided a clear view of Bristol Bay on the 14th. SST gradients were distinguishable within Bristol Bay

Figure 28a. Infrared image for 12 April 1981; GMT 06:40:25; enhanced with Table 64P.

Features of interest are: the cyclonic, cold core eddy just south of St. George Island, the region of warm surface water extending from the Gulf of Alaska, through the Aleutian passes and into the Bering Sea, the area just northeast of St. Paul (along the 70-m bathymetric contour) with the curling structure along the edges.

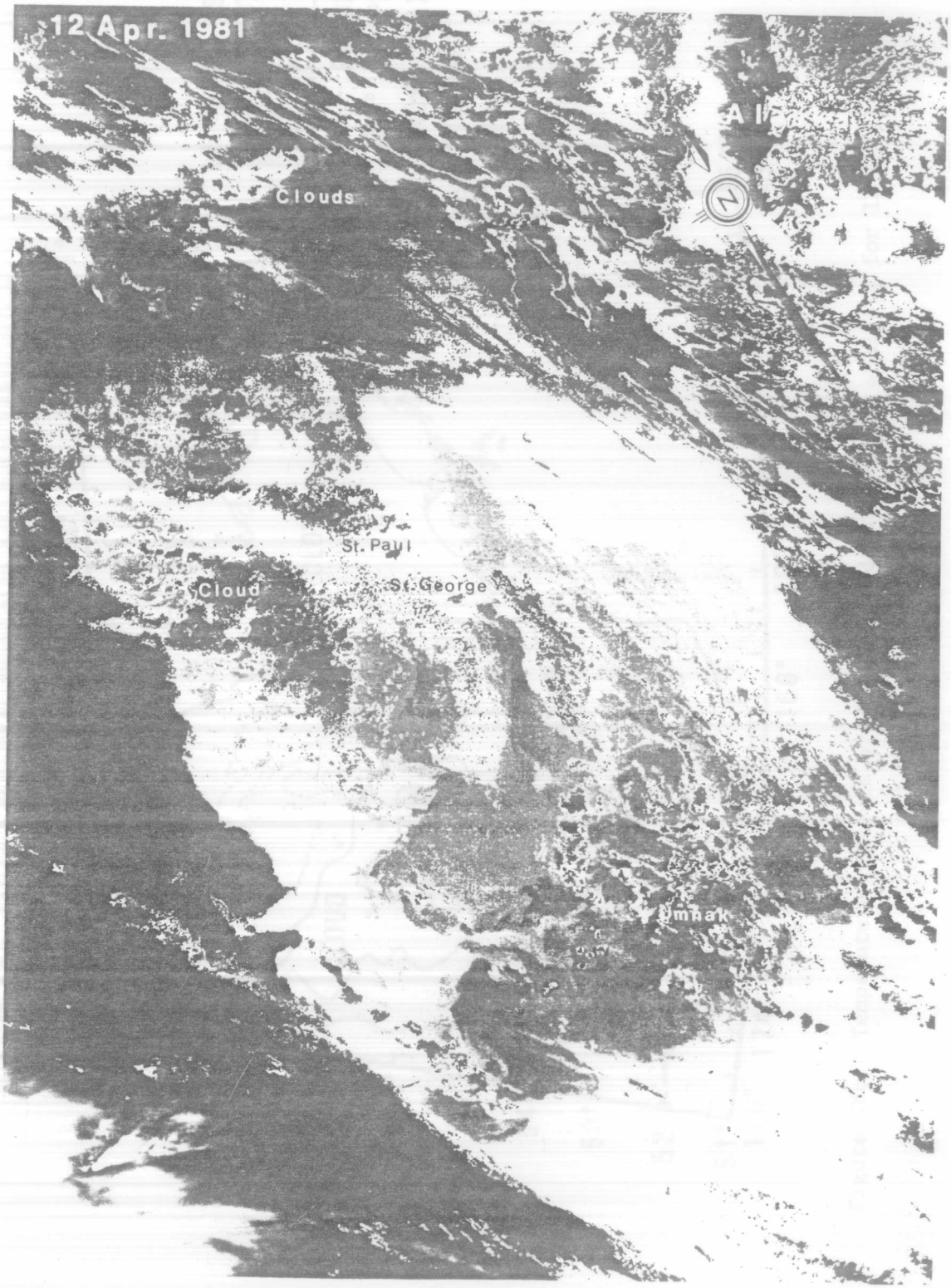
12 Apr. 1981
Clouds
St. Paul
St. George
Cloud
Umnak

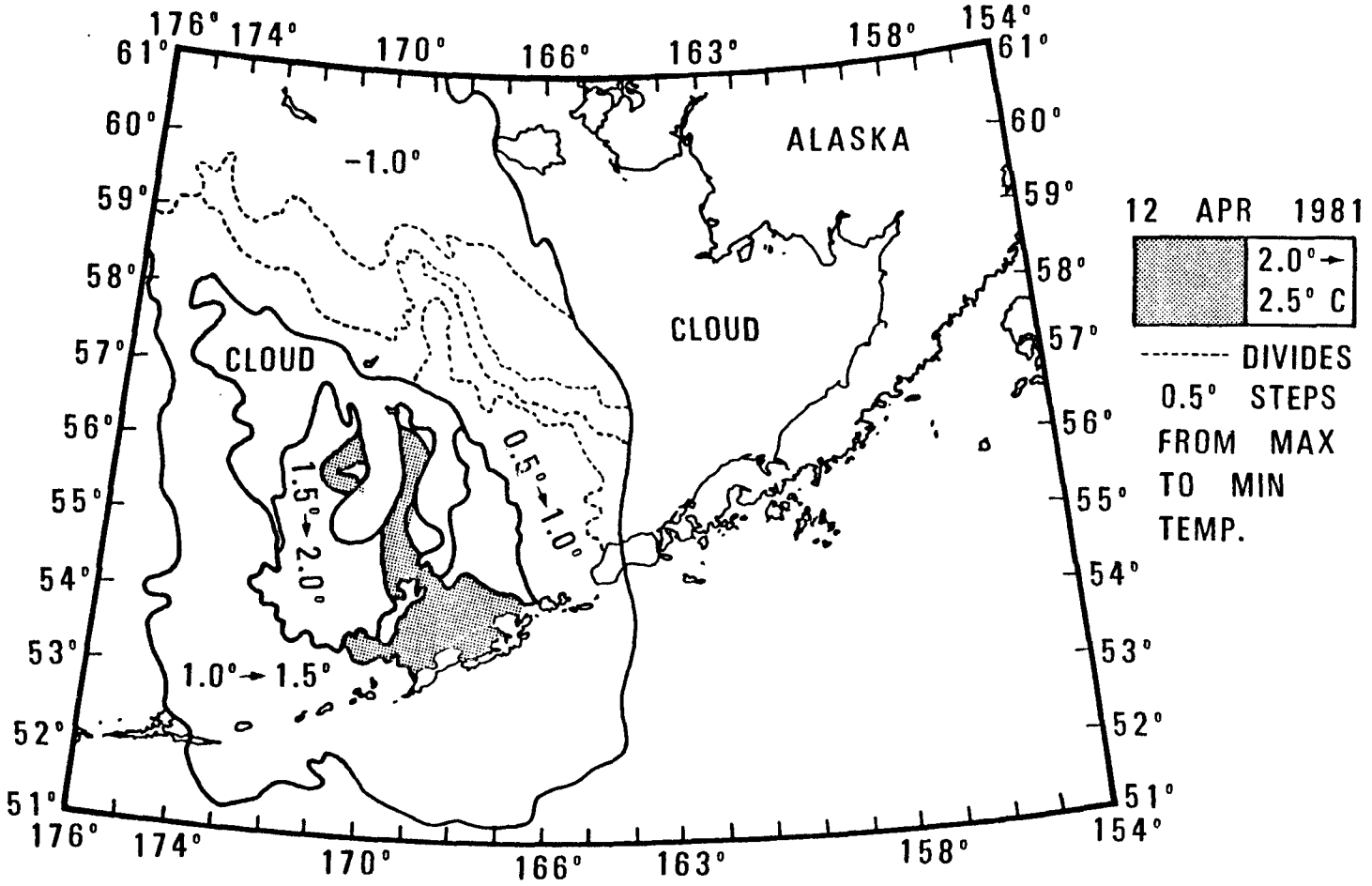

Figure 28b. Temperature contours produced from densitometric analysis for 12 April 1981.

Figure 29a. Infrared image for 13 April 1981; enhanced with Table 6MC.

Features of interest are: the large indistinct curl of warm water located where the eddy was seen in the previous image, the region of warm surface water extending from the Gulf of Alaska to the Bering Sea through the Aleutian passes, also seen in the Gulf of Alaska along the Alaska Peninsula, the area just northeast of St. Paul (near the 70-m bathymetric contour) with the curling structure along the edges.

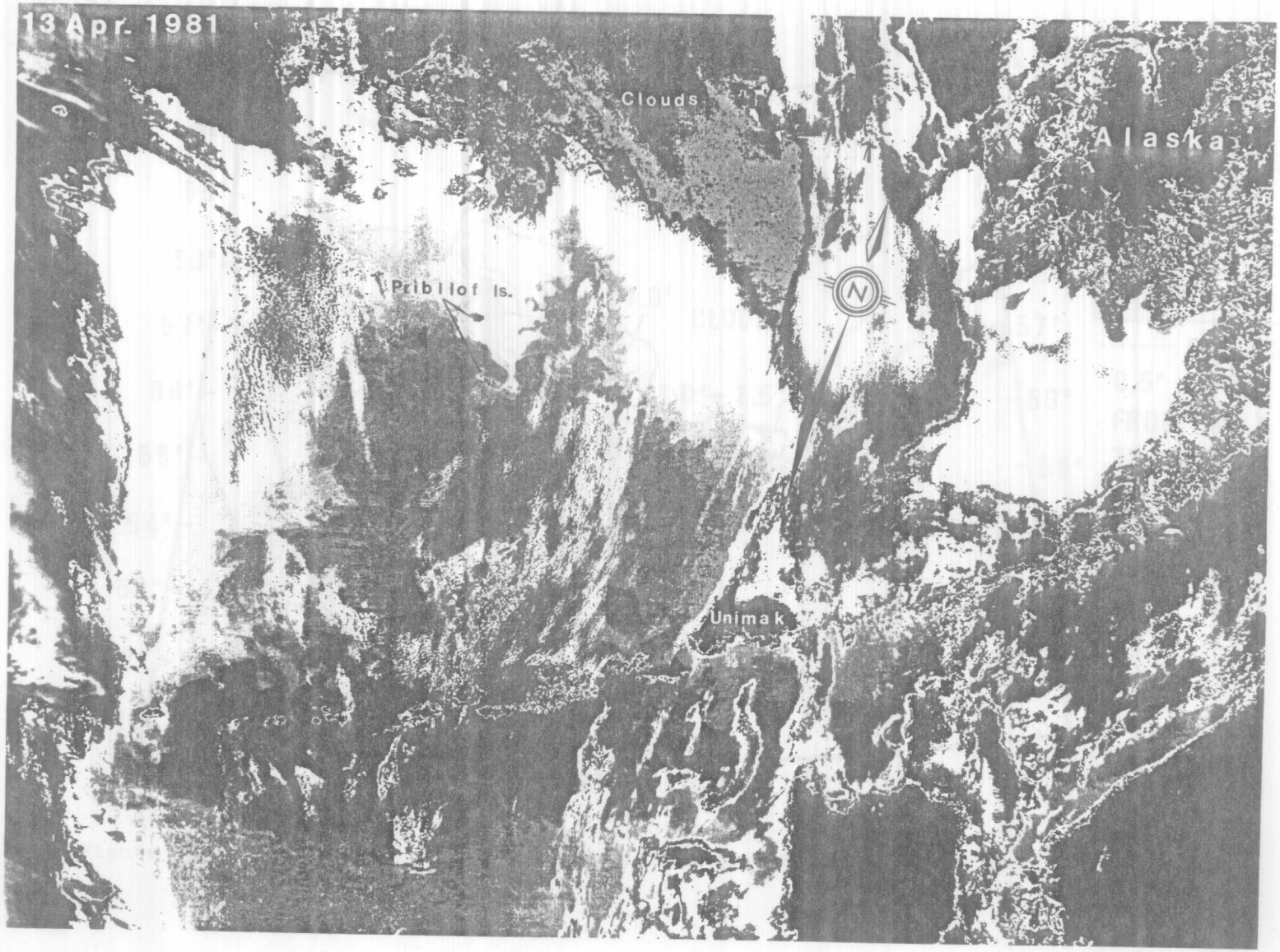
13 Apr. 1981
Clouds
Alaska
Pribilof Is.
N
Unimak

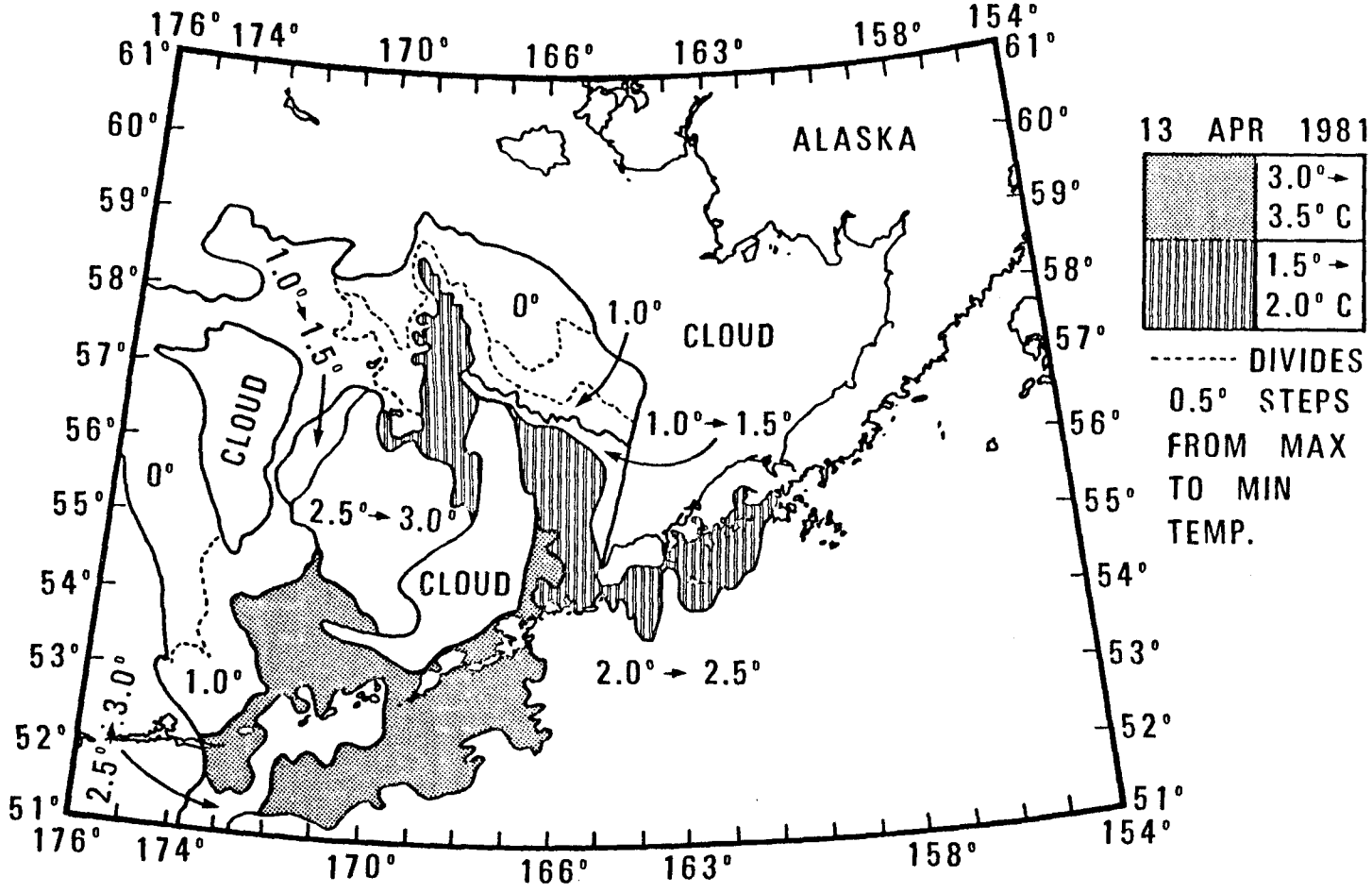

Figure 29b. Temperature contours produced from densitometric analysis for 13 April 1981.

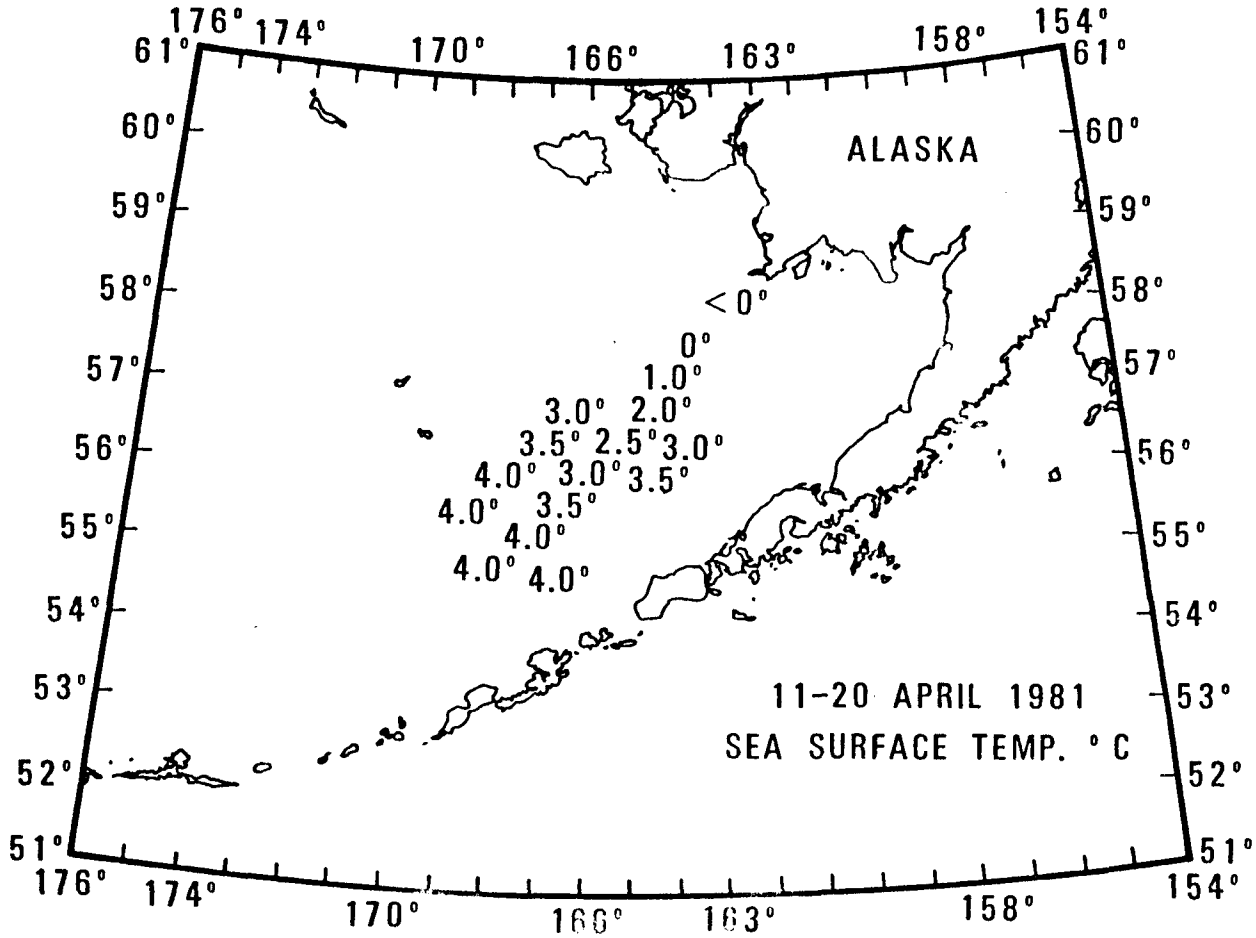

Figure 30. Sea surface temperatures for April 1981 to be used for surface truth data.

but did not follow the bathymetry as before. The feature at 70 m was still clear and distinct on 15 April. On April 20 a band of warm water was seen along the coast of Bristol Bay. SST gradients were noticeable along the 60-m isobath. Proceeding seaward from the coast, there was the warm band, then cooler water between the 50-m and 60-m isobath, with warmer water seaward of the 60-m isobath. The April 22 image showed the same pattern of SST gradients in Bristol Bay as were seen the previous day. Near St. Paul Island cooler water was seen extending south and curling around the island. Beyond, there was a distinct SST gradient following the 100-m isobath.

Clear images were found for 8, 9, 27, and 28 May. On 8 and 9 May there were SST gradients following the 70-m, 100-m, and approximately 3000-m isobaths (Figures 31a, 32a). The finger-like structure at 70 m (previously described) was still apparent. The warm band between 100-3000 m was also very distinct. On the 8th warmer features of a circular nature were seen within the warm band (Figure 31a); on the 9th the south-east portion of the warmer water still was seen (Figure 32a).

June 1981 - August 1981

On the 17 June image, SST gradients in Bristol Bay were well defined. The gradients corresponded with the isobaths with the coolest water contained in the center of the Bay near the 50-m isobath. On the 18th these contours were still seen, in addition to a large patch of warm water between 60 and 100 m. St. George was surrounded by cool water, and small eddy-like features were seen near Unimak Pass.

Figure 31a. Infrared image for 8 May 1981; enhanced with Table 64Z.

Features of interest are: the region of warm surface water along the shelf break and extending onto the shelf just northeast of St. George Island, the warmer patches of water (within the region) with the circular nature.


8 May 1981
N
Alaska
Nunivak
St. Matthew

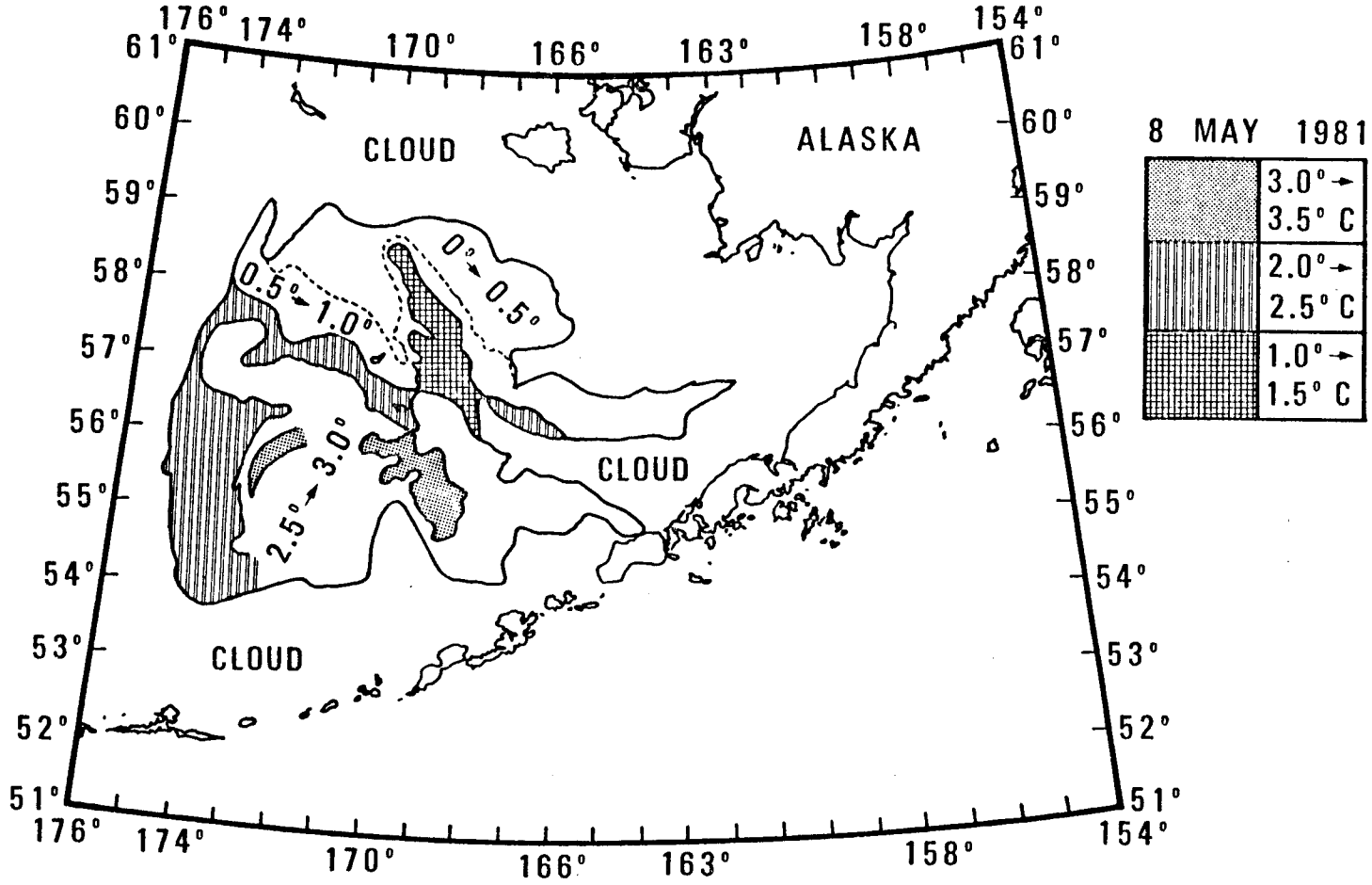

Figure 31b. Temperature contours produced from densitometric analysis for 8 May 1981.

Figure 32a. Infrared image for 9 May 1981; enhanced with Table 64Z.

Features of interest are: the region of warm surface water paralleling the shelf break and extending onto the shelf just northeast of St. George Island, the region of still warmer water to the southeast of the Pribilof Islands.

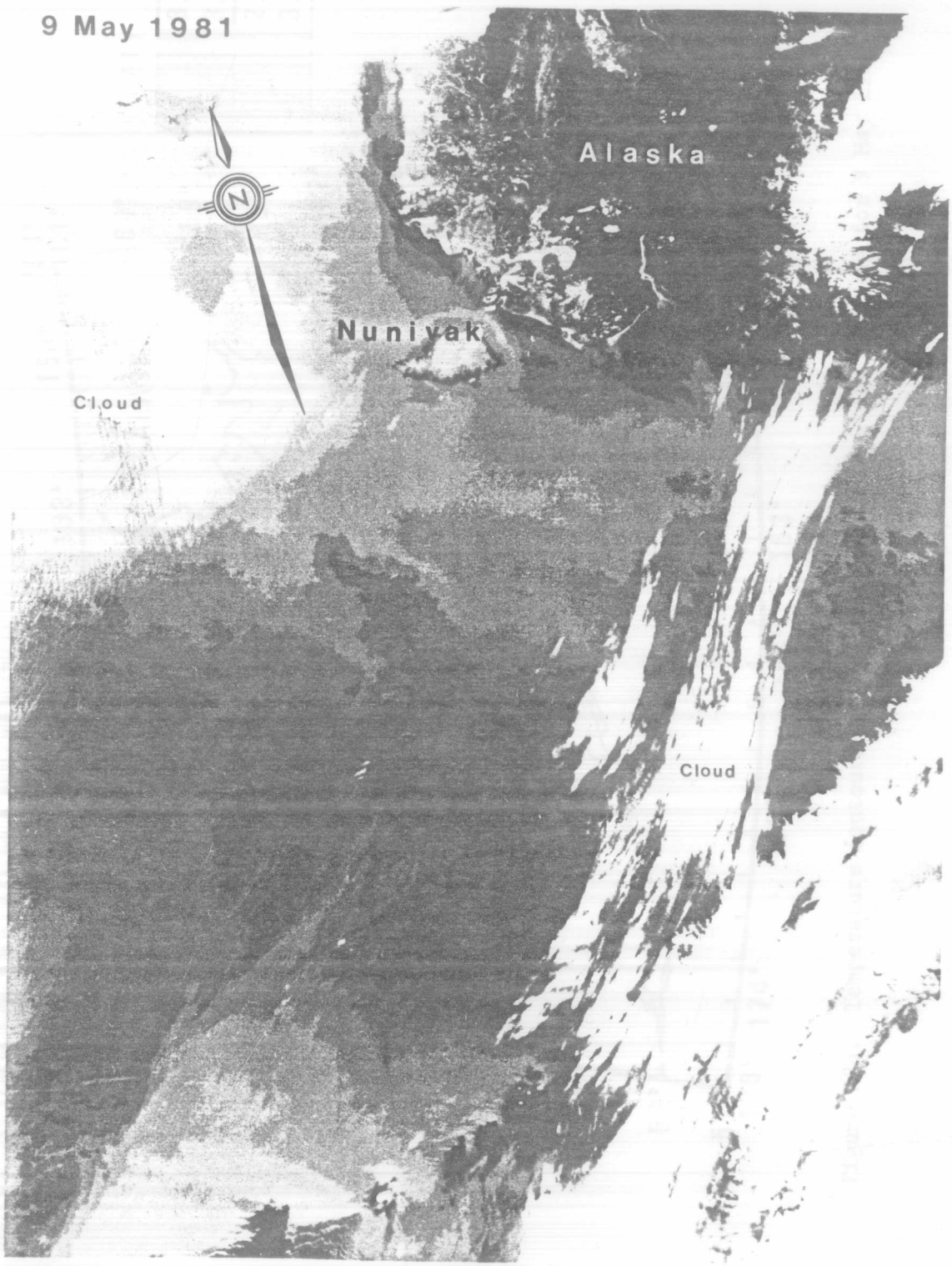
9 May 1981
N
Alaska
Nunivak
Cloud
Cloud

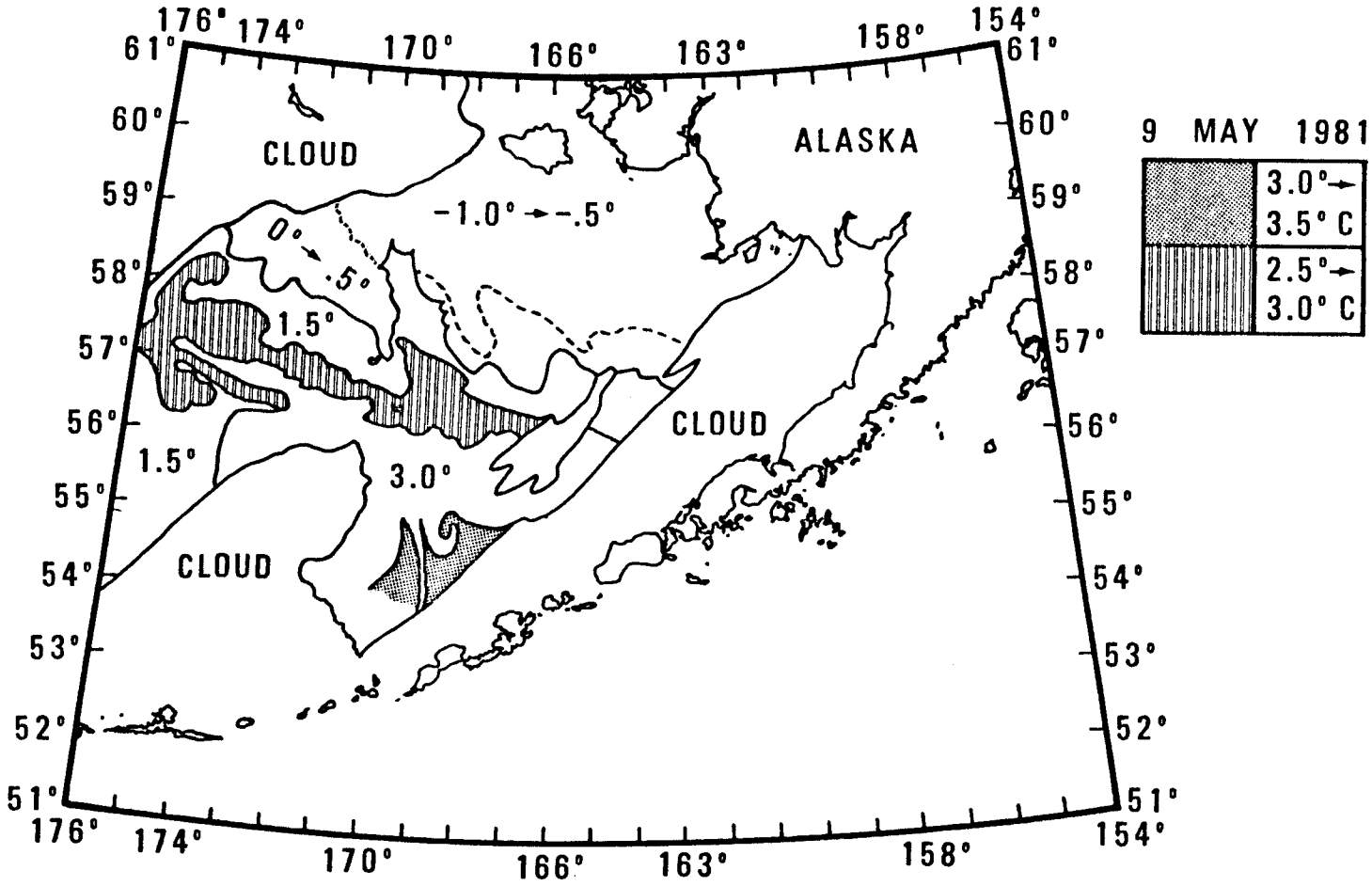

Figure 32b. Temperature contours produced from densitometric analysis for 9 May 1981.

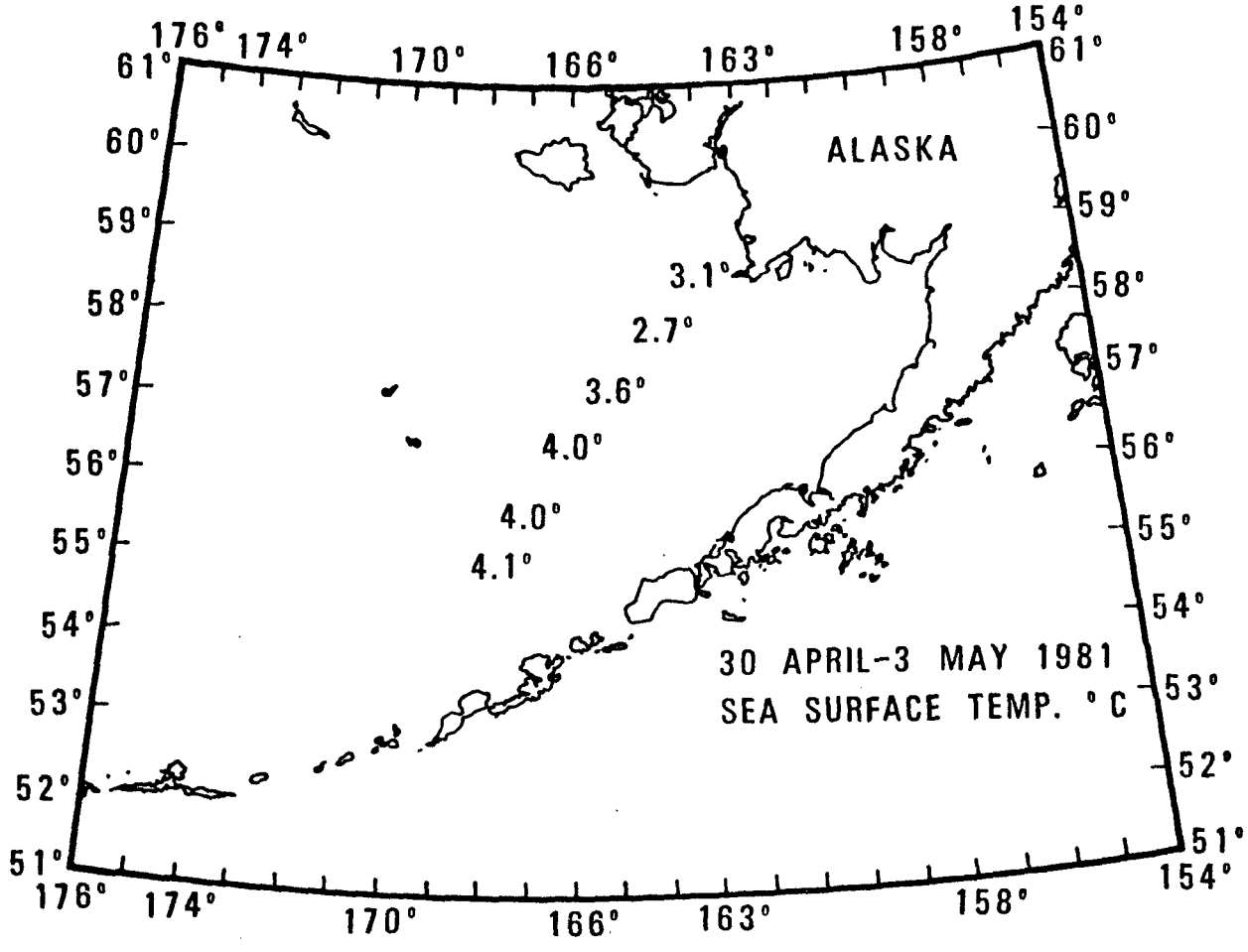

Figure 33. Sea surface temperatures for 30 April to 3 May 1981 for use as surface truth data.

On 27 July an image showing the Near and Rat Islands (far western Aleutian Islands), and a portion of the Bering Sea was obtained. A large, yet diffuse, eddy-like feature was seen in the area just south of Zhemchung Canyon (Figure 8a,b,c). The feature was cyclonic, with a warm outer ring, and was located in approximately 3700 m of water. Clouds covered this area on the 28th, and confirmation of this feature was not possible.

Bristol Bay was seen on the 4th of August, and gradients coinciding with the 50-m, 60-m, and 70-m isobaths were visible. The water was warmest inshore of the 50-m isobath and coolest between the 60- and 70-m isobaths. On the 5th the far western Aleutian Islands were clear, and small eddy-like features were noted in Amchitka Pass and south of Amchitka and Kiska Islands.

Features: Similarities and Differences

In the analysis of the 1980-81 images, several repetitive features were noted. A summary of these features can be seen in Figure 34 which shows their spatial relationship. Ice coverage, although not shown on the schematic (Figure 34), was an obvious feature which had a definite seasonal trend; it was seen in the images from December through April. It was noted that the ice filled in the Bering Sea in a similar manner in both winters for which images were analyzed. Ice generally was observed along the coast first, then surrounding Nunivak Island, filling in Bristol Bay and the western portion of the Bering Sea. In both winters it progressed no further south than St. Paul Island in the

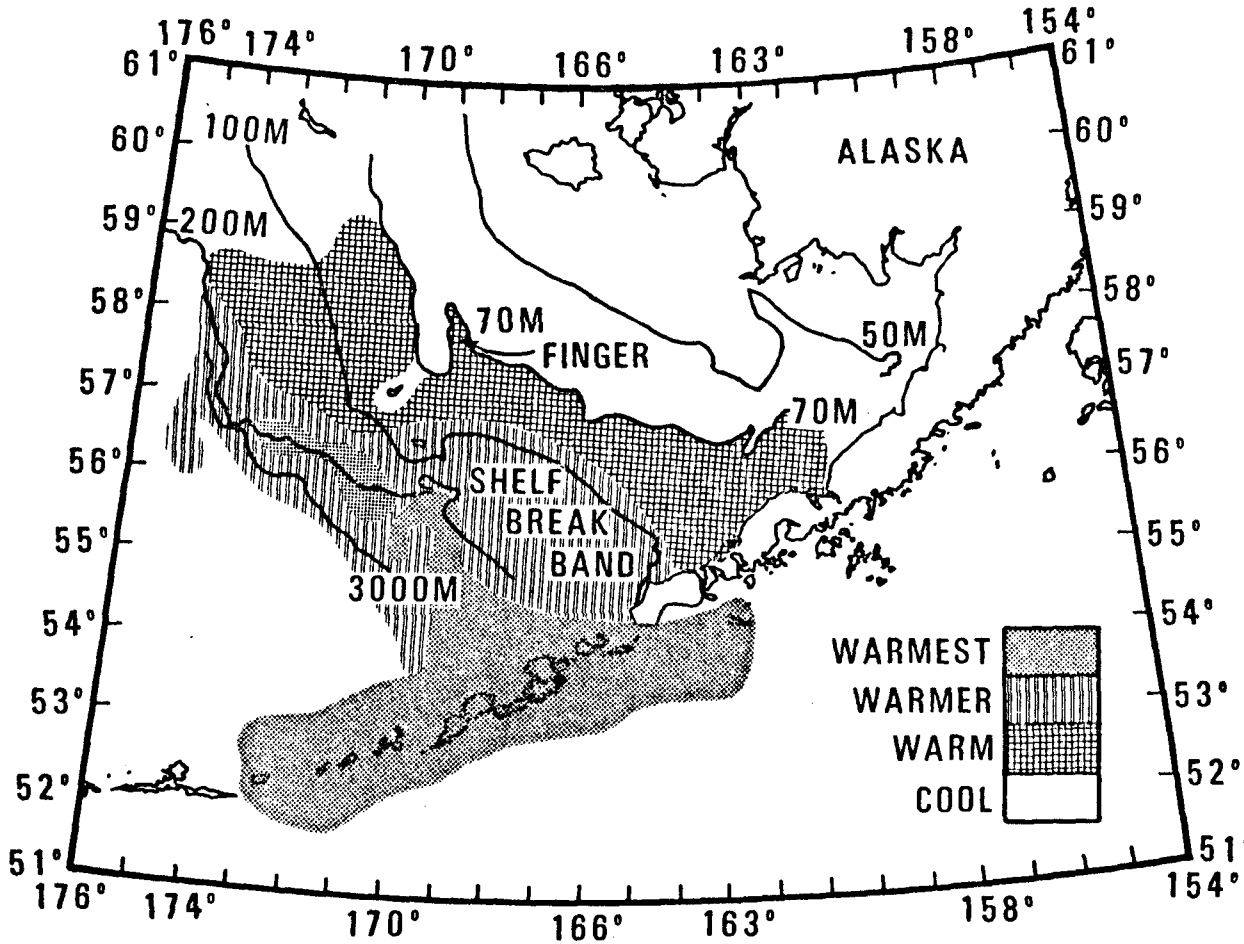

Figure 34. Summary of physical features; schematic shows: warm band over shelf break bounded roughly by 100-3000 m bathymetric contours, the warmer region extending from the Gulf of Alaska through Aleutian passes and into the Bering Sea, and warmest dynamic features such as eddies (from satellite imagery).

Pribilofs. Figure 35 shows a time series of ice edge progression in 1981. It was noted that the tendency for the ice edge to follow the bathymetric contours. A difference in the time and manner of break-up and retreat of the ice pack was also noted. In 1980, the ice left in April, melting from the coastline, then westward; in 1981, the ice began to break up in March with several leads forming in the western portion as well as along the coast.

Another very obvious and persistent feature was the SST gradients and the coincidence of these contours with bathymetric contours (Figures 9, 10, 11). This tendency was pronounced in December of both years, January 1980, and also in the spring months for the shelf region. In March and April only nearshore gradients were well established; this was also true of March and April 1981. In 1981, surface truth information indicated temperatures between 2° and 1°C, as did the satellite imagery. By June the gradients were more apparent and in 1981 could be seen closely paralleling isobaths, but in 1980 this trend was not as apparent until July. Comparison of the summer images showed that sea surface temperature gradients in Bristol Bay tended to follow the isobaths, yet the alignment of the surface temperature contours with the isobaths occurred at different times: June in 1981 and July in 1980. Once the gradients were aligned, they maintained that configuration throughout the summer. Moving seaward from the coast, the same temperature trend was noted both years. There was a warm band nearest the coast which was the first noticeable gradient both years. The surface water then became cooler with distance

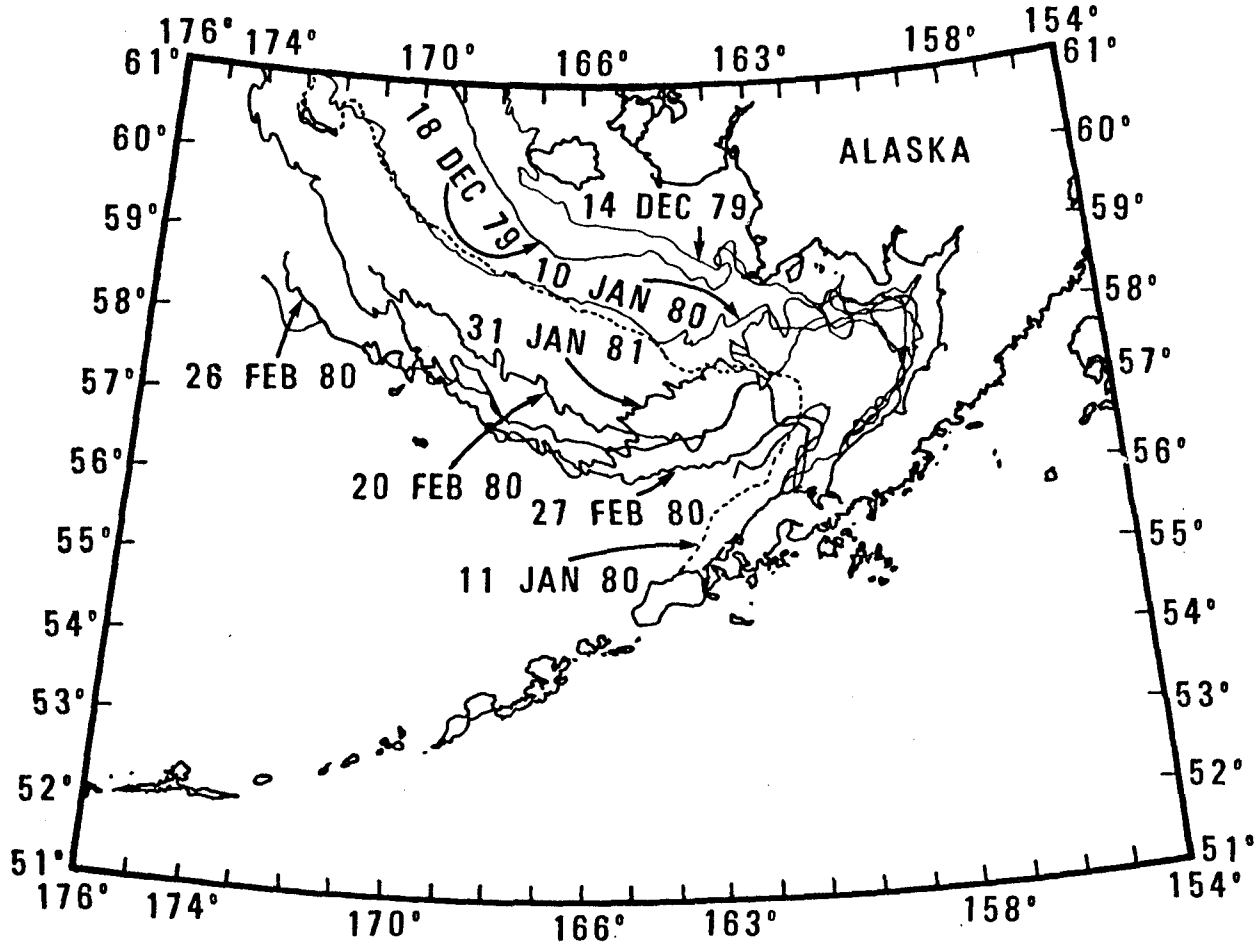

Figure 35. Ice edge extent seen in 1979-1980 (from satellite imagery).

off-shore. The coldest area was reached at approximately 50 m in the middle of the bay but became warmer farther offshore.

On the outer shelf, surface temperature gradients also tended to follow isobaths. Most noticeable were the gradients seen paralleling the 70-m and 100-m isobaths (Figure 34). These contours were seen in both years and in all seasons for which imagery and coverage allowed viewing of that area. These contours were most well defined in the winter imagery (Figures 9, 10, 11 and Figures 13, 14), probably because thermal contrast is best. They have also been clearly seen in April 1981 (Figures 28, 29), May 1981 (Figures 31, 32). SST gradient corresponding to the 70-m isobath was most noticeable because the isobath has a finger-like extension pointing on shelf. The temperature structure in this region was warmer seaward of 70 m and cooler on shelf (Figure 34). The warmer water reaches up into the finger and cooler water comes down and surrounds St. Paul in April and May 1981 (Figures 28, 29, 31, 32, 34). The edges of this structure were unusual and differed from the previous and latter examples in that the edges were curled which could indicate mixing or lateral advection or diffusion of heat.

On images which include the shelf area, the Pribilof Islands, and the Bering Sea basin area, additional sea surface temperature structure could be seen. Between the 100 m and 3000 m isobaths the water was warmer than the water shallower than 100 m and deeper than 3000 m (Figure 34). The structure closely followed the shelf break and was also curled cyclonically at the northwest end near Zhemchung Canyon.

A good example of this structure is shown very clearly in Figures 10, 11, Figure 13, Figures 24, 25, 26, Figure 27, Figures 28, 29, and Figures 31, 32. The seasonality of this feature cannot be determined because of the scarcity of imagery in the basin area during the summer.

In the January (Figures 9, 10, 11), August (Figure 20), December (Figures 24, 25, 26), and April (Figures 28, 29) images, there appears to be water of a similar temperature along the western Aleutian passes, along the western edge of the basin, and in and along the area near Unimak Pass. This warm surface water feature occurred along with the warm shelf break band (Figure 34). Within the band of warm water between the 100 and 3000 m isobaths, 0.5 to 1.0°C warmer water could be seen, usually coinciding with the 200-m isobath. This water was the warmest water detected in the Bering Sea area (Figure 34), and when the coverage of the imagery allowed, it could be matched with temperatures on the Gulf side of the Aleutian Islands and within Unimak and other western Aleutian passes (Figures 9b, 10b, 11b, 12, 13b-18b, 19, 28b, 29b, 30).

These incidences of warmest water within the shelf break band appeared as several types of distinct features. On 9 October 1980 (Figure 22a,b), and 9 May 1981 (Figure 32), a large, warm patch of water appeared in the southeast corner of the shelf break. The temperature analysis maps and the surface truth data (Figures 22c, 22d, 23 and Figures 31b, 32b, 33) confirm the existence and temperature of this feature.

Another feature that appeared within the shelf break band was an undulating band of warmer water, following the 200-m contour and narrowing at the northwestern portion (Figure 34). Very distinct examples of this feature were seen on 31 January 1980 (Figure 13), 20 February 1980 (Figure 14), 25 and 26 December 1980 (Figures 24, 25, 26), and 22 March 1981 (Figure 27). The temperature analysis sections show this band to be approximately half a degree to one degree warmer than the surrounding temperatures (Figures 13b, 14b, 24b-26b, and 27b).

The most distinct features were eddies which could be seen on 10 and 11 January 1980 (Figures 9, 10), 26 and 27 February 1980 (Figures 15-18), 23 August 1980 (Figure 20), and 12 April 1980 (Figure 28). The 10 and 11 January and 12 April eddies appeared to be very similar. They were cyclonic, with cooler core, warm outer ring, and were centered near the Pribilof Canyon and appeared as a warmer signal within the warm shelf break band. Water of a similar temperature to the eddies outer ring was seen along the south side of the Aleutians and in and around the western Aleutian passes and western edge of the Bering Sea basin. The temperature analysis (Figure 9b-11b, 12, Figure 15b-18b, 19, Figures 20b, 21, and Figures 28b, 29b, 30) shows these features clearly defined and shows their similar temperature structure. The surface truth data for the January eddies shows good agreement between temperatures; that is, ship temperatures showed the slope water to be between 2.5 and 3.0 degrees, as did the imagery. The February images from the TIROS-N satellite also showed good agreement with the surface truth data. The NOAA-6 images showed the same

temperature patterns and relative gradients but showed colder temperatures than the surface truth information. This was also true in April. The 26 and 27 February 1980, and the 23 August 1980, eddies differ from the other two eddies. In February there were what appear to be three eddies: one east of the Pribilof Canyon was cyclonic with a cold core, one centered over the Pribilof Canyon was anticyclonic with a warm core and cold outer ring, and the other east of Zhemchung Canyon was anticyclonic with a cooler core and warm outer ring. The temperature analysis for this imagery shows a wave-like feature of warmer temperature and the three eddies (Figures 15b-18b) within the warm shelf break band. The August eddy was anticyclonic with a warm core and cold outer ring. It was near the Pribilof Canyon but further offshore and in deeper water than any of the other eddies. This eddy was quite different than any of the others, with the cold outer ring matching cooler water along the western Aleutian passes and western edge of the basin. This is also seen in the temperature analysis (Figures 20b, 21). Although the temperatures (cold *vs.* warm) were opposite for the August eddy (Figure 20), the pattern and distribution was similar to the 10 and 11 January 1980 (Figures 9, 10), and 12 April 1981 (Figure 28), eddies and SST patterns. The possibility that there were several other eddies must be considered as they could exist and not be sensed because they were hidden by clouds or they did not have a surface temperature signal.

Surface winds from Unimak and St. Paul Island climatological data were analyzed for the period of time in which the eddies occurred.

Stick plots were constructed to show magnitude and direction and also to be used to present trends in the wind direction (Figure 36).

In December the winds were largely from the southeast between 5-15 m/sec. At the end of the month (16th-31st), the winds were from the north to northwest up to 10 m/sec. Again in January, the first part of the month, winds were generally from the southeast followed by northerly winds from the 8th on through the 31st. In February again, there were winds from the southeast until February 15, then northerly winds.

Stick plots for the Pribilof Islands (Figure 37) in December, January, and February show the winds from the south to southeast in the first part of December, then again from the north in the later part. In January, for the first part of the month, there were strong south and southeast winds, up to 13 m/sec, and from the 8th to the end of the month the winds were from the north and northeast. The north/northeast winds continued on into February.

In August (Figure 38a), the stick plots indicated winds from the south and southwest until the 7th; then winds from the north/northwest dominated except for short interludes, then the wind was from the southwest or southeast. The speed of the wind was still between 5 to 15 m/sec but did increase toward the end of the month.

The April stick plots (Figure 38b) showed southwest winds in the beginning and end of the month, with winds from the north between the 10th and 20th.

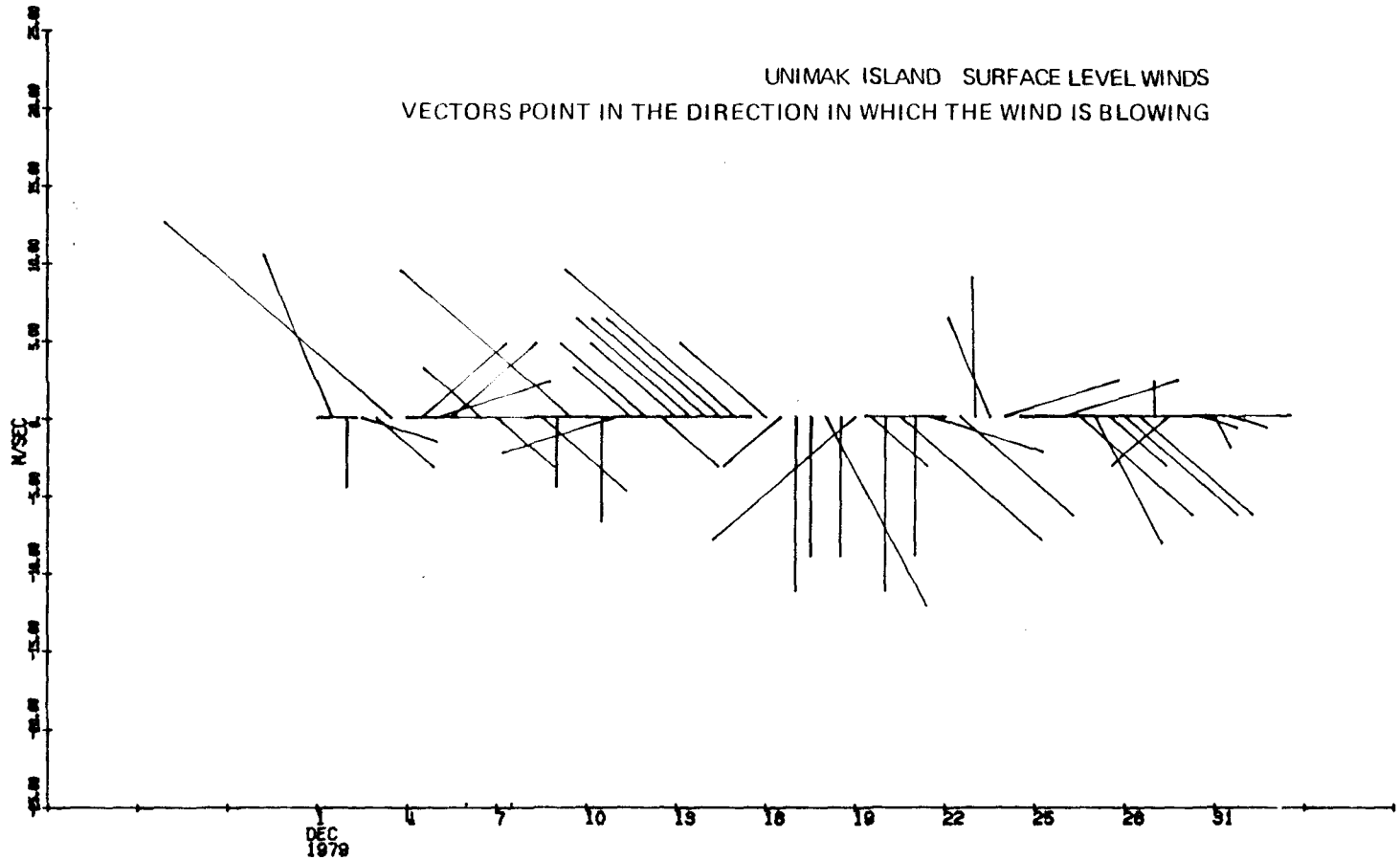

Figure 36a. Stick plots of wind at Unimak Pass; December 1979.

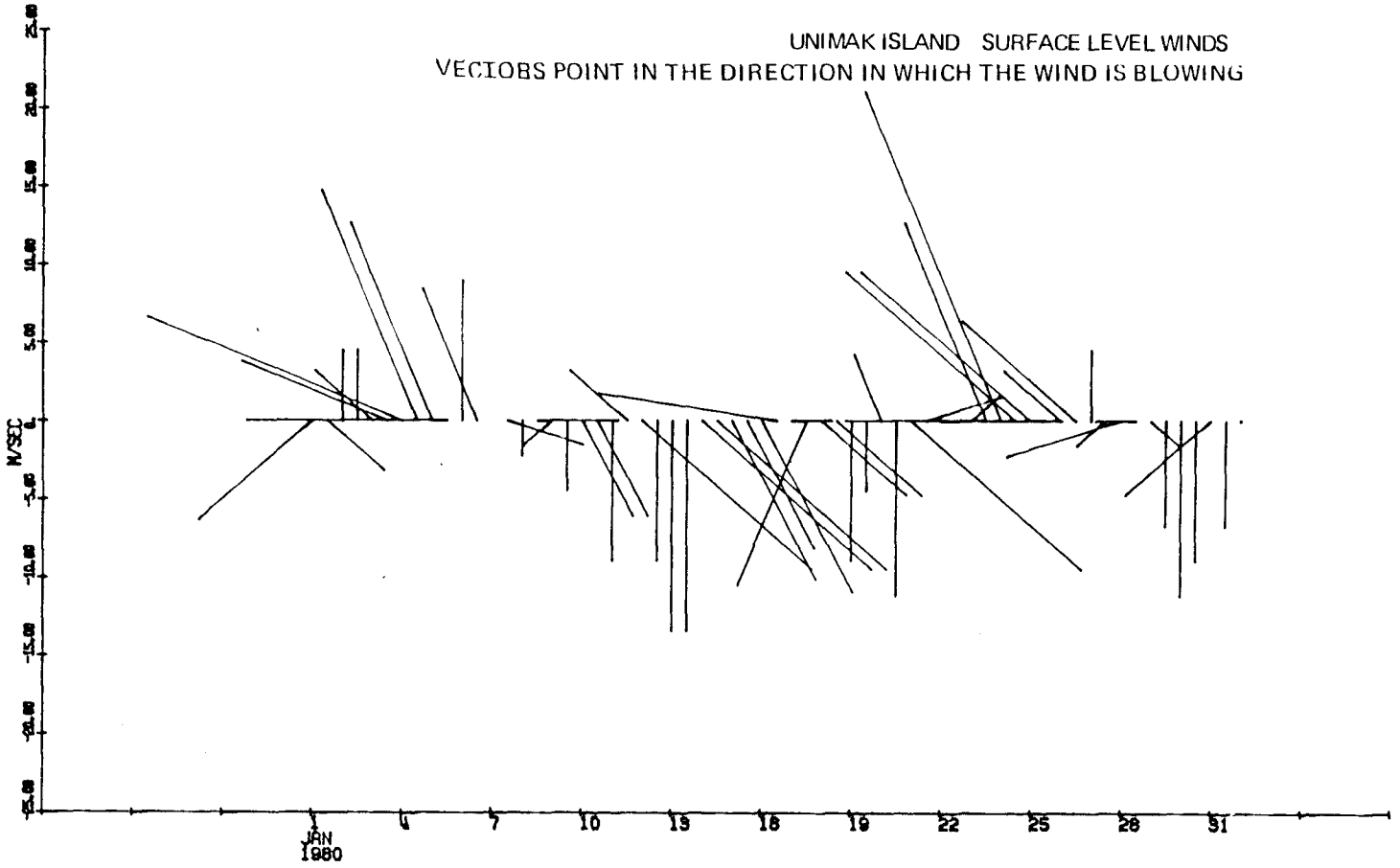

Figure 36b. Stick plots of wind at Unimak Pass; January 1980.

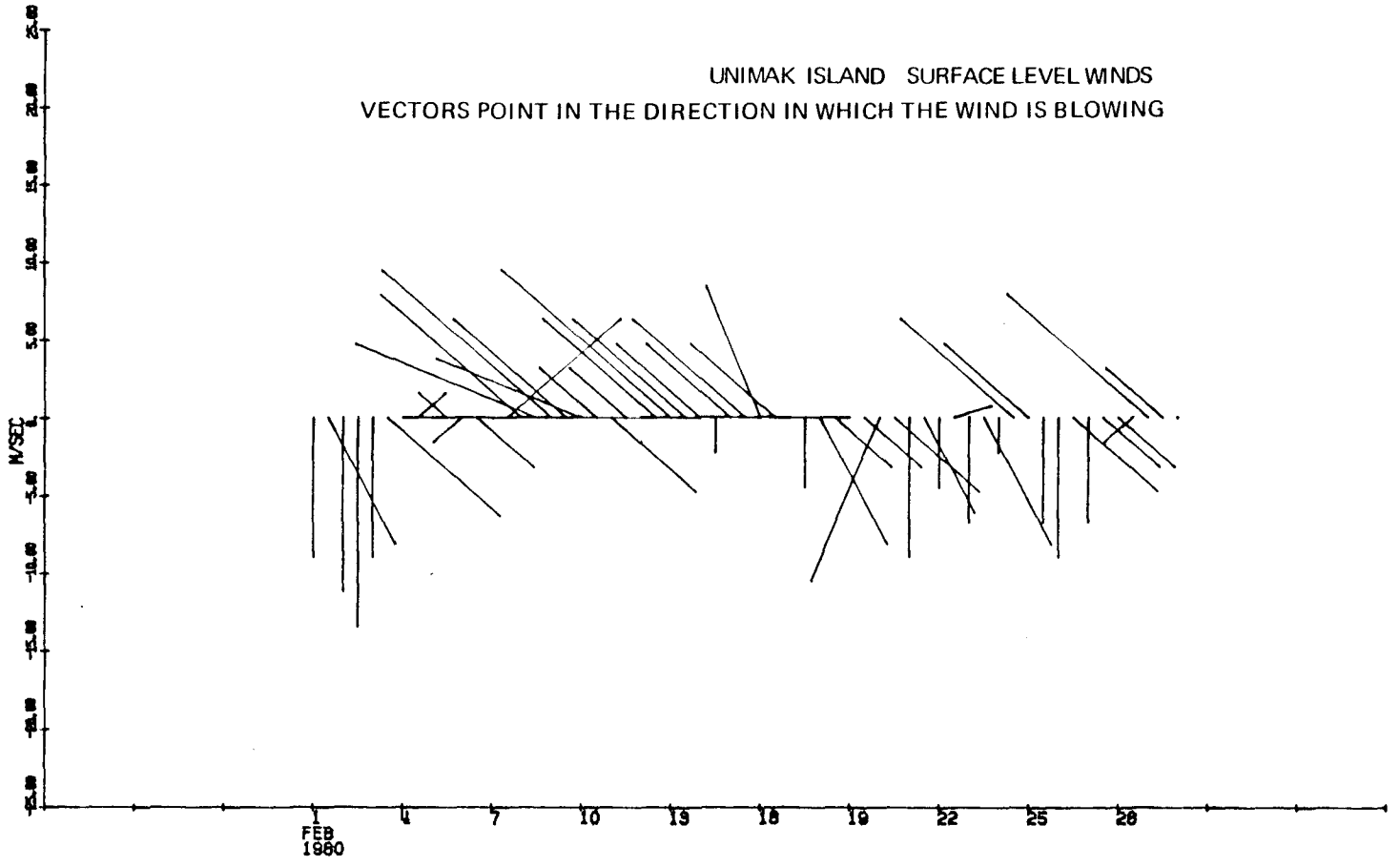

Figure 36c. Stick plots of wind at Unimak Pass; February 1980.

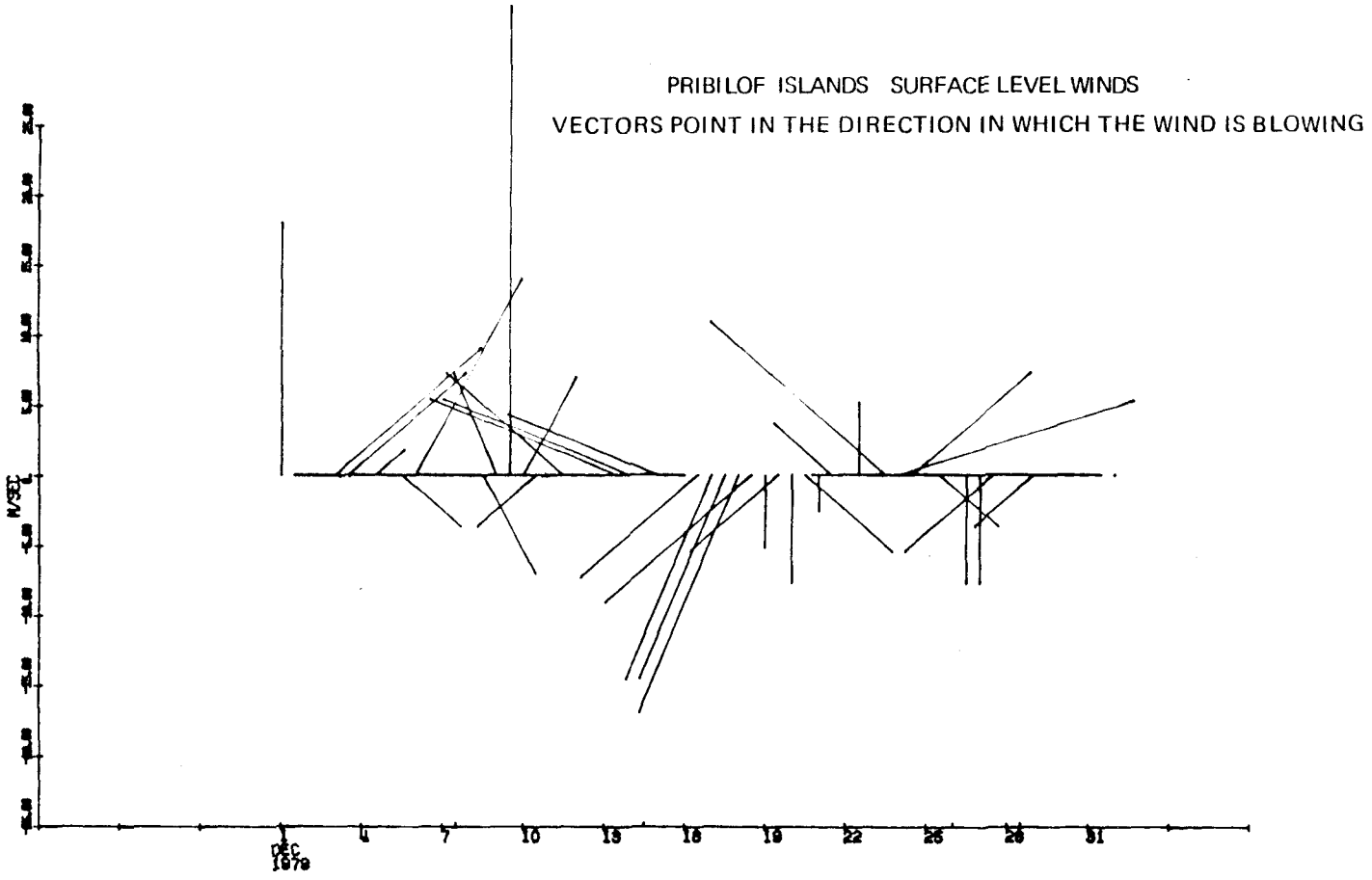

Figure 37a. Stick plots of wind at the Pribilof Islands; December 1979.

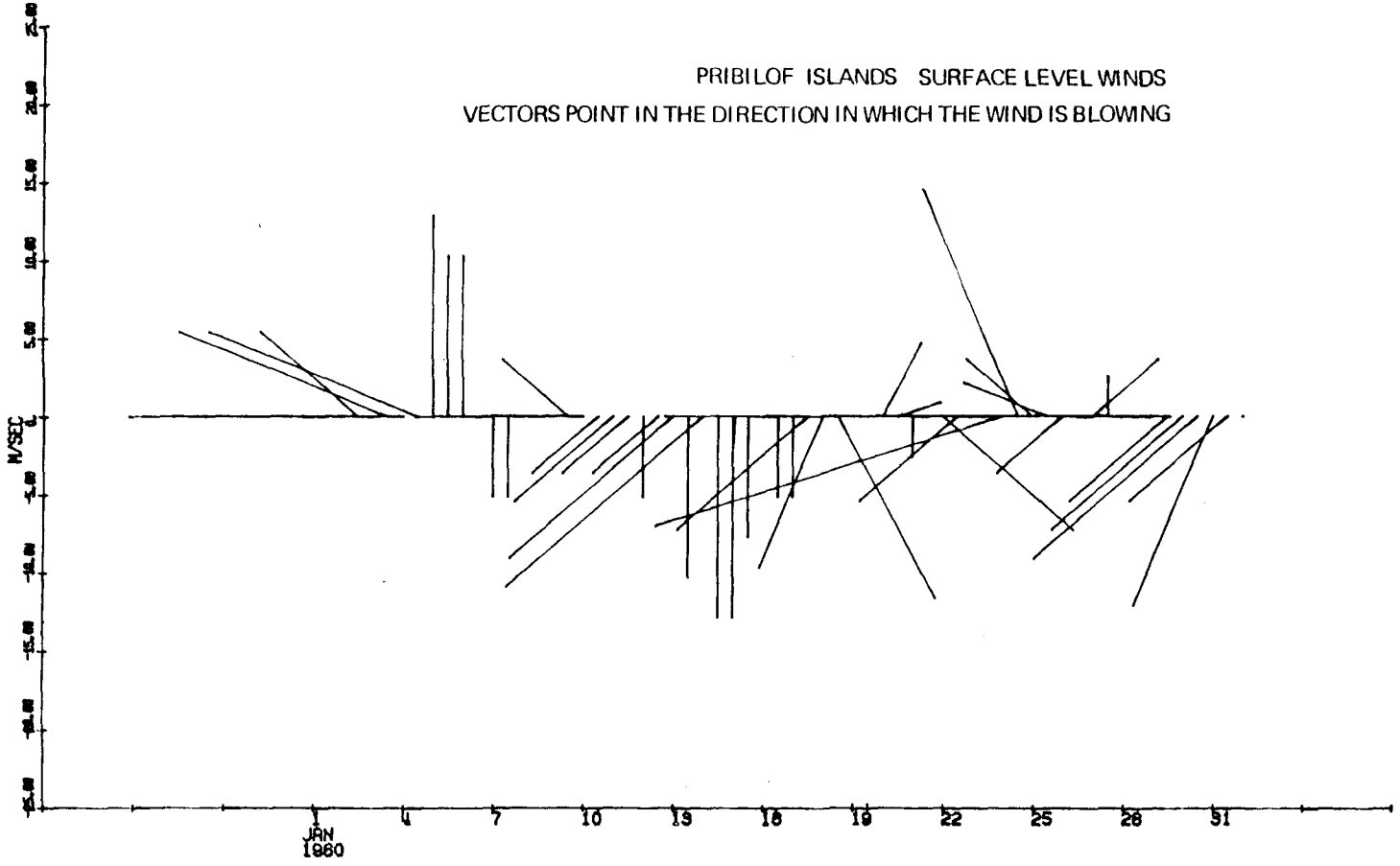

Figure 37b. Stick plots of wind at the Pribilof Islands; January 1980.

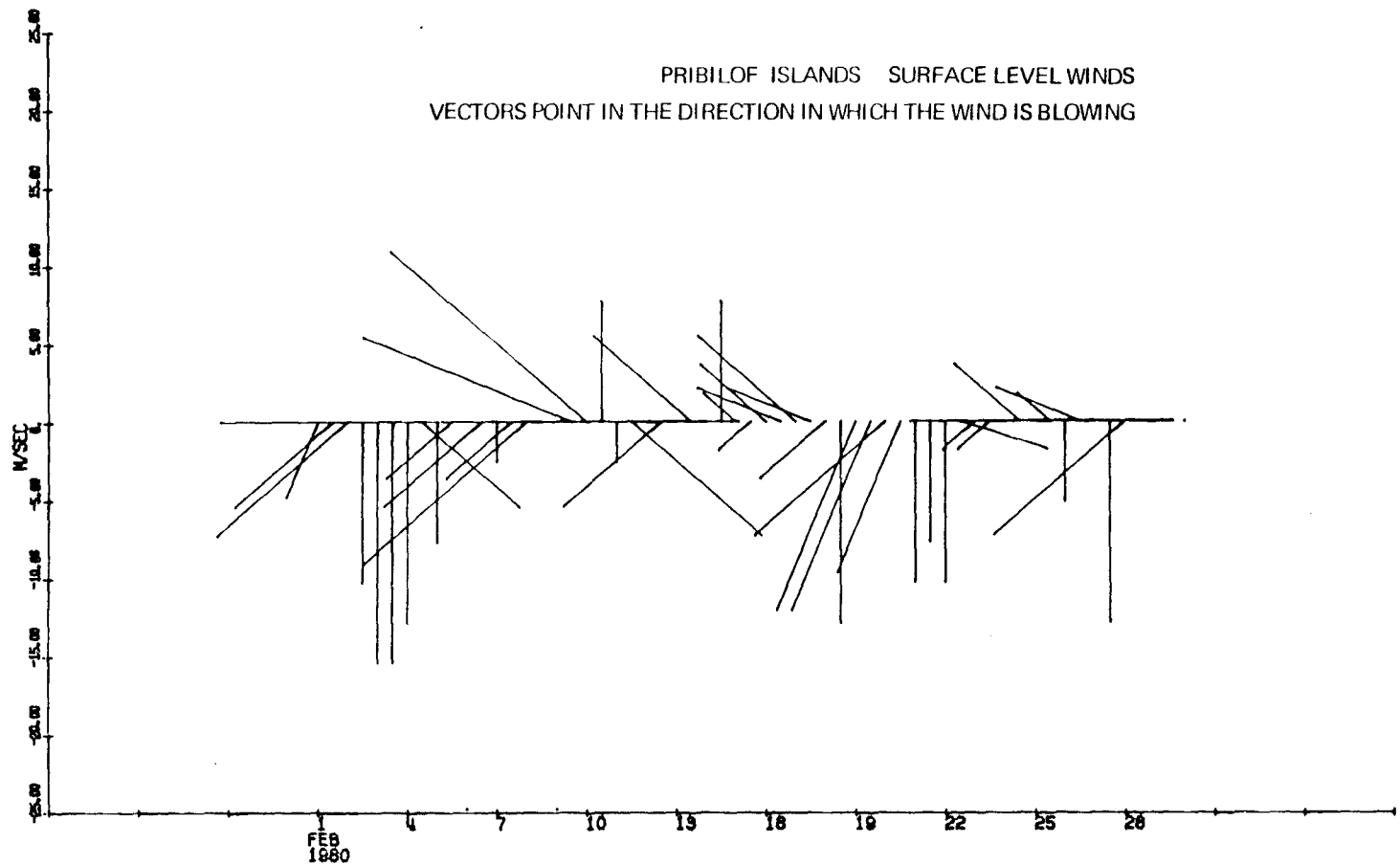

Figure 37c. Stick plots of wind at the Pribilof Islands; February 1980.

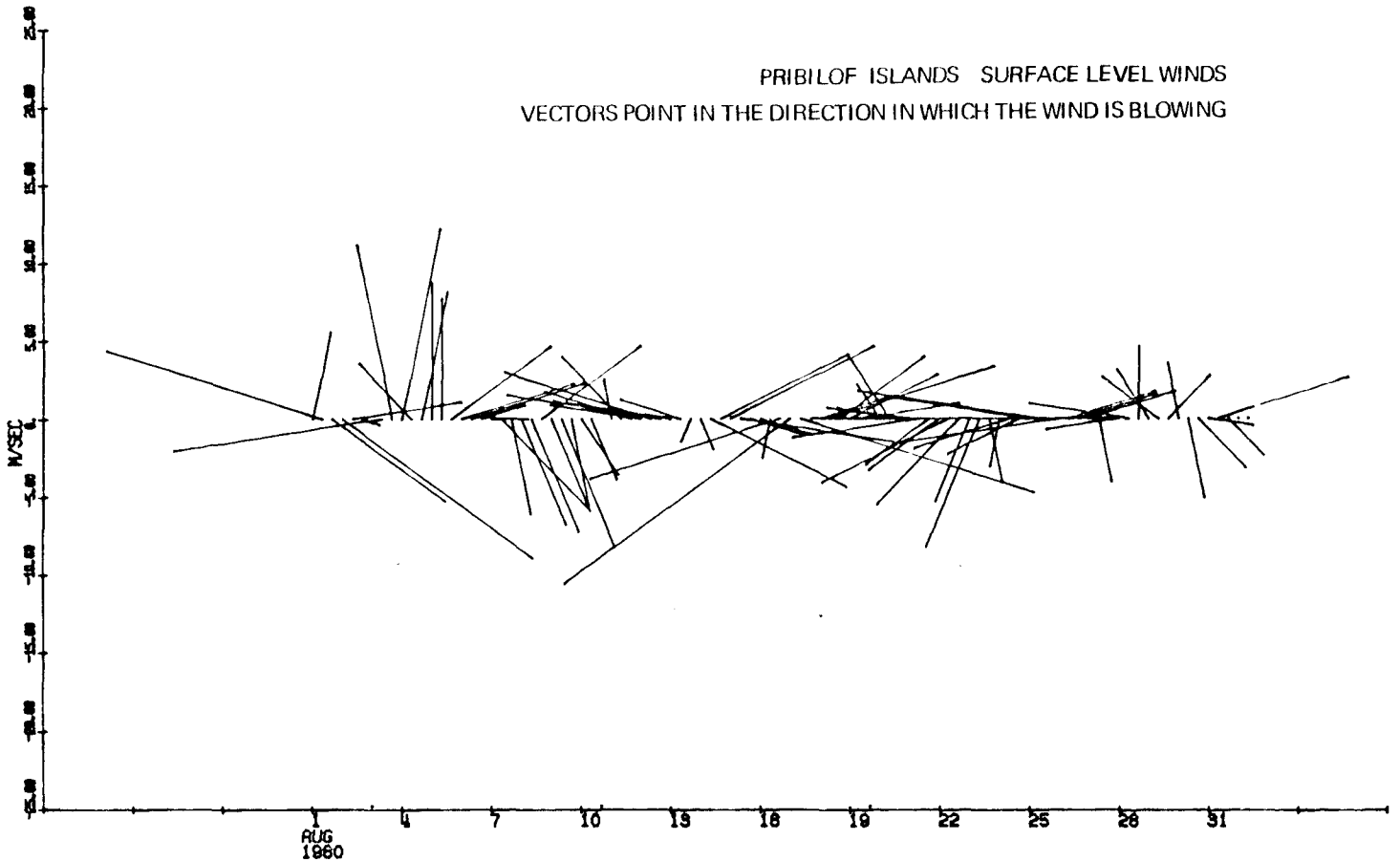

Figure 38a. Stick plots of surface winds for the Pribilof Islands; August 1980.

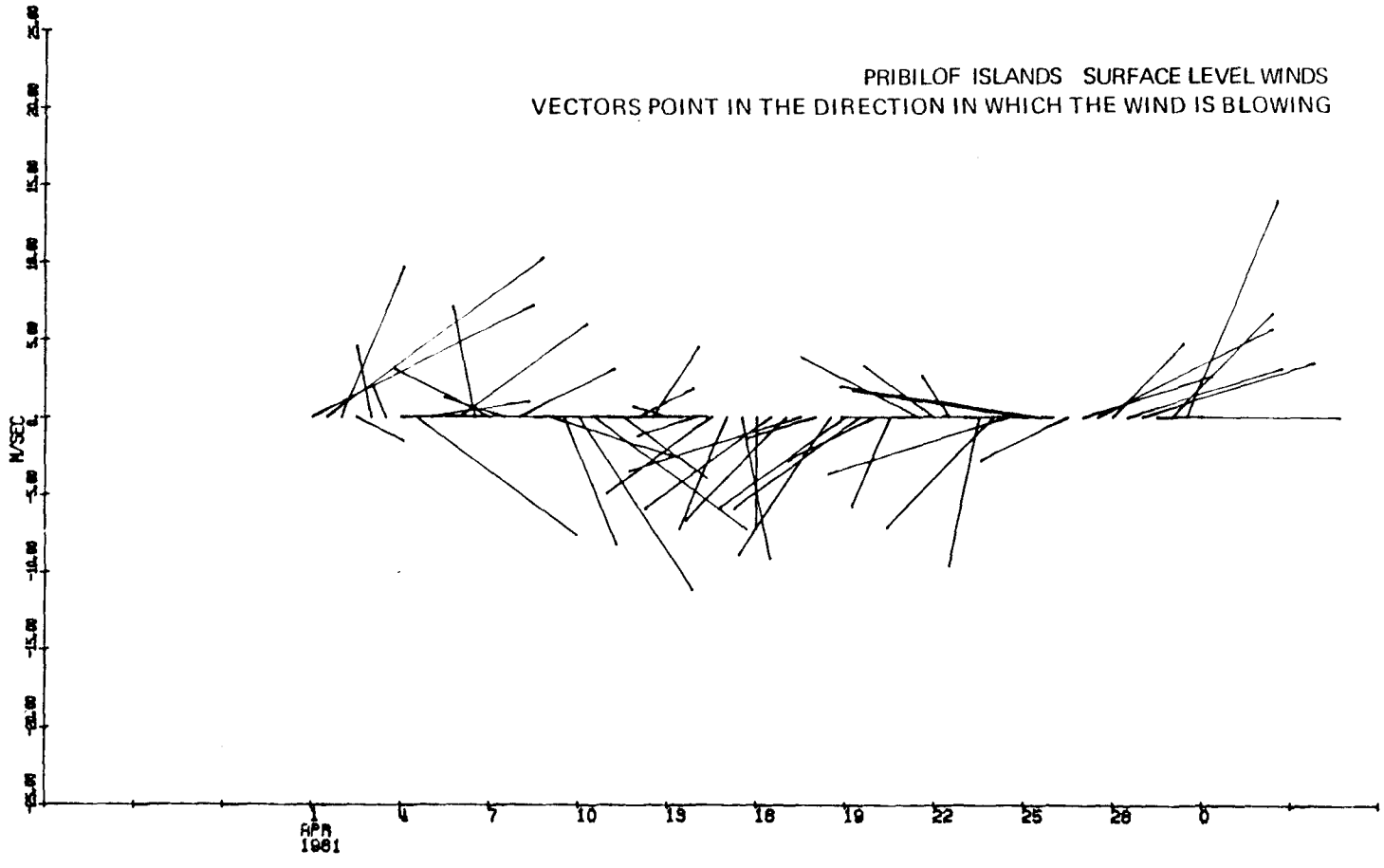

Figure 38b. Stick plots of surface winds for the Pribilof Islands; April 1980.

Table 3 shows the locations of the atmospheric highs and lows in the northern North Pacific for the time spanning the dynamic events, such as the eddies. The high pressure centers are usually located above 65°N, implying they are bringing in the cold, drier arctic air to the Bering Sea during the time at which the images are received. For the times presented low pressure centers are located within the 50°N to 55°N latitude band — that is, they are over or just south of the Aleutian Island chain, also for these time periods low pressure centers are also found in the Gulf of Alaska.

In the stick plots of the winds there is a correlation between the winds from the north and the clear days which allow acquisition of the satellite images in which the eddies were seen. The winds from the north and northeast correspond to the high pressure systems in the Arctic and Bering Sea. As was mentioned before, these circulation systems tend to bring in cool, dry air which creates favorable conditions for the infrared sensing.

The south and southeast winds correspond to low pressure systems in the Bering Sea and over and south of the Aleutian Islands.

Table 3. Atmospheric surface pressure center location versus time.

1-15 JANUARY 1980

Day	1	2	3	4	5	6	7	8	9	10	11	12	13	14	15
Above 70°N		Low							High	High	High		High		
65°N								High				High			
60°N						Low	High						Low	Low	Low
55°N	Low				Low							Low			
50°N	Low			Low						Low	Low				
45°N		Low	Low						Low						
40°N															

15-30 FEBRUARY 1980

Day	15	16	17	18	19	20	21	22	23	24	25	26	27	28	29	30
Above 70°N								High	High							
65°N	Low					High				Low			High	High		
60°N								Low			Low	High				
55°N	High			Low	Low		Low			Low				Low		
50°N			Low			Low			Low		High	Low	Low			Low
45°N	Low	Low				Low			Low						Low	
40°N					Low		Low	Low		Low	Low					

10-25 AUGUST 1980

Day	10	11	12	13	14	15	16	17	18	19	20	21	22	23	24	25
Above 70°N								High								
65°N									High							
60°N	Low				Low		Low	Low	Low	Low			High	High		
55°N		Low				Low					Low	High			High	High
50°N			Low	Low	Low		Low	Low		Low		Low		Low	Low	Low
45°N	High				Low								Low			Low
40°N										Low						

1-15 APRIL 1981

Day	1	2	3	4	5	6	7	8	9	10	11	12	13	14	15
Above 70°N							High	High	High	High	High	High	High		
65°N														Low	Low
60°N	Low				Low							Low	Low		
55°N		Low	Low	Low		Low					Low	Low	Low	Low	
50°N						Low	Low		Low	Low	Low			Low	Low
45°N						Low	Low	Low							
40°N															

For area between 155°W to 175°W
The Aleutian Islands, from Unimak Island to Attu Island, are within the latitude band from 50°N to 55°N; above 55°N is the Bering Sea; below 50°N is the Gulf of Alaska.

DISCUSSION

The features observed in the satellite images, delineated by sea surface temperature patterns, are interpreted and related to physical processes occurring in the Bering Sea. This section will relate the information from the satellite imagery with other data in an effort to relate the sea surface temperature structure seen with the physical processes responsible. The large, instantaneous coverage of the satellite reveals temporal and spatial relationships between features indicated by sea surface temperature patterns. The implications of these relationships will also be discussed in this section.

The Shelf Region

Ice

Ice and sea surface temperature patterns which corresponded with bathymetric contours appeared in the shelf region. The time series for 1979-1981 of satellite imagery reveals that ice is present in the Bering Sea between December to March or April (Figure 35). Visual correlations between rapid advances in the ice extent (Figure 35) and winds from the north (Figures 36 and 37) can be seen for January and February 1980. The maximum extent of the ice was slightly south of St. Paul Island (Figure 35) and corresponded with the boundary of the warm band near the 100 m bathymetric contour. Muench and Ahlnäs (1976) also noted that the ice edge was aligned with the isobaths near the shelf break. They suggest the Bering Slope current as a factor in governing the extent of ice. The imagery relating this spatial relationship between

the ice and the warm band adds support to their hypothesis by suggesting the interaction between the shelf and shelf break/basin region.

The melting and the formation of ice in Bristol Bay and over the shelf are directly related to the salinity of the upper water column (Schumacher *et al.*, 1979; Kinder and Schumacher, 1981) and in conjunction with atmospheric fluctuations are also related to sea surface temperatures. Niebauer (1980) notes that the mean winter atmospheric circulation is the driving force among year-to-year fluctuations in ice cover, freezing degree days, and ultimately sea surface temperature, which correlate with the previous year's freezing degree days. The spatial and temporal relationships observed in the satellite images also imply a relationship between ice cover and the sea surface temperature patterns on the shelf. In early March through late April (1980-1981), the satellite imagery reveals the retreat of the ice on the shelf and a resulting layer of very cold water (Figures 27-29). The very cold water appears as the grey-black speckled region on the shelf. Temperature analysis (Figure 27b) reveals that this water is between -1.0°C and 2.0°C. As time progresses, late May through early June, sea surface temperature patterns which correspond with the isobaths become distinct. A temporal relationship between retreat of the ice, establishment of the cool surface layer, and establishment of sea surface temperature gradients is implied. The surface layer of cool, fresh, and hence stable water is left behind by ice melt. This layer remains visible until mixing by the wind and tidal action establish a new thermal signature.

Hydrography

On those areas of the shelf shallower than 70 m, sea surface temperature patterns visually correspond to isobaths in the June through August (1980-1981) images. This visual correlation is most pronounced at 70 m and 50 m. The region near the 50-m isobath and inshore is homogeneous, and the thickness of the tidally mixed layer is equal to the depth of the water (Pingree *et al.*, 1974). During the heating season, shallower water will be warmer because there is less volume for incoming radiation to heat, likewise as with deeper water, the incoming radiation has more volume to heat, and, consequently, the overall temperature will be less. Because the region is well mixed, the temperature of the surface is representative of the column of water, and as the depth changes, so does the heat content of the water, hence the corresponding sea surface temperature patterns align with the isobaths on the shelf. Schumacher *et al.* (1979) calls this region around the 50-m isobath a front because it delineates the coastal well mixed region and the middle two-layered region. The temperature contour seen along the 50 m depth contour on the satellite imagery is a result of this front, and it indicates that the conclusions drawn from the hydrographic data taken on a station line holds for Bristol Bay and for as far west as Nunivak Island. McRoy (unpublished report, 1981) shows hydrographic data which supports the conclusion drawn from the images; indeed, the 50-m front found on the shelf extends as far west as the Pribilof Islands.

Figures 9-11, 13, 24-32 show seasonal sea surface temperature contours which align with the 70-m isobath. This is particularly noticeable because of the finger-like extension located near 58°N 169°W (Figure 2) just northeast of St. Paul Island. The temperature distribution shows warmer water seaward of the 70-m isobath, in the finger-like extension, and cooler water landward and on each side of the extension. This region is also well mixed (Kinder and Schumacher, 1981). The top 20-50 m are mixed by the wind and the bottom 50 m are mixed by the tidal layer. The area is strongly stratified, and a front occurs along the 100-m isobath. Also, in this area, there is a subsurface cold pool which follows the bottom contours and lies between the 60-100 m isobath (Kinder and Schumacher, 1981). Mean flow in this region is very small (Kinder and Schumacher, 1981), and finestructure has been found in this area. Given this information, it is suggested that a likely physical explanation for the coincidence of the surface temperatures with the bottom contours would be that flow in this region is geostrophic in the along shelf direction. It is realized that in shallow water, friction may translate geostrophic flow into quasi-geostrophic flow. The geostrophic velocities are perpendicular to the horizontal pressure gradient, hence the fluid flows along and not across the lines of constant pressure, which tend to parallel the isobaths (Pedlosky, 1979).

Considering the fact that there is a large tidal effect in this area, one would expect that there is a large component of cross isobath flow and hence friction, which would invalidate the conclusion

that the flow is geostrophic. However, Kinder and Schumacher (1981) note that the tidal motion in the middle domain, between 50-100 m, is ellipitical with the major axis parallel to the isobaths, and, therefore, there is no major cross-isobath tidal effect. Since the tidal motion is along isobath and the geostrophic component of motion is along isobath, this is a likely means by which the flow and characteristic temperatures in the 70-m water column also align with the isobaths.

Figures 9-11, 25-27, 28, 29 are examples of incidences where cooler water is seen surrounding St. Paul Island. Since the flow is along the 70-m isobath, as described above, then it is possible that the finger-like extension is instrumental in directing the flow south into the region near St. Paul Island. Around St. Paul Island the depth becomes shallow very quickly (Figure 2a), and tidal mixing could establish a front similar to the inner coastal front. The tidal mixing would establish the cooler surface temperature structure by mixing some of the subsurface cold pool through the water column. This cooler water may also be a factor in the control of the maximum ice extent. The ice edge has been seen encompassing St. Paul Island (Figures 16-18) but not St. George, which is surrounded by deeper water. Another possibility is the cold subsurface pool follows the finger and curves northwestward again with the regular trend of the isobath (Figure 2a). Overall, the temperature contour at 70 m could be considered evidence of the middle front (as described by Kinder and Schumacher, 1981) and also could show evidence of the fate of the cooler subsurface water.

In the shelf region, the ice covers the shelf with a maximum extent reaching the shelf break. The maximum extent could be controlled by two factors suggested by spatial relationships seen in the imagery. The warm shelf break band, possibly evidence of the Bering Slope current or Alaska Stream/Bering Sea water, bounds the southernmost extent and could be the factor which controls the maximum extent. Also the cool water around St. Paul, which could be the cool subsurface water directed to the area by the 70-m bathymetric contour and is then tidally mixed through the water column could explain why ice has formed around St. Paul Island (Figures 16-18). St. George Island is within the warm band, and the deeper water surrounding it plus the presence of this warmer water are probably the reasons why the ice does not surround this island also.

The Slope/Basin Area

The features in this area include a warm band between the 100-3000 m bathymetric contours, warmer patches of water over the 200-m contour, eddies in the basin and near the shelf break, and a region of warm surface water which extends from the Gulf of Alaska, through the Aleutian Passes, and into the Bering Sea (Figure 34). The interpretations and interrelationship of these features are discussed in this section.

Circulation

The warm shelf break band (Figure 34) is seen in Figures 9-10, 13, 14, 15-18, 22, 24-32. The band generally follows the shelf break and

turns cyclonically at the northwest end bounded by the 100 m and 3000 m bathymetric contour. In the above figures and Figure 20, the region of warm surface water warm band extending from the Gulf of Alaska, through the Aleutian Passes, and into the Bering Sea is also present. The temperature analysis charts (accompanying above figures) show that the temperature of the warm band over the shelf break matches the temperature of the warm surface water within the Aleutian Passes and on the Gulf and Bering sides of the Aleutian Islands. It seems unlikely that insolation and resultant surface heating would be responsible for the distinct temperature patterns for two reasons: (1) the majority of images in which this band is seen occur in the winter when insolation is minimum, and (2) there is no reason that insolation would heat this particular area and not the shallower and deeper region. The warm band seen over the shelf break is related to the temperature pattern along the Aleutians and is possible evidence of advection of Gulf of Alaska water into the Bering Sea. Since the northern boundary of this warm band (the 100 m bathymetric contour) coincides with the region in which the outer front is found, this also indicates that the warm band is related to interactions between the Gulf of Alaska water and the Bering Sea. Kinder and Schumacher (1981) describe the middle front which occurs near the 100-m isobath as a thermal front, which separates the middle and outer regime. The outer domain, seaward of 100 m, is characterized by the occurrence of finestructure. This finestructure is believed to be due to the mixing of shelf and oceanic water masses.

In the southeast corner of the basin (< 150 m), Coachman and Charnell (1979) identify a water mass which they term the Alaska Stream/Bering Sea water, a mixed product of Alaska Stream water and shelf water. This also indicates that there is advection of Gulf of Alaska water into the shelf break band. Hughes *et al.* (1974), Takenouti and Ohtani (1974), and Kinder and Schumacher (1981) discuss possible transport of Gulf of Alaska water into the Bering Sea through the far western passes. Figure 34 shows a summary of the information gained from the images and clearly illustrates the continous distribution of warmer water in the Gulf, in the passes, and in the Bering Sea. Reed and Taylor (1965) and Favorite (1967) establish that the Alaska Stream near 175°W has a warmer, fresher character. Takenouti and Ohtani (1974) propose that Alaska Stream water is transported into the Bering Sea through Aleutian Passes and becomes mixed. They show the distribution of this mixed product and this distribution closely resembles the temperature distributions seen in the images referenced previously. Hughes *et al.* (1974), and Favorite (1974) believe that an increase in winter winds intensifies flow into the Bering Sea. The images which show the warm surface water extending from the Gulf of Alaska and through the Aleutian passes occur in the months of December, January, February, and April, when intense low pressure systems can be found over the Aleutians. Transport of the Alaska Stream water through the far western passes would account for the warm temperature signal seen in many of the images. The density gradient resulting from the mixing of the basin and gulf water is probably a

contributing factor in driving the overall cyclonic basin circulation. Figure 26a shows a very distinct temperature distribution which matches the approximate circulation in the basin as given in Figure 6. The Aleutian low, which sits roughly over the Aleutian chain for a major part of the year (Table 3), would impart cyclonic vorticity to the basin area. This wind stress curl is probably a major factor in driving the upper layer circulation of the basin. Figures 9-11, 14, 24-26, 28 seem to indicate that some of this water transported in through the passes does travel toward the shelf and is probably transported along the shelf break by the Bering Slope Current.

There is a possibility that the major exchange of properties occurs nearer the slope, through the shallower passes. Figures 9-11, 13-18, 22 show temperature distributions which indicate flow through Unimak Pass. If this flow is sufficient, it would help explain the warm band over the shelf break. A recent study by Schumacher *et al.* (1981) revealed that there is a mean westward flow through Unimak Pass with reversals in both winter and summer. The magnitude of the low frequency current was seasonal, higher in winter (approximately 15 cm/sec) and lower in summer (9 cm/sec). The flow was coherent at certain frequencies with the atmospheric pressure gradient normal to the Alaska Peninsula. The investigators suggest that a large portion of the observed flow is driven by wind set-up and coastal divergence on either side of the pass. The long-term forcing for the inflow appeared to be related to the coastal current flowing westward on the Gulf of Alaska side of the Aleutians. This latest evidence

supports the flow indicated by the temperature distributions seen in the images. Table 3 shows that during the time period for which the images indicate flow through the Aleutian passes into the Bering Sea, there are lows centered over or south of the Aleutians. Atmospheric lows centered south of the Aleutian chains would be favorable for enhanced transport into the Bering Sea. The set-up would result in a barotropic flow, while there would also be a baroclinic component from the influx of the Gulf of Alaska water.

The warmer water centered over the 200-m contour (Figures 34 and 13, 14, 24-27, 31-32) correlates with the position of the temperature maximum presented by Kinder (1976). However, the temperature maximum layer is located at depths of 350-500 m. Kinder (1976) proposed that this was water characteristic of that which came through the deeper passes. The temperature analysis accompanying the time series (Figures 24-26) indicate that the surface phenomena may also have been water whose source was originally the Gulf of Alaska, and it had not yet lost its characteristic through mixing. The temperature analysis shows that the temperatures of the patches match the temperatures in the Gulf, and the time series show that on the 2nd and 3rd day the 200-m patch is no longer distinct and in its place is water similar in temperature to the shelf break band. Kinder and Schumacher (1981) and Kinder and Coachman (1978) described a haline front over the continental shelf which they termed the outer front. This haline front marks the change from the oceanic regime to the outer shelf regime. It is possible that the

temperature distributions along the 200-m bathymetric contour are representative of this front.

Overall, there is a coincidence of the boundary of the shelf break band with the region identified as the 100-m front and outer domain. In this outer domain Alaska Stream/Bering Sea water is found. Warm surface water extending from the Gulf of Alaska, through the Aleutian passes and into the Bering Sea, occur simultaneously with the shelf break warm band. Documented flow through Unimak Pass and the far western passes lends support to the interpretation that the temperature distributions imply flow of Alaska Stream or Gulf of Alaska water into the Bering Sea and eventually into the warm band. The possible source of the warm water seen between the over the shelf break in the Bering Sea was indicated as the Gulf of Alaska and the Alaska Stream by both the temperature distributions in the satellite imagery and historical research. The satellite images show this warm water structure as a continuous band extending along the shelf break as far west as 176°W. The Bering Slope Current is a likely means by which the warm water entering the Bering Sea through the Aleutian passes could be transported across the shelf. The general directional flow of the current is toward the northwest along the shelf break. This would explain the correlation with the temperature distribution which parallels the shelf break.

Kinder (1976) identified a northwestward flow along the shelf break as the Bering Slope Current. Figure 5 shows the approximate location and speed of this current. Note that correlation between

the location of this current and the warm band over the shelf break, located between 100 m and 3000 m bathymetric contours (Figures 24-26). Hydrographic data (Figure 39) and PROBES data (unpublished) also show sloping isopycnals which could indicate northwestward baroclinic flow along the shelf break. Occasionally (Figure 40) isopycnals also indicate southwestward flow. The station locations did not extend far enough off shelf or along the shelf to resolve this feature and determine whether it was an eddy-like feature, a meander, or a current. These stations are located near a region influenced by Unimak and Akutan Pass. Flow through these passes, the Bering Slope current, and the general cyclonic basin circulation could be responsible for the flow implied by these hydrographic data. While Kinder (1976) had suggested a counter-current located next to the near-shelf component of the Bering Slope Current, he also noted that the counter-current may not be a permanent feature and may be due to fluctuations in the flow regime. The hydrographic data which occasionally indicate flow to the southeast support the latter interpretation.

A visual correlation with certain weather patterns is noticeable in the images showing the warm band over the shelf break, the warmer water within the band (over the 200-m bathymetric contour), and eddies near the shelf break (Figure 34). All these images (Figures 19 and 22-32) were found in winter and early spring. During the time of the January, February, and April images, lows were centered south of and over the Aleutian chain, while a high pressure was present between 60°N and 70°N, affecting the Bering Shelf area (Table 3). Figures 36-38

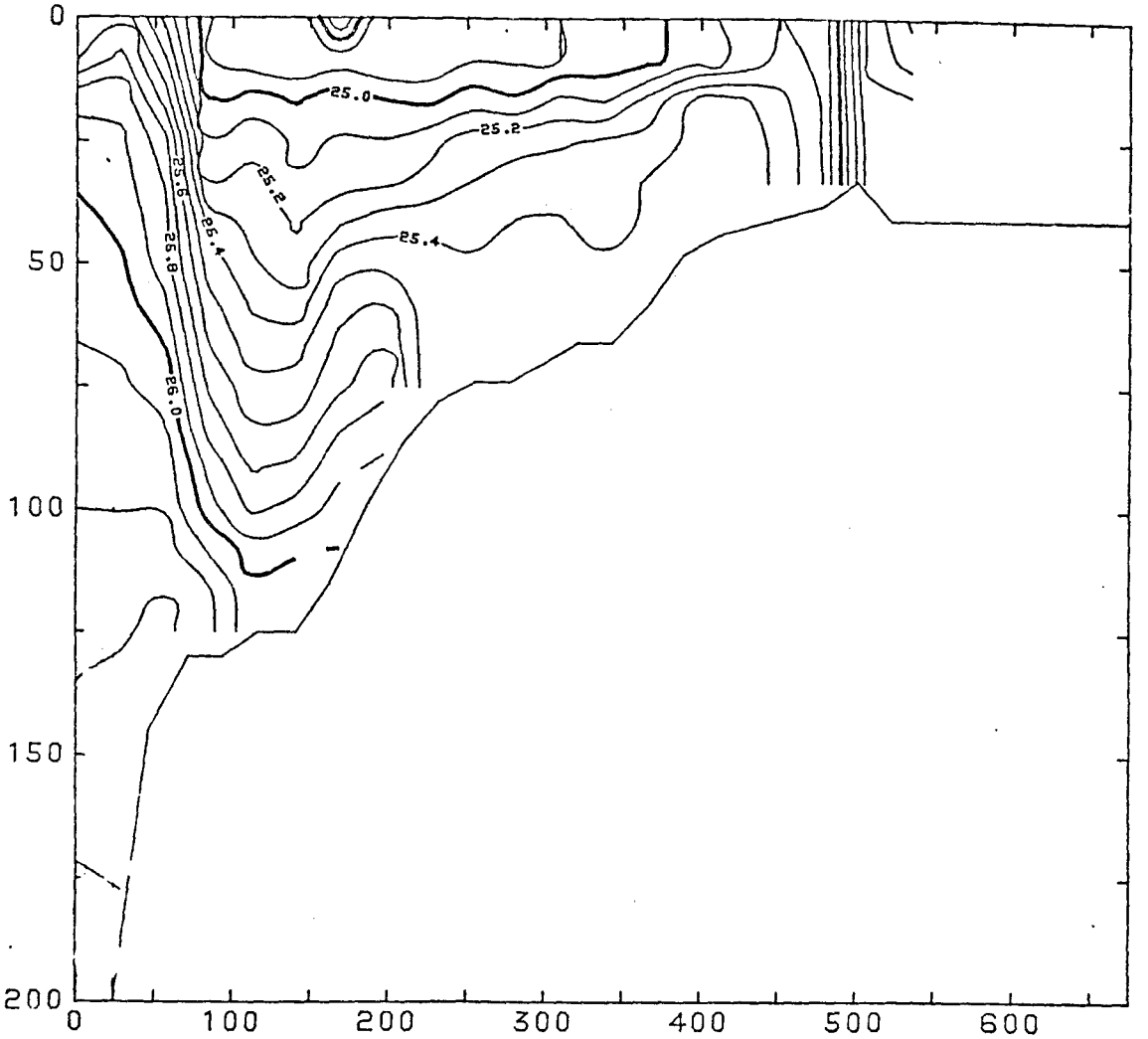

Figure 39. Cross-shelf hydrographic section for June 1981; note the sloping isopycnals which indicate northwestward flow along the shelf break, the strong front at 50 m and near 100 m.

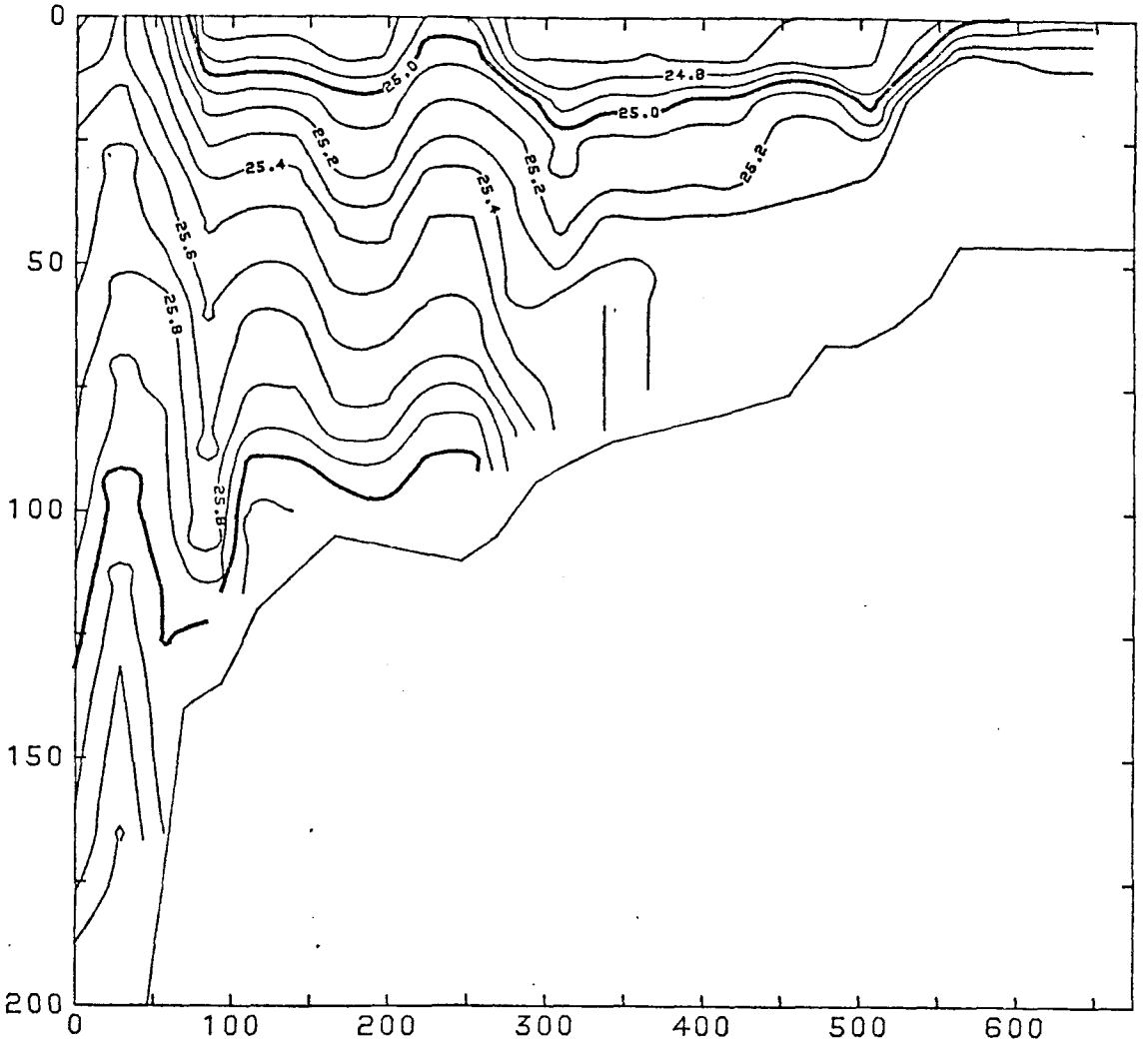

Figure 40. Cross-shelf hydrographic section for mid-June; note the sloping isopycnals which indicate northwestward and southeastward flow along the shelf break.

show that winds from Unimak Pass (near 54° latitude) and the Pribilof Islands (near 56° latitude) were mostly affected by the high pressure systems near 65°N with resulting winds from the north. The south and southeast winds at the Unimak Pass station are probably from the low pressures. Location of the pressure centers is such that the lows south of the Aleutians result in a set-up along the Aleutian Chain and resulting transport into the Bering Sea. The high in the northern part of the Bering Sea results in a set-down, reinforcing the barotropic portion of the flow (Figure 41). The flow through the passes and resulting pressure gradient would also lead to a barotropic flow directed northwestward along the Bering Sea side of the Aleutian Chain. This reinforces the proposed circulation (Figure 6) in the basin.

Hughes *et al.* (1974) and Takenouti and Ohtani (1974) proposed increased transport through the western passes in the winter. This transport of water into the Bering Sea in periods of low pressure systems will also tend to strengthen density gradients which will enhance the baroclinic component of flow in addition to the barotropic component. This could act to intensify the outer front and the Bering Slope Current. Schumacher *et al.* (1981) propose that the flow through Unimak Pass of the fresher Alaskan coastal water enhanced the middle front. The transfer of vorticity from the atmosphere to the western Bering Sea is the proposed forcing mechanism for the overall circulation and the Bering Slope Current by Kinder (1976) and Hughes (1974). Table 3 shows that there is a change from dominant lows in the Bering

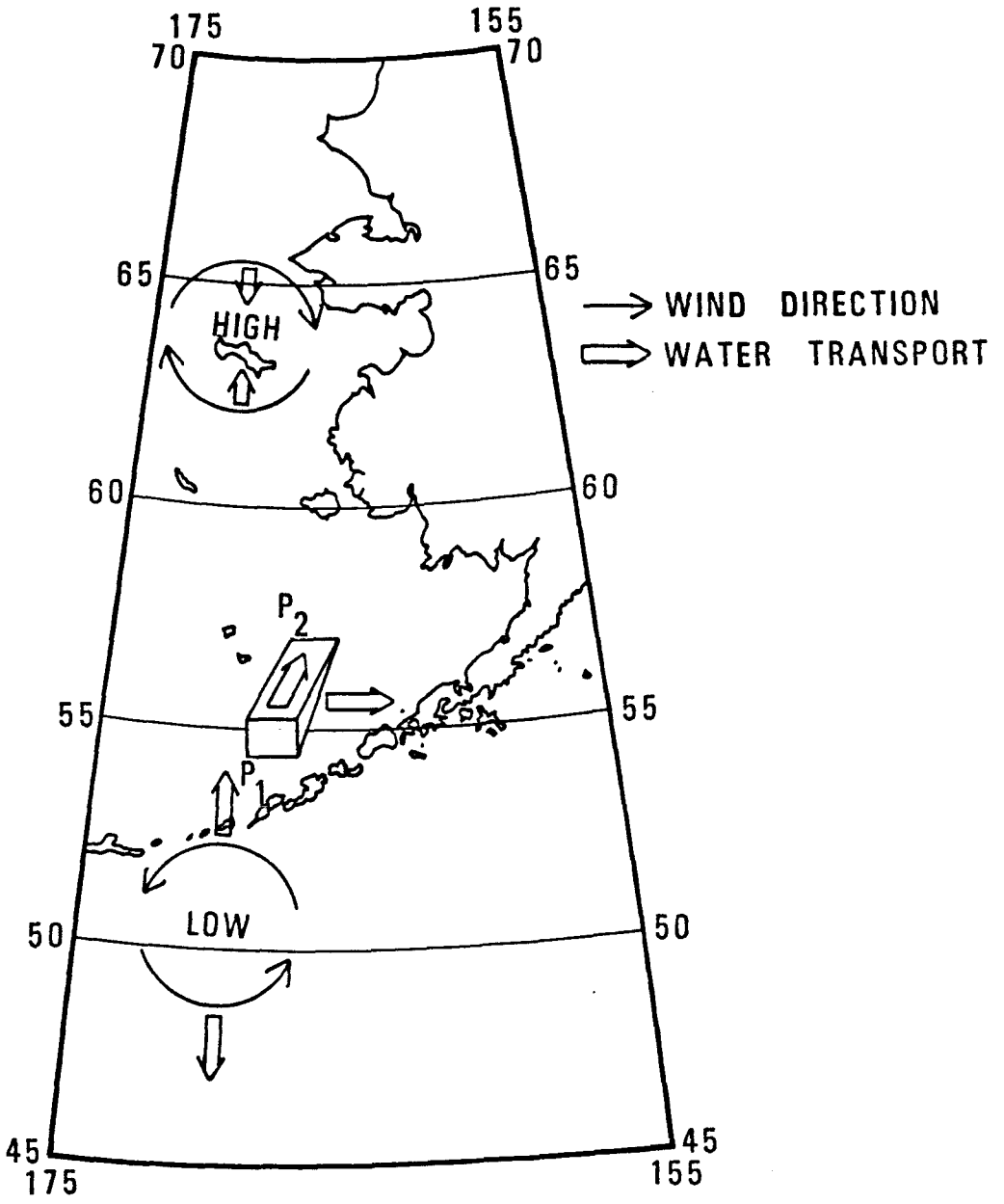

Figure 41. Schematic of wind related surface water transport into the Bering Sea.

Sea to a high then back to dominant lows. This change will result in a change in vorticity on less than annual scales.

These processes would provide a source of warmer, less dense water, and a forcing mechanism to transport this water across the shelf. At the times when these processes first occur (before mixing destroys the signature of the Gulf of Alaska water), the satellite imagery provides a snapshot of the distribution of the warmer Gulf of Alaska water, and from this distribution, the transport process can be implied. The images are collected usually on the first day of northerly winds, and they reveal the process. On several instances, Figures 9-11 24-26, 28-29, the signature of warmer water at the 200-m bathymetric contour becomes less noticeable in the latter images of each 3-5 day time series. The warm water over the shelf break, located between the 100 m and 3000 m bathymetric contours, is still visible. This may imply that the warmer water patches within the shelf break band (Figure 34) are original warm water from the Gulf and the water in the shelf break band is the product of the Gulf water mixed with Bering Sea water. Coachman and Charnell (1979) have referred to the water found from Unimak Pass to Pribilof Canyon as the mixed product of the Alaska Stream and the Bering Sea. This would tend to support the relationship described above. The spatial and temporal relationships seen in the image indicate that the shelf break band, the warmer patches within it, and the temperature pattern extending from the Gulf of Alaska, through the Aleutian Passes, and into the Bering Sea

represent processes which are part of the circulation in the Bering Sea basin and along the shelf.

Eddies

An eddy is defined as a circular movement of water found throughout the water column or limited to certain depths (Baker *et al.*, 1966). The eddies found in the Bering Sea have all been located near the shelf break. The eddies described here are more spiral than circular in appearance and are found in the infrared imagery because the water temperature of the arm of the spiral and the core are different. Temperature is used to distinguish the eddy and define its shape and orientation, but temperature structure does not necessarily imply the dynamics of the eddy as is the case with others, e.g., Gulf Stream eddies, because salinity gradients are more important to density gradients than temperature gradients in cold water regions.

Certain similarities and differences exist between the different eddies and their temperature distributions. A summary of the eddies found is given in Table 4. In all of the images which revealed eddies, the water seen near the Aleutians on the Gulf of Alaska side, in the passes, in the Bering Sea along the Aleutian Islands, and as eddies was the same or nearly the same temperature. This temperature distribution was seen as a continuous contour in January 1980 (Figures 9-11), August 1980 (Figure 20), and April 1981 (Figure 28). In February 1980 (Figures 15-18), the band did not appear continuous.

Table 4. Comparison of eddies (first half of table after Kinder *et al.*, 1980).

Date	Source	Location	Diameter	Structure & Orientation	Method
Sept. 70	Favorite & Ingraham (1972)	Eddies near Bower's Ridge		One anticyclonic, One cyclonic	STD
May - June 71	Int. N. Pacific Fisheries Commission	Eddy in S.E. Aleutian Basin		Anticyclonic	STD - drogue
Aug. 72	Kinder *et al.* (1975)	Eddies along continental slope	Not given	One anticyclonic, one cyclonic near Zhemchung Canyon	STD - drogue
July 74	Kinder and Coachman (1977)	Current ring near Pribilof Canyon. Outer canyon seaward of inner branch of Bering Slope current	100 km x 80 km Elipital Extends to 100 km depth	Cyclonic, salty core	Hydro-cast, current meter
Jan. 76 - June 77	Solomon and Ahlnäs (1978)	Vortices in Kamchatka current east of Kamchatka		Cold core (3°C), Anticyclonic	IR & Vis. satellite imagery
July 77 - May-Oct. 77	Kinder, Schumacher, & Hansen (1980)	Eddy in Eastern Aleutian Basin 55°00N 169°30W	150 km Extends to 1500 m depth	Cyclonic, cold, salty core	CTD, drifters
Jan. 10, 80	This study	Eddy near Pribilof canyon	74.1 km	Cyclonic, cold core	IR satellite imagery
Jan. 11, 80	This study	Eddy near Pribilof canyon, plus warmer water near Zhemchung canyon	92.6 km	Cyclonic, cold core	IR satellite imagery
Feb. 26, 80	This study	One "eddy" in mouth of Pribilof canyon (slightly to S.W. of main axis, and one eddy within Zhemchung canyon)	In Pribilof canyon 81.5 km In Zhemchung canyon 44 km	Difficult to determine in Pribilof canyon — but most probably anti-cyclonic with warm core; in Zhemchung — also anticyclonic but with a cold core	IR satellite images
Feb. 27, 80	This study	Same (except better developed)			
Aug. 23, 80	This study	Eddy S.E. of Pribilof canyon on the "fan" in deep 1000-3000 m deep water	118 km	Anticyclonic, warm core	IR satellite images
Apr. 12, 81	This study	Eddy over Pribilof canyon	102 km	Cyclonic, cold core	IR satellite images

All of the eddies were seen in a time series. Usually, the eddy appeared on the first and second days of the time series, disappearing on later images. From these images it appears that the signature of the eddy can manifest itself only under certain conditions. All of these eddies were found during north winds, after the wind switched from south to north. Later in the time series the eddies were not visible.

Kinder *et al.* (1980) found an eddy near the Pribilof Canyon at depth; no surface signature was seen. The temperature signature can disappear from the surface because of mixing, and the eddy, while it may still be present, will not be revealed on satellite imagery.

The January (Figures 9-11) and April (Figure 28) eddies were similar to each other in surface temperature distribution, position, and surrounding conditions. It is assumed that the surface temperature pattern is representative of the whole water column, although cases have been found where the orientation and temperature structure reverse at depth. Both January and April eddies were cyclonic, with colder cores, and located nearly over the Pribilof Canyon. The February eddy (Figures 15-18) is less distinct, and had a cold outer ring and warm core, and was anti-cyclonic. It appeared as a series of swirls near the Pribilof Canyon. Further along the shelf there was an anti-cyclonic, cold core eddy, which was most pronounced on the first day of the time series. This series of eddies differs from all the others. The cool temperature pattern appears almost wave-like, cresting around the eddy in the Pribilof Canyon and then cresting again with the other

eddy nestled in its western-most trough. The August eddy (Figure 20) also differed in temperature and location, but was similar in structure and surrounding conditions tc the January and April eddies. The August eddy had a cool outer ring, warmer core, and the temperature distribution was continuous from along the passes. This eddy is located further from the canyon, in deeper water.

The temperature analysis maps accompanying the above figures show that the sea surface temperature of the eddies matches that of the water in the passes and on either side of the Aleutian Islands. This temperature distribution might lead one to hypothesize that they are eddies generated by the flow through the passes and then were somehow transported along the slope. While this may be possible, it is not probable because the size of each of the eddies was much greater than the width of the passes, so it is believed that these eddies are generated within the Aleutian basin of the Bering Sea.

Although it is not possible to determine the depth to which these eddies extend, previous eddies found in the Bering Sea (Kinder *et al.*, 1975; Kinder and Coachman, 1977; and Kinder *et al.*, 1980) have been found to depth (Table 4). It seems probable that these eddies also extend to depth and are not mere surface features.

The January 1980 (Figures 9-11) and the April 1981 (Figure 28) eddies seem similar to an eddy Kinder and Coachman's (1977) 1974 study. The warm outer layer would be suggestive of the Bering Slope Current, with the cooler water similar to the water in the basin. If formed by a pinched-off meander or trapped ring, these eddies would retain

the sense of the current, and they do. The February 1980 (Figures 16-19) eddies are most similar to the eddies implied by dynamic topographies in Kinder *et al.* (1975). The February eddies are also anticyclonic and oriented along the shelf break as Kinder *et al.* (1975) showed (Figures 2.4 and 2.6; Kinder, 1976). The August 1980 (Figure 20) eddy does not resemble any of the other eddies. Its cold water structure, orientation, and the corresponding conditions in the images are not similar to other Bering Sea eddies discussed in the literature.

Possible Generating Mechanisms for Bering Sea Eddies

The sea surface temperature patterns seen in the satellite imagery imply interrelationships in time and space between inflow through the Aleutian Passes, the Bering Slope Current, and eddies. The differing structures of the eddies (Table 4) leads one to believe that the January, February, August, and April eddies are not the same eddy, also the differing structures and locations of the eddies indicate that the eddies could be generated differently. Generating mechanisms such as bathymetrically trapped meanders, reflected planetary waves, combinations of current instability, wind forcing, and topographic interaction have been suggested previously by Kinder (1976), Kinder and Coachman (1977), and Kinder *et al.* (1980).

The size, location, orientation, and temperature structure of the January 1980 and the April 1981 eddies suggest that the generating mechanism of the eddies is related to the Bering Slope Current and interactions with the complex topography of the region. These eddies

have a warm outer ring, similar to the temperature of the water seen along the Gulf and Bering sides of the Aleutians; they curl cyclonically as would a trapped ring or meander from the Bering Slope Current. It seems possible that the Bering Slope Current which flows northwest along the shelf break will encounter the canyon and become unstable in that area. The January and April eddies are found directly over the canyon and may be the result of either the currents meander into the canyon being pinched off as in Kinder and Coachman (1977) or through a process of vorticity conservation.

The Bering Slope Current flows from the southeast to the northwest. This current is generally believed to be geostrophic. As the current follows along the shelf, it encounters a change in topography, i.e., the Pribilof Canyon. A parcel of water which is moving along the current in geostrophic equilibrium will encounter topography and follow the isobaths in order to keep the pressure gradient and the Coriolis acceleration in balance.

The absolute vorticity of the flow given by:

$$f - \frac{\partial u}{\partial y}(\text{geostrophic}); \text{ if } f - \frac{\partial u}{\partial y}(\text{geostrophic}) \begin{cases} > 0 \text{ stable} \\ = 0 \text{ neutral} \\ < 0 \text{ unstable} \end{cases} \quad \text{(Holton, 1979)}$$

u = eastward velocity and y = northward displacement D = constant

so that for the flow to remain stable the absolute vorticity must be positive. If the absolute vorticity becomes negative, as it may when the parcel ventures into the canyon and $\frac{\partial u}{\partial y}$ (geostrophic) > f, inertially unstable motions would occur. The depth does not change

because the canyon is deep; however, $\frac{\partial u}{\partial y}_{\text{geostrophic}}$ does. The Coriolis parameter would not change significantly. Inertial instability results from an imbalance between the pressure gradient and the Coriolis force. In the atmosphere, amplification of perturbations of an unstable zonal current result in cyclogenesis (Holton, 1979).

Another possibility, as suggested by Kinder and Coachman (1977) is that the eddy pinched-off by the canyon is a baroclinic instability. According to Wright (1980), mean currents are affected by low-frequency quasi-geostrophic wave perturbations. The energy of a quasi-geostrophic disturbance increases with time by extracting energy from the available potential energy of the mean state. This is known as baroclinic instability. These low-frequency perturbations can extract their energy from horizontal and vertical shear. Wright (1980) considered a baroclinic instability as a source for eddies seen in the California undercurrent off Vancouver Island. He found good agreement between results from a three-layer model of baroclinic instabilities and observations.

Fluctuations in the Bering Slope Current could occur when there is greater influx of water from the Gulf of Alaska. This increased influx could (1) increase horizontal and vertical density gradients, thereby intensifying the outer and middle front and likewise intensifying the Bering Slope Current, and/or (2) increase the general cyclonic circulation in the Bering Sea Basin and likewise intensify the Bering Slope Current. Increases in transfers of vorticity through the curl of the wind stress and corresponding intensifications in the overall basin circulation could also affect the Bering Slope

Current. These periods of intensification could create a quasi-geostrophic perturbation of the mean current with the increased horizontal and vertical shear providing a source of baroclinic instability. Saltzman and Tang (1975) used an analytical model to demonstrate that cut-off cyclonic cold pools and anticyclonic warm pools resulted from a baroclinic instability that would arise when non-geostrophic effects modified a baroclinic system causing perturbations of a uniform zonal current. It is possible that a similar process could occur in the Bering Sea resulting in a cyclonic cold pool which could become "trapped" in the Pribilof Canyon and form an eddy. Saltzman and Tang (1975) suggest that cut-off thermal pools, meanders, and fronts could be viewed as a "simultaneous consequence of baroclinic instability of a broader, more uniform, current that might tend to be forced by the wind stress and large-scale thermohaline processes". If this mechanism occurs along the slope, it could explain the reoccurrence of the eddies and their correlation the intrusion of Gulf of Alaska which would serve as the forcing functions of the baroclinic instability within the uniform current.

The brief lifetime of the Bering Sea eddies is probably because of the low velocities of around 15-30 cm/sec (Kinder *et al.*, 1980) and hence lower potential and kinetic energy than Gulf Stream eddies to be dissipated. Saunders (1971) notes that eddy energy is reduced by two processes: (1) seasonal cooling of the eddy water column greater than in the surrounding water or seasonal salinity changes, and (2) dissipation of kinetic energy by molecular viscosity into heat.

The entrainment of outside water and the resulting mixing will result in dissipation of heat and aid the first process. The imagery indicates that the temperature differences are not large (0.5 to 1.0°C) and the velocities are low (Kinder, 1976), hence the lifetime of these eddies should be short.

The information from the images and hydrographic information from the Pribilof Canyon is used to estimate the fastest growing baroclinic instability. Using an example of an off-shelf station near the Pribilof Islands, a two-layered system is approximated.

Using λ = internal Rossby radius of deformation

$$= \frac{g \frac{\Delta\rho}{\rho} h_1 h_2}{f^2 (h_1+h_2)}$$

$h_1 = 80$ m, $h_2 = 1320$ m, $f = 1.169 \times 10^{-4}$, $\rho_1 = 1.02597$, $\rho_2 = 1.02699$

$\lambda = 7.46$ km is found

A criterion for a baroclinic instability is that $\frac{4\lambda^2}{L^2} < 1$, Eady (1949) and Saunders (1971). λ = Rossby radius of deformation, r = eddy radius. For the January eddy r = 46.3 km, $\sim\lambda$ = 7.46 km, $\frac{4\lambda^2}{L^2} = .103 < 1$, and for the April eddy r = 51 km, $\sim\lambda$ = 7.46 km, $\frac{4\lambda^2}{L^2} = .0854 < 1$, and a baroclinic instablity could occur.

$L = 2\Pi\lambda$ is the wavelength of the fastest growing baroclinic instability, which would be 46.9 km. This wavelength matches closely with the width of the Pribilof Canyon ($\sim$ 45 km), and this match could imply that the baroclinic instability could be trapped in the canyon. Kinder and Coachman (1977) found similar results for their eddy.

The February 1980 and August 1980 eddies are anticyclonic, warm core eddies. These would not be eddies characteristic of a trapped meander of the Bering Slope Current because their orientation and temperature structure would be incorrect. Anticyclonic gyres have been inferred from STD data by Favorite and Ingraham (1972) off Bower's Ridge in 1980, and from 1971 data they showed an anticyclonic gyre just south of Pribilof Canyon (International North Pacific Fisheries Commission, 1972). The August 1980 eddy was found in nearly the same position as the 1971 eddy with the center of the eddy at ∿ 170°W and 54°35'N. The temperature distribution indicates that the eddy is the same temperature as the warm water surrounding the western Aleutian Passes from Unimak Pass to Amchitka Pass. Water along the south side of the Aleutians is much warmer, but the temperature distribution shows that it is confined and does not communicate with the Bering Sea in this instance. The characteristic warm band over the shelf break is not distinguishable.

The temperature analysis map (Figure 20b) shows that the outer ring of the eddy is near 5°C, and the surrounding water in the Bering Sea and in the core of the eddy is between 6° and 7°C. The warm patch of water on the Gulf side is 9°C. Surface temperatures from Schumacher *et al.* (1980) were taken on a path from the Gulf of Alaska to the Bering Sea through Unimak Pass (September 4-5) and show 9-10°C water on the Gulf side and 7-8°C water in the pass and on the Bering Sea (Figure 21). It can be assumed that the temperatures in the imagery are reasonably dependable and indicate that the eddy at 5°C is

representative of cooler, perhaps subsurface, water. The surface truth data indicate 5°C at 100 m near Unimak Pass. Winds from the 17th to the 20th of August were from the southeast blowing to the northwest paralleling the Bering side of the Aleutian Islands. Ekman transport (90° right of the wind) would result in a set-up off shore of the islands and possible upwelling of cooler water near the islands and passes. Cooler surface water has been found in this area (173-175°W) by Kinder (1976) and Royer (pers. comm., 1981) on other occasions, indicating that upwelling in this region may not be the only factor in governing this cooler water. The eddy could be a result of the topographic influence of the Umnak Plateau on the general circulation in the Bering Sea basin. The Umnak Plateau is located slightly south of the Pribilof Canyon, and that correlates well with the position of the eddy (Figures 2a and 20). As the current encounters the Plateau and the depth decreases, the vorticity of the water column must also decrease, through the conservation of potential vorticity.

$$\frac{d}{dt}\ \frac{\xi + f}{D} = 0, \text{ therefore } \frac{\xi + f}{D} \text{ must be a constant}$$

ξ = relative vorticity

f = planetary vorticity (assumed constant in this case)

D = depth

For ξ to decrease, the vortex tubes must shrink, thereby producing negative vorticity and anticyclonic motion. The Unmak Plateau is a topographic high of 2200 m. Water coming in the western passes and circulating cyclonically around the basin will encounter this plateau;

the depth change would be from > 3000 to 2200 m. This plateau is situated roughly in the corner between the basin and the shelf break. Also located in this corner (Figure 2b) are the Bering and Bristol Canyons both at depths 2600 m to 1000 m (Figure 3b). As the water flows along the basin in a general circulation pattern, it encounters abrupt rises in topography. The corresponding shrinking of the vortex tubes will give rise to the anticyclonic vortex. The flow encounters still shallower waters and canyons which would reinforce this gyre and perhaps contain it, also preventing the cyclogenesis that occurs in the lee of topographic high places. The temperature distribution (Figure 20b) from the images indicates that water is also distributed near the western Aleutian Passes and that the gyre is located near Umnak Plateau, slightly south of the Pribilof Islands.

Eddies generated by this process were found in the Atlantic Ocean by Richardson (1980) over the Corner Rise Seamounts. Richardson's eddy was anticyclonic with a warm core and was formed over the seamounts and then drifted southwestward with the mean flow. The August eddy and Richardson's eddy have characteristics which match the model topographic eddies of Hogg (1973), McCartney (1975), and Huppert and Bryan (1976). These models predict that a Taylor column, as indicated by closed stream lines, will form over topographic features. A feature with anticyclonic vorticity will form above the bump and cyclonic features can be formed or shed downstream of the bump. Huppert and Bryan (1976) have demonstrated in their model that for a flow, on the order of 5 cm sec^{-1}, the following temperature pattern will evolve:

upwelling will occur on the upstream side of the feature resulting in a cold anamoly which remains stationary over the feature; for slower flows, on the order of 1 cm sec^{-1} more of the flow goes around, to the left of the feature. This would result in the cold outer ring of the anticyclonic vortex, and consequently, a warmer core. The velocity of flow (an integrated value) would probably be on the order of 1 cm sec^{-1} for the Bering Sea basin area. Hughes *et al.* (1974) presents measured surface velocities as between 4-6 cm sec^{-1} with a maximum value at 22 cm sec^{-1}. It seems likely that the integrated (top to bottom) flow would be on the order of 1 cm sec^{-1}. Richardson (1980) explains that if lateral advection is greater than vertical advection, the eddy will have a warm core, with the opposite the eddy will have a cold core. The temperature distribution (Figure 20b) indicates that the core is warmer and matches areas surrounding the eddy, hence it seems likely that the lateral advection term is greater than the vertical advection term. These comparisons indicate that the August eddy is generated by the basin circulation interaction with Umnak Plateau, a topographic high.

The February 1980 eddies (Figures 15-18) were not similar to the August or January-April eddies. Their arrangement along the shelf break suggests a wave-like pattern. A thin band of cool water delineates a crest and trough pattern in which a cyclonic eddy and two anticyclonic eddies are situated (Figure 15). This pattern and the alternating cyclonic, anticyclonic sense seen in the surface temperatures indicates that a wave-like disturbance is a possible generating

mechanism for these eddies. Longuet-Higgins (1964) and Veronis (1966) have described slow period barotropic oscillations of several days period that can exist in enclosed basins. Longuet-Higgins (1964) and Willmot and Mysak (1980) suggest that these motions may be a response to wind stress. A planetary (Rossby) wave, described by Holton (1979), is an "absolute vorticity conserving motion" and it owes its exsitence to the variation of Coriolis force with latitude, the beta effect, $\frac{\partial f}{\partial y}$. Topography can play an important role because the bottom slope will affect the potential vorticity gradient due to vortex tube stretching and compression (Pedlosky, 1979). The change in planetary vorticity due to a meridional displacement of fluid will cause a negative vorticity. In order to conserve vorticity, the fluid motion would be displaced southward; movement over the sloping bottom topography will add to the perturbation of vorticity by vortex tube stretching and squashing. The pattern of vorticity maxima and minima will propogate westward or along a topographic contour, constituting a Rossby wave. It is possible this could occur within the Bering Sea basin. The eddies found along the shelf break, over Umnak Plateau, and near Kamchatka (Ahlnäs and Solomon, 1978) could be indicative of the vorticity maxima or minima of the potential vorticity waves traveling around the topographic contours in the basin. Kinder (1976) and Kinder *et al.* (1975) suggested a topographic Rossby wave incident upon the continental slope as an explanation for eddy-like patterns in their dynamic topographies.

A simple model for continental shelf waves or topographic Rossby waves (Mooers, 1976) is used to estimate the wave period which would

be responsible for the February eddies along the shelf break. The wave is assumed to be barotropic because: (1) the temperature contours have indicated that the temperature patterns could be a result of spatially (x, y) displaced water rather than vertically displaced water, (2) the effect of bottom slope is critical [$\mu f \beta^{-1} \sim 1$; from Kinder (1976) and Veronis (1966); $\mu \sim 10^{-4}$ km^{-1} for the Aleutian basin where $h = h_o e^{\mu x}$ gives the depth variation; $\beta = 1.28 \times 10^{-8}$ km^{-1} sec^{-1} and $f = 1.169 \times 10^{-4}$ sec^{-1}]; (3) the time between the January and February eddies indicates the period is short.

Mooers' (1976) model considers the case for coastally trapped waves which exist because of the proportional discontinuity in depth and the earth's rotation, f. These trapped wave modes are constained to travel in one direction. The non-dimensional parameters, s and δ, are used where $s = \sigma f^{-1}$, $\delta = \ell L_c$, ℓ = along shore wave number; 140 km measured from the wave in the image, L_c = the width of the zone of bathymetric variation; 100 km for the Bering Sea Slope, σ = frequency (to be determined), f = Coriolis parameter; = 1.169×10^{-4} sec^{-1} for a latitude of 53°N; $h = e^{-mx}$, $0 \geqslant x \geqslant -1$; the form used to represent the exponential form for bottom topography where m = .033. A disperson relationship for the maximum value of s is derived where

$$Su = \frac{m\delta}{\delta^2 + m^2/4}$$

$Su = 7.37 \times 10^{-3}$ for the wave along the slope, $\delta = 8.62 \times 10^{-6}$ sec^{-1}, and the period, $T = 2\Pi/\sigma = 7.2 \times 10^{5}$ sec = 84.3 days, or 2.8 months.

The phase speed would be 1.9 cm sec^{-1} and the phase diagram (drawn according to Longuet-Higgins, 1964) indicates the direction of propogation of the phase velocity is along the shelf break, to the northwest. The direction of propogation of the group velocity would be to the south or slightly southeast. These diagrams were constructed using the wave numbers calculated from the image.

It is possible that a wave with a period on the order of two months could possibly be responsible for the eddies seen in the February images since the appearance and disappearance of the eddies is approximately the same as the period of the wave. The lifetime of the eddies along the shelf break was estimated as on the order of a month, the time between the January and February eddies. The waves could be generated in the basin and propogate along the boundaries of the basin; in areas where the ambient potential vorticity gradient is enhanced, like topographic highs and canyons, the eddies can be seen. The eddies would indicate the presence of the topographic wave since they represent regions of increased local relative vorticity.

The period and wave speed, just presented, are only estimates. The beta effect should be considered as should the effects of stratification and consequent baroclinic modes. The effect of stratification would trap the maximum vertical velocities near the bottom and diminish through the water column (Pedloskey, 1979). Pure baroclinic waves have a much slower propogation speed and are much smaller in scale. Willmot and Mysak (1980) indicate a wave length on the order of 600 km and a period between 4-6 years for the baroclinic waves they modelled in the

Gulf of Alaska. If there is a wave mechanism responsible for the February eddies, it is probably a barotropic wave because of the scale and period indicated previously.

CONCLUSIONS AND RECOMMENDATIONS

Infrared satellite images are used to study the temporal and spatial relationships of physical features and processes, such as ice, fronts, surface currents, and eddies in the Bering Sea. The infrared imagery is obtained from the advanced very high resolution and radiometers (AVHRR) onboard NOAA-6 and TIROS-N orbiting satellites. The infrared images are enhanced to reveal surface temperature patterns more clearly. The positions of the isotherms are visually correlated with bathymetric contours and land masses to establish locations and spatial relationships. A densitometer is used to verify the density patterns initially detected by visual examination and to reveal relative temperatures.

Imagery collected from December 1979 to August 1981 revealed several reoccurring features and relationships. The extent of the ice and its pattern of formation was studied. The ice was confined to the shelf area, it did not extend past the Bering Shelf slope on either year, although it did surround St. Paul Island. The ice retreats and advances occurred on short (day-to-day) time scales and correlates well with winds from the south and north, respectively. Establishment of sea surface temperature patterns with bathymetric contours was seen in both years, although the dates on which these patterns aligned with the bathymetric patterns with the 50-m and 70-m isobaths appears related to processes which establish fronts as described by Kinder and Schumacher (1981) in those regions. The correlations of sea surface

temperature patterns with isobaths occurs on the shelf and is seen through June-September on the images.

The imagery reveals a broad warm band of water located over the shelf break, situated roughly between the 100-3000 m bathymetric contours. Occasionally, particularly warm patches of water located over the 200-m isobath are present. The warm shelf break band occurs simultaneously with a sea surface temperature pattern extending from the Gulf of Alaska, into Bering Sea, through the Aleutian passes. The temperature of water in the warm shelf break band, and the surface temperature pattern extending through the Aleutian passes into the Bering Sea matches the temperature in the Gulf of Alaska. On some occasions the warm band is cooler than the Gulf of Alaska water while along the 200-m isobath the water matches the temperature in the Gulf. It is proposed that these sea surface temperature patterns imply inflow through Aleutian passes into the Bering Sea, a cyclonic circulation in the basin and the Bering Slope Current along the shelf. These sea surface temperature patterns occur during and after periods where low pressure systems are situated in the Bering Sea and south of the Aleutians and winds can cause transport from the Gulf to the Bering Sea. These atmospheric conditions correlate well with proposed inflow through the Aleutian Passes as described by Takenouti and Ohtani (1974), Hughes *et al.* (1974), and Schumacher *et al.* (1981).

Eddies are seen along the shelf break in January 1980, February 1980, August 1980, and April 1981. These eddies were seen simultaneously with the sea surface temperature patterns described above.

Information from the satellite images yields size, location, and temperature structure of the eddies. These results were compared with similar eddies described by Kinder (1976), Kinder and Coachman (1977), and Kinder *et al.* (1980). The locations and size of the eddies imply that the eddies are probably generated by one of the following three mechanisms. It is proposed that the January and April eddies were generated by interactions of the Bering Slope Current with the Pribilof Canyon resulting in a cut-off cyclonic cold pool as described by Saltzman and Tang (1975). The August eddy was thought to be a result of topographic interactions of the basin circulation as it encounters Umnak Plateau, resulting in an anticyclonic gyre to conserve vorticity. A topographic Rossby-wave propogating along the shelf is proposed to explain the multiple eddies and wave-like pattern in the February images.

In this study it became obvious that circulation in the Bering Sea basin is not yet well understood. The Golden Triangle, a term used by PROBES to describe the rich pollock fishing grounds in the Bering Sea, extends out from Bristol Bay to the Bering Sea shelf break. A line from Unalaska Island in the Aleutian chain to Cape Newenham on the Alaska mainland intersects this triangle (Coachman and Walsh, 1981). The Bering Slope current and all of the eddies fall within this area. In order to evaluate how the circulation contributes to the productivity of this region, it should be better understood. The Bering Slope current has been identified but fluctuations of the current over time have not been studied. It might be helpful to understand

how its volume and velocity react to inflow from the Gulf of Alaska. Is there a constant trickle of inflow, or a surge? Do fluctuations in flow and location affect the productivity and marine life cycles? Is there upwelling or downwelling associated with the shelf break eddies, and do they add significantly to the resupply of nutrients to the surface waters? How exactly does inflow through the Aleutian passes influence the Bering Slope current and the basin circulation? The answers to these questions can be implied from the satellite imagery, but hydrographic data is needed to answer questions about magnitudes of velocities and density gradients. It would be useful to biological and physical studies to have this information about the circulation in the Bering Sea basin.

REFERENCES

Ahlnäs, K. 1979. I.R. enhancement techniques to delineate surface temperature and sea-ice distributions. Proc. of Thirteenth Intern. Symposium on Remote Sensing of Environment. Vol. II. pp. 1067-1079.

Ahlnäs, K. 1981. Surface temperature enhanced: NOAA-satellite infrared imagery for the Bering, Chukchi, and Beaufort Seas and the Gulf of Alaska — May 1974 to September 1980. Publ. R80-2, Inst. Mar. Sci., Univ. of Alaska, Fairbanks. 96 p.

Ahlnäs, K. and G. Wendler. 1977. Arctic sea-ice conditions in early spring viewed by satellite. *Arctic and Alpine Res.* 9(1):61-72.

Baker, B. B., Jr., W. R. Deebel, and R. D. Gersenderfer (eds.). 1966. *Glossary of Oceanographic Terms.* 2nd edition. 204 p.

Coachman, L. K. and R. L. Charnell. 1979. On lateral water mass interaction — A case study, Bristol Bay, Alaska. *J. Phys. Oceanogr.* 9:278-297.

Coachman, L. K. and J. J. Walsh. 1981. A diffusion model of cross-shelf exchange of nutrients in the southeastern Bering Sea. *Deep-Sea Res.* 28(8A):819-846.

Dalu, G., C. Prabhakara, R. C. Lo, and M. J. Mack. 1979. An improved scheme for remote sensing of sea surface temperature. NASA Technical Memorandum 80332, July 1979.

Eady, E. T. 1949. Long waves and cyclone waves. *Tellus* 1:33-52.

Favorite, F. 1967. The Alaskan Stream. Bull. 21, Int. North Pac. Fish. Comm.

Favorite, F. and W. J. Ingraham, Jr. 1972. Influence of Bowers Ridge on circulation in the Bering Sea and influence of Amchitka Branch, Alaska Stream, on migration paths of sockeye salmon. pp. 13-29. *In* A. Y. Takenouti (ed.), *Biological Oceanography of the Northern North Pacific Ocean.* Idemitsu Shoten, Tokyo.

Favorite, F. 1974. Flow into the Bering Sea through Aleutian island passes. pp. 3-38. *In* D. W. Hood and E. J. Kelly (eds.), *Oceanography of the Bering Sea.* Occ. Publ. No. 2, Inst. Mar. Sci., Univ. of Alaska, Fairbanks.

Hogg, N. G. 1973. On the stratified Taylor column. *J. Fluid Mech.* 58:517-537.

Holton, J. R. 1979. *An Introduction to Dynamic Meteorology*. Academic Press, New York.

Hood, D. W. and J. A. Calder (eds.). 1981. *The Eastern Bering Sea Shelf: Oceanography and Resources*. Vol. I. O.M.P.A. 625 p.

Hood, D. W. and E. J. Kelly (eds.). 1974. Oceanography of the Bering Sea: with emphasis on renewable resources. Occ. Publ. No. 2, Inst. Mar. Sci., Univ. of Alaska, Fairbanks. 623 p.

Hughes, F. W., L. K. Coachman, and K. Aagaard. 1974. Circulation, transport, and water exchange in the western Bering Sea. Ch. 3. *In* D. W. Hood and E. J. Kelly (eds.), *Oceanography of the Bering Sea*. Occ. Publ. No. 2, Inst. Mar. Sci., Univ. of Alaska, Fairbanks.

Huppert, H. E. and K. Bryan. 1976. Topographically generated eddies. *Deep-Sea Res.* 23:655-679.

International North Pacific Fisheries Commission. 1972. Annual Report. Vancouver, B.C. pp. 95-96.

Iverson, R. L., L. K. Coachman, R. T. Cooney, T. S. English, J. J. Goering, G. L. Hunt, Jr., M. C. Macauley, C. P. McRoy, W. S. Reeburgh, and T. E. Whitledge. 1979. Ecological significance of fronts in the southeastern Bering Sea. From: *Ecological Processes in Coastal and Marine Systems*. Edited by Robert J. Livingston. Plenum Publ. Co.

Kinder, T. H. 1976. The continental slope regime of the eastern Bering Sea. Ph.D. dissertation, Univ. of Washington. 272 p.

Kinder, T. H. and L. K. Coachman. 1977. Observation of a bathymetrically trapped current ring. *J. Phys. Oceanogr.* 7:946-952.

Kinder, T. H. and L. K. Coachman. 1978. The front overlaying the continental slope in the eastern Bering Sea. *J. Geophys. Res.* 83(C9):4551-4559.

Kinder, T. H., L. K. Coachman, and J. A. Galt. 1975. The Bering Slope Current system. *J. Phys. Oceanogr.* 5:231-244.

Kinder, T. H., J. D. Schumacher, and D. V. Hansen. 1980. Observation of a baroclinic eddy: An example of mesoscale variability in the Bering Sea. *J. Phys. Oceanogr.* 10:1228-1245.

Kinder, T. H. and J. D. Schumacher. 1981a. Hydrographic structure over the continental shelf of the southeastern Bering Sea. pp. 31-52. *In* D. W. Hood and J. A. Calder (eds.), *The Eastern Bering Sea Shelf: Oceanography and Resources*. Vol. I.

Kinder, T. H. and J. D. Schumacher. 1981b. Circulation over the continental shelf of the southeastern Bering Sea. pp. 53-75. *In* D. W. Hood and J. A. Calder (eds.), *The Eastern Bering Sea Shelf: Oceanography and Resources*. Vol. I.

Longuet-Higgins, M. S. 1964. Planetary waves on a rotating sphere. *Proceed. Roy. Soc.* (A) 279:446-473.

McCartney, M. A. 1975. Inertial Taylor columns on a beta plane. *J. Fluid Mech.* 68(1):71-95.

McClain, E. P. 1980. Multiple atmospheric-window techniques for satellite-derived sea surface temperatures. Oceanography from space. COSPAR/SCOR/IUCM Symposium, May 26-30, 1980. Venice, Italy.

Mooers, C. N. K. 1976. Wind-driven currents on the continental margin. pp. 29-52. *In* D. J. Stanley and D. J. P. Swift (eds.), *Marine Sediment Transport and Environmental Management*. John Wiley and Sons, Inc.

Muench, R. D. and K. Ahlnäs. 1976. Ice movement and distribution in the Bering Sea from March to June 1974. *J. Geophys. Res.* 81(24):4467-4476.

Niebauer, H. J. 1980. Sea ice and temperature variability in the eastern Bering Sea and the relation to atmospheric fluctuations. *J. Geophys. Res.* 85(12):7507-7515.

Niebauer, H. J. 1981a. Recent short period wintertime climatic fluctuations and their effect on sea surface temperature in the eastern Bering Sea. pp. 23-30. *In* D. W. Hood and J. A. Calder (eds.), *The Eastern Bering Sea Shelf: Oceanography and Resources*. Vol. I.

Niebauer, H. J. 1981b. Recent fluctuations in sea ice distributions in the eastern Bering Sea. pp. 133-140. *In* D. W. Hood and J. A. Calder (eds.), *The Eastern Bering Sea Shelf: Oceanography and Resources*. Vol. I.

NOAA. 1979. Technical Memo. Ness. 95. The TIROS-N/NOAA A-G Satellite Series.

NOAA. 1980. National Environmental Satellite Service 107, Satellite Activities of NOAA 1979.

Ohtani, K. 1973. Oceanographic structure in the Bering Sea. Memoirs of the Faculty of Fisheries, Hokkaido University 21:65-106.

Overland, J. E. 1981. Marine climatology of the Bering Sea. pp. 15-22. *In* D. W. Hood and J. A. Calder (eds.), *The Eastern Bering Sea Shelf: Oceanography and Resources.* Vol. I.

Pedlosky, J. 1979. *Geophysical Fluid Dynamics.* Springer-Verlag, New York. 19 p.

Reed, R. K. and N. E. Taylor. 1965. Some measurements of the Alaska Stream with parachute drogues. *Deep-Sea Res.* 12:777-784.

Reeves, R. G., A. Anson, and D. Landen (eds.). 1975. *Manual of Remote Sensing.* Falls Church, VA, Amer. Soc. Photogramm.

Saltzman, B. and C. Tang. 1975. Formation of meanders, fronts, and cutoff thermal pools in a baroclinic ocean current. *J. Phys. Oceanogr.* 5:86-92.

Saunders, P. M. 1981. Anticyclonic eddies formed from shoreward meanders of the Gulf Stream. *Deep-Sea Res.* 18:1207-1219.

Scholl, D. W., E. C. Buffington, and D. M. Hopkins. 1968. Geologic history of the continental margin of North America in the Bering Sea. *Marine Geol.* 6:297-330.

Scholl, D. W., E. C. Buffington, D. M. Hopkins, and T. R. Alpha. 1970. The structure and origin of the large submarine canyons of the Bering Sea. *Marine Geol.* 8:187-210.

Schumacher, J. D., T. H. Kinder, D. J. Pashinski, and R. L. Charnell. 1979. A structural front over the continental shelf of the eastern Bering Sea. *J. Phys. Oceanogr.* 9:79-87.

Schumacher, J. D., C. A. Pearson, and J. E. Overland. 1981. On exchange of water between the Gulf of Alaska and Bering Sea continental shelves through Unimak Pass, Alaska. Submitted to *J. Geophys. Res.*

Sharma, G. D. 1974. Contemporary depositional environment of the eastern Bering Sea. pp. 517-540. *In* D. W. Hood and E. J. Kelly (eds.), *Oceanography of the Bering Sea.* Occ. Publ. No. 2, Inst. Mar. Sci., Univ. of Alaska, Fairbanks.

Simpson, J. H., C. M. Allen, and N. C. G. Morris. 1978. Fronts on the continental shelf. *J. Geophys. Res.* 83(9):4607-4614.

Smith, W. L., P. K. Rao, and R. Koffler. 1970. The determination of sea surface temperature from satellite high resolution infrared window radiation measurements. *Monthly Weather Rev.* 98: 604-611.

Solomon, H. and K. Ahlnäs. 1978. Eddies in the Kamchatka Current. *Deep-Sea Res.* 25:403-410.

Tabata, S. and J. F. R. Gower. 1980. A comparison of ship and satellite measurements of sea surface temperatures off the Pacific coast of Canada. *J. Geophys. Res.* 85(C11):6636-6648.

Takenouti, A. Y. and K. Ohtani. 1974. Currents and water masses in the Bering Sea: A review of Japanese work. pp. 39-57. *In* D. W. Hood and E. Kelly (eds.), *Oceanography of the Bering Sea.* Occ. Publ. No. 2, Inst. Mar. Sci., Univ. of Alaska, Fairbanks.

Veronis, G. 1966. Rossby waves with bottom topography. *J. Mar. Res.* 24:338-349.

Willmott, A. J. and L. A. Mysak. 1980. Atmospherically forced eddies in the Northeast Pacific. *J. Phys. Oceanogr.* 10:1769-1791.

Wright, D. G. 1980. On the stability of a fluid with specialized density stratification. Part I: Baroclinic instability and constant bottom slope. *J. Phys. Oceanogr.* 10:639-666.

APPENDIX. Listing of Images

AREA	DATE	JULIAN DATE	PASS NUMBER	BAND	SATELLITE	TABLE	SPECIAL FEATURES
Bering Strait to below Pribilof Is. Good coverage of Bristol Bay to St. Matthew	14 Dec 79	348:15:40:07	6025	#4-IR	TN	N4P Temp. Corr. +3°C stretched	Ice above is well defined — above St. Matthew well defined structure in water doesn't follow bathymetry except "canyons" on both sides of Cape Newenham — structure seems to follow ice edge — structure seen off shelf not well defined because of clouds
Bering Strait to Aleutians. Kodiak to St. Lawrence. Good coverage of Bristol Bay to St. Matthew	18 Dec 79	352:01:03:34	6073	#4-IR	TN	N4P stretched	Ice edge well defined. More cooler open water near west side of ice edge. Temp. structure well defined — appears to follow bathymetry but not closely — so does ice edge.
Bering Strait to Pribilof St. Matthew to Aleutian Peninsula	10 Jan 80	010:15:46:21	6406	#4-IR	TN	N4P	Note: Image distorted (compressed horz.) vertical is good. Ice edge near St. Matthew. Well defined temperature structure. Warm eddy in (C.C.) Pribilof Canyon, water same temperature as water through Unimak Pass. Warm water follows 100 m, 70 m contour — or will if distortion removed — structure near 50 m and Bristol Bay too distorted to determine trends.
Bering Strait to slightly below Aleutian Chain. Aleutian Peninsula to St. Matthew	11 Jan 80	011:01:42:21	6412	#4-IR	TN	N4P	Horz. distortion (compressed) eddy seems more developed and water of same temp. is seen along Gulf side of Aleutian Chain and through Unimak Pass — also west of eddy along shelf water of temp. cooler than eddy covers whole shelf w/ slightly cooler water to west. Seems to extend to where shelf becomes 120-100 m. Ice nearly covers St. Matthew. Temp. structure following contours — as does ice edge — distinctly warmer water seen going into Pribilof Canyon.

Tables: These are the enhancement tables used by Gilmore Tracking Station and are available at the station; the code denotes the table used to perform these enhancements.

NOTE: TN = TIROS-N; N6 = NOAA-6. TN sensors were "off" 5 density counts (approx. 2°C) January 21-March 21; overall, the image appear darker.

APPENDIX. Continued

AREA	DATE	JULIAN DATE	PASS NUMBER	BAND	SATELLITE	TABLE	SPECIAL FEATURES
Bering Sea to Aleutian Chain. Bristol Bay to St. Matthew.	11 Jan 80	011:15:36:21	6420	#4-IR	TN	N4P	Horz. distortion. Ice edge extent to St. Matthew. Structure well defined. Eddy appears broken up — hard to tell. Clouds obscure visibility. Warmer water still seen on Gulf side of Aleutians w/ bits and pieces on shelf. Warm water extends 100 m to 3000 m then gets cooler deeper and shallower, cools as it approaches ice edge — some warmer water intrusion up along St. Paul and into the "canyon"??
Nunivak to Unimak Pass, Kodiak to mid-Bering Sea	29 Jan 80	29:19:38:27	3072	#5-IR	N6	64P	Somewhat distorted — Zoom 2 ice edge not yet covering all of Bristol Bay — temp. structure well defined. Warmer out on shelf — one warmer spot in the middle of Bristol Bay. On Gulf side, eddies seen in Shelikof Strait — on the other side of Kodiak warm water band may be Alaska Stream — with colder, water on each side — some meanders and eddies.
Norton Sound to below Aleutian Chain. St. Matthew to Bristol Bay	31 Jan 80	031:05:42:01	3093	#4-IR	N6	64P	Ice edge covers St. Matthew to approx. 65-70 m contour. Warm water seen along Aleutian Chain (Gulf side). Warm water on slope extends to slope between 200-100 m contours. Some bits of warmer water on shelf water.
Bering Sea Norton Sound-Aleutian Chain	20 Feb 80	051:01:15:21	6976	#4-IR	TN	N4P-7°	Some structure visible near shelf break.

APPENDIX. Continued

AREA	DATE	JULIAN DATE	PASS NUMBER	BAND	SATELLITE	TABLE	SPECIAL FEATURES
Bering Sea ice edge to Aleutian Chain	20 Feb 80	057:15:33	7069	#4-IR	TN	N4P-7°	Clearly visible temp. gradient following the 200 m contour and the shelf break — see bathymetric overlay
Bering Sea ice edge to Aleutian Chain	26 Feb 80	057:20:05	3471	#4-IR	N6	64P-7°	Temp. difference visible as in above but not as clearly.
Bering Sea ice edge to Aleutian Chain	27 Feb 80	058:19:43	3485	#4-IR	N6	64P-7°	Some temp. differences seen along the shelf break, indicates warmer water along break, cooler on the shelf — some eddy-like features.
Bering Sea above Norton Sound to Aleutian Chain	27 Feb 80	058:05:56	3477	#4-IR	N6	64P-7°	Same as above although not as clearly — some clouds obscuring.
Bering Sea ice edge to Aleutian Chain	12 Mar 80	072:19:39	3684	#1-VIS	N6	Zoom and Enhancement	Some temp. difference following the edge of the ice. It appears dark gray on the enhancement and could indicate snow blown off the ice or ice melt.
*This enhancement was done by Anchorage Satellite Service, the table was not listed.							
Bering Sea above Norton Sound to Aleutian Chain	4 Apr 80	095:19:33	4011	#1-VIS #4-IR	N6	Zoom and Enhancement	No clearly defined differences, but bits of dark and light intermixed — very confused image — it may perhaps indicate water temp. close to that of ice edge and/or the clouds (black = 1)
*With reference to enhancement — same as above.							
Bering Sea above Norton Sound to Aleutian Chain	8 Apr 80	099:19:46	4068	#1-VIS #4-IR	N6	64P-7°	No definite temp. structure indicates water in that area may be very close in temp. — some swirls and blobs of a darker shade appear.

APPENDIX. Continued

AREA	DATE	JULIAN DATE	PASS NUMBER	BAND	SATELLITE	TABLE	SPECIAL FEATURES
Bering Sea above Norton Sound to Aleutian Chain	10 Apr 80	101:19:06	4096	#1-VIS #4-IR	N6		Some temp. structure along shelf – indicates warmer water as you proceed off shelf.
Bering Sea above Norton Sound to Aleutian Chain	11 Apr 80	102:04:57	4102	#4-IR	N6	64P-7°	Some structure, as above; however, distortion in area of interest.
Bering Sea Norton Sound to Aleutian Chain	11 Apr 80	102:18:40	4110	#1-VIS	N6	None	Use to identify clouds for above image (4102)
Bering Sea above Norton Sound to Aleutian Chain	18 Apr 80	109:19:27	4210	#1-VIS #4-IR	N6	64P-7° and UA3 (-4 to +4°C)	Well defined gradient in Bristol Bay – corresponding with 20-50 m contours.
Above Nunivak to mid-Aleutian Chain – good coverage of Bristol Bay	5 May 80	126:19:58:19	4452	#4-IR	TN	64Z enlarged (-3 to 12°C)	Bristol Bay free of ice. Outer Bristol Bay cloud covered. Closer in, warmer water following coastline.
Bering Strait to below Aleutian Chain	8 May 80	129:18:49:32	4494	#1-VIS #4-IR	N6	UA2	A great deal of interference from clouds. In Bristol Bay warm water seen close to coast – cooler away – gradient of approx. 20-30 m contour warmer patch water seen out near 50-70 m slope.
Bristol Bay – Aleutian Chain	19 May 80	140:19:52:21	4651	#1-VIS #4-IR	N6		No structure visible.
Kuskokwim Bay	20 May 80	141:19:29:26	4665	#4-IR	N6	64X enlarged	Warmest water near shore.
Nunivak to below Aleutian Chain – mainly Bristol Bay – Some Gulf of Alaska	8 Jun 80	160:00:53:34	8514	#5-IR	TN	Enlarged N4X	Warm water along coast – with some cooler water in mid-bay.

APPENDIX. Continued

AREA	DATE	JULIAN DATE	PASS NUMBER	BAND	SATELLITE	TABLE	SPECIAL FEATURES
Bristol Bay — Cape Newenham over to Kodiak	8 Jun 80	160:05:22:14	4927	#4-IR	N6	Enlarged	Warmer water out to 10-20 m then cooler water.
Bristol Bay and Kodiak	23 Jun 80	175:04:54:20	5140	#4-IR	N6	64Y Enlarged	Spots of warmer water — no discernable pattern.
Bering Strait to Aleutian Chain	9 Jul 80	191:05:44:06	5368	#4-IR	N6	6MA *All images stretched from this point on	Many clouds, low ground fog; no SST features noticeable.
Bering Strait to Aleutian Chain	19 Jul 80	201:19:06:59	5518	#1-VIS #4-IR	N6	64V	Partly cloud covered; area of St. Lawrence to St. Paul, however, low clouds around St. Paul. Temperature gradient apparent; consistent with 50 m isobath. Interesting structure in Norton Sound.
Bristol Bay Nunivak Is. to Unimak Is.	20 Jul 80	202:01:21:25	9107	#4-IR	N6	N4U N4V	Some clouds obscuring the Aleutian Peninsula; temperature gradients following 50 m isobath with colder water within the center of Bristol Bay — seaward of 50 m isobath. N4V reveals the gradients with greater clarity.
Nunivak Is. to Aleutian Chain	20 Jul 80	202:18:45:11	5532	#1-VIS #4-IR	N6	64V	Clear view of Bristol Bay, some clouds obscuring the Aleutian Peninsula, one streak across Bristol Bay. Temperature gradient also well pronounced at the 50-m isobath with colder water seaward; a great deal of structure seen at the mouth of the Kuskokwim River. Warmer water on the Gulf side, and what looks like the Alaska Stream paralleling the Aleutian Peninsula.

APPENDIX. Continued

AREA	DATE	JULIAN DATE	PASS NUMBER	BAND	SATELLITE	TABLE	SPECIAL FEATURES
Bristol Bay Nunivak to Unimak	21 Jul 80	203:01:10:00	9121	#4-IR	TN	N4V	Clear view of all of Bristol Bay. 50-m isobath temperature gradient well pronounced. There are temp. gradients shoreward of 50 m which also seem to correspond with the isobaths, except near the mouth of the Kuskokwim where structure is more confused. A cold spot once again appears seaward of 50 m.
St. Lawrence to Aleutian Is. on east slightly south of St. Matthew	21 Jul 80	203:20:07:04	5547	#1-VIS #4-IR	N6	64V	Clouds cover all but the area from St. Lawrence to Bristol Bay, the temperature gradient which follows the 50-m isobath is obvious again.
St. Lawrence to the Aleutian Chain	22 Jul 80	204:05:57:51	5553	#4-IR	N6	64V	Clouds cover the area west of St. Matthew; however, Bristol Bay is clear. The temperature gradient at the 50-m isobath is visible. There is an area of colder water shoreward of the 50-m isobath, SW of Nunivak Island.
Bering Strait to Aleutian Chain	22 Jul 80	204:19:40:59	5561	#1-VIS #4-IR	N6	64V	Mostly cloud free from the Strait to south of St. Matthew, some scattered clouds of Bristol Bay; temperature structure is confused and may be questionable due to cloud contamination.
Bering Strait to Aleutian Chain	23 Jul 80	205:05:35:39		#4-IR	N6	64V	Extensive low cloud cover over Bristol Bay and west of St. Matthew, some clear areas near the Aleutian Chain which show temp. gradients relatively parallel to isobaths.

APPENDIX. Continued

AREA	DATE	JULIAN DATE	PASS NUMBER	BAND	SATELLITE	TABLE	SPECIAL FEATURES
Southern portion of Bristol Bay and areas east of the Pribilof Islands	24 Jul 80	206:19:00:45	5589	#1-VIS #4-IR	N6	64V	Low clouds and fog make temperature structure suspect; some indications of a temp. gradient aligned with the 100- and 200-m isobaths; some structure roughly associated with the 70-m isobath.
South of St. Matthew to the Aleutian Chain	25 Jul 80	207:06:27:18	5596	#4	N6	64V	Low fog near the Aleutian Chain and west of the Pribilof Islands. Temp. gradient along 50-m isobath. Some warmer water appears over the basin near the Pribilof Canyon.
Bering Strait to the Aleutian Chain	21 Aug 80	234:20:23:41	5988	#1-VIS #4-IR		64V	The area around the Pribilof Islands is clear; however, clouds were found west, east, and south of the Islands. Some cold water appears around St. George, with small fingers of the cold water around St. Paul and out into the basin. Temp. gradients follow the 40-m, 50-m, 60-m isobath from the Bristol Bay past St. Matthew.
Bristol Bay to the Aleutian Chain	22 Aug 80	235:19:57:28	6002	#1-VIS #4-IR	N6	64V	The area over the Pribilof Islands is clear; the cool water, seen in previous image, is still present and surrounds both St. Paul and St. George; it seems to match same water over basin and the area between the 40-m isobath and the 60-m isobath. Part of the cool water surrounding the Pribilof Islands curls around the Pribilof Canyon.

APPENDIX. Continued

AREA	DATE	JULIAN DATE	PASS NUMBER	BAND	SATELLITE	TABLE	SPECIAL FEATURES
Nunivak Island to the Aleutian Chain	23 Aug 80	236:19:35:23	6016	#1-VIS #4-IR	N6	64X	The area around the Pribilof Islands is clear except for low ground fog over St. Paul, the northern island. The major feature seen is an eddy, anticyclonic, with a warm core off the shelf near the Pribilof Canyon. The core looks as if it is shelf water. The outer ring appears to be water of a temperature similar to that along the Aleutian Islands. The temp. gradient paralleling the 50-m isobath is apparent. Several swirling eddy-like features appear around and within the passes of this portion of the Aleutian Chain. Warmer water is seen on the Gulf side of the Aleutian Islands.
Bristol Bay to the Aleutian Chain	24 Aug 80	237:19:13:11	6030	#1-VIS #4-IR	N6	64X	Clouds cover St. George and the area where the eddy was seen previously. Some cooler water structure is seen around St. Paul. Warmer water is seen over the basin and along the shelf break.
Bristol Bay to Aleutian Chain	25 Aug 80	238:05:04:30	6036	#4-IR	N6	64X	Clouds and low fog are present to the west and north; however, the 50-m isobath temp. gradient is visible and a temp. contour which follows the 100- and 200-m isobath. The temp. between the 100- and 200-m isobath appears to be the same and is warmer than the basin and shelf water.
Bristol Bay to the Gulf of Alaska including Kodiak	25 Aug 80	238:01:14:51	9615	#4-IR	TN	N4V	Temperature contours appear to follow bathymetric contours in the shallow region of Bristol Bay.

APPENDIX. Continued

AREA	DATE	JULIAN DATE	PASS NUMBER	BAND	SATELLITE	TABLE	SPECIAL FEATURES
Bristol Bay to the Aleutian Chain	29 Sep 80	273:05:34:40	6534	#4	N6	64X	Clouds cover most of the area west and north of Bristol Bay; a temperature gradient follows the 80-m isobath.
Bristol Bay to the Aleutian Chain	8 Oct 80	282:05:31:38	6662	#4-IR	N6	64X	Entirely cloud or fog covered.
Inner Bristol Bay	8 Oct 80	282:19:21:33	6670	#4-IR	N6	64X	Temperature gradients coinciding with 10-, 20-, 30-, 40-m isobaths.
St. Lawrence to the Aleutian Chain	9 Oct 80	283:19:00:32	6684	#1-VIS #4-IR	N6	64X 64Z 6MG	Area over Pribilof Islands to Aleutian Chain is clear. Warmer water on shelf appears to be curling around the Pribilof Canyon. Colder water is seen over the basin and between the 70-m and 50-m isobath. 64Z enhancement reveals this same structure with yet a warmer section of water, along the eastern edge of the shelf break; smaller eddy-like features are seen within this. 6MG enhancement again narrows the temperature range and reconfirms features seen in the first two enhancements.
Inner Bristol Bay	10 Oct 80	284:04:49:39	6690	#4-IR	N6	64X	Clouds and ground fog make structure seen questionable. Generally, temp. gradient seen at 50-m isobath.
Outer Bristol Bay, south of Nunivak	27 Oct 80	301:05:14:57	6932	#4-IR	N6	6MG	Clouds and ground fog obscure temp. structure.
No clear images in November.							

APPENDIX. Continued

AREA	DATE	JULIAN DATE	PASS NUMBER	BAND	SATELLITE	TABLE	SPECIAL FEATURES
St. Lawrence to Bristol Bay	10 Dec 80	345:05:36:57	7558	#4-IR			The ice has reached St. Lawrence and is forming along the coast and around the edges of St. Matthew. SST gradients are well defined and follow bathymetric contours closely. Table 6MG was too warm and is not useful in this season.
St. Lawrence to St. Paul Islands	10 Dec 80	345:19:23:50	7566	#4-IR	N6	64P 6MG	Much the same as above.
St. Lawrence to the Aleutian Chain including St. Paul	11 Dec 80	346:05:14:50	7572	#4-IR	N6	6MG	Same as above.
St. Matthew to St. George Island	11 Dec 80	346:06:56:08	7573	#4-IR	N6	64P 6MG Zoom 3	Clouds cover all the area except that from St. Matthew to St. Paul. The SST gradient visibly follows the 100-m and 70-m isobath closely.
Bering Strait to the Aleutian Chain	24 Dec 80	359:19:09:21	7765	#4-IR		64P	Ice extent has passed Nunivak Island and reaches its max between 59-58°N. The temperature contours follow the isobaths, especially at 100 m. A very warm spot is present SE of the Pribilof Islands between 100-130 m of water.
St. Lawrence to the Aleutian Chain	25 Dec 80	360:06:40:25	7772	#4-IR	N6	64P	The ice edge has reached the 50-m isobath and follows this very closely. New ice surrounds St. Matthews. A band of warmer water is very prominent. It follows the 200-m isobath very closely and spreads up to the 100-m isobath in the southern end and narrows as it proceeds NW along the 200-m contour. Other SST gradients follow the isobaths, including the 100-m, 70-m, 80-m, isobaths. Note that cooler water surrounds St. Paul than St. George.

APPENDIX. Continued

AREA	DATE	JULIAN DATE	PASS NUMBER	BAND	SATELLITE	TABLE	SPECIAL FEATURES
Nunivak to the Aleutian Chain	25 Dec 80	360:05:01:35	7952		N6	64P	This enlargement of this area reveals that the ice edge has formed around the coastline. SST gradients also follow isobaths; it is interesting to note the 70-m isobath, which has a "finger" reaching up onto the shelf and is usually well defined.
St. Lawrence to Aleutian Chain	25 Dec 80	360:20:27:40	7780	#4-IR	N6	64P	As earlier in the day the broad band of warm water is still present over the 200-m isobath; within this is yet another warmer band which extends from the Pribilof Canyon northwestward. It has a wave-like structure. Warmer water can be seen out in the basin; on either side of the warm band, cooler water is found.
St. Lawrence to Aleutian Chain	26 Dec 80	361:06:18:06	7786	#4-IR	N6	64P	Clouds obscure the southeastern part of the Bering Sea; however, the Pribilof Islands and west are clear. The ice edge has not changed. The band of warm water is still apparent, and is still centered over the 200-m isobath. Warmer water can be seen out in the basin and around the Aleutian Islands; however, the warm band is still isolated by cooler water on either side.
Bristol Bay to the Pribilof Is.	27 Dec 80	362:05:56:31	7800	#4-IR	N6	64P	Clouds are obscuring both the upper and lower portions of the scene; however, the Pribilof Islands and the warm band along the shelf break are still visible.

APPENDIX. Continued

AREA	DATE	JULIAN DATE	PASS NUMBER	BAND	SATELLITE	TABLE	SPECIAL FEATURES
Bering Strait to the Aleutian Chain	23 Feb 81	054:05:59:40	8625	#4-IR	N6	64P	The ice edge has advanced to the 60-m isobath in the western portion of the Bering Sea, but is still no further than the 50-m isobath within the Bering Sea. Surface fog obscures the SST structure even though the regular if indicated the area was clear.
St. Lawrence to Aleutian Chain	21 Mar 81	808:20:03:30	9003	#1-VIS #4-IR	N6	64P	The ice has been retreating. A very large lead/open area is seen going past Nunivak, up along the coast. Other large leads can be seen in the western portion of the ice pack. Some surface structure can be seen. A warm band is seen following the 200-m contour. A band of clouds near that area may cause question in the accuracy.
St. Lawrence to Bristol Bay	22 Mar 81	081:05:53:30	9009	#4-IR	N6	64P	More large openings in the ice can be seen in the area of Norton Sound and west, also in Bristol Bay. The SST structure is more apparent and the same warmer band of water band of water appears over the 200-m isobath. Curls and swirls are seen on the edges of this band, there is cooler water on the shelf and in the basin.
Portions of outer Bristol Bay	25 Mar 81	084:06:26:45	9052	#4-IR	N6	64P	The area is largely cloud covered with only a portion of Bristol Bay clear. In this portion some SST gradients can be seen.
Nunivak to Aleutians and inner Bristol Bay	31 Mar 81	090:05:51:26	9137	#4-IR	N6	64P 64Z Zoom 2	It appears that the water south of Nunivak to approx. 50-m isobath is very cold, i.e., newly melted ice. The SST gradients south of that were masked by cloud contamination. Table 64Z is too warm.

APPENDIX. Continued

AREA	DATE	JULIAN DATE	PASS NUMBER	BAND	SATELLITE	TABLE	SPECIAL FEATURES
Bristol Bay	10 Apr 81	100:19:14:09	9287	#4-IR	N6	64Z	Temperature gradients could be distinguished but did not seem to correspond well to isobaths.
Nunivak to the Aleutian Chain	12 Apr 81	102:20:09:00	9316	#1-VIS #4-IR		6MC 64Z Zoom 2	The SST structure reveals an eddy-like feature located near the Pribilof Canyon, cyclonic, with a cool core. This feature is superimposed on a warm band which parallels the 100-m isobath, but also extends out into the basin. On either side of this warm band are cooler temperatures. Another interesting feature is an influx of this warmer water up the 70-m finger which extends onto the shelf; around the edges of this finger swirls of the warmer water go into the cooler shelf water. Also, note the warm water along the Aleutian Chain on both the Gulf and Bering sides.
St. Matthew to Aleutian Chain	13 Apr 81	103:05:58:30	9322	#4-IR	N6	64P	The warm water band over the 200-m contour is still visible but is less distinct; the eddy is well defined, but there is a swirl with a cyclonic curvature and its temperature is warmer than that of the band; the feature at the 70-m finger near the Pribilof Islands. The swirling fingers at the edge of this warm water extension are much more defined that previously. Warm water can be seen along the Aleutian Chain and the temp. structure seems continuous from Kodiak on down. There is structure in Bristol Bay, but no well defined. The water there is much colder than on the western part of the shelf.

APPENDIX. Continued

AREA	DATE	JULIAN DATE	PASS NUMBER	BAND	SATELLITE	TABLE	SPECIAL FEATURES
Bristol Bay	14 Apr 81	104:05:36:28	9336	#4-IR	N6	64Z	The SST gradients in inner Bristol Bay roughly conform to the isobaths but not as closely as previous years. The cold patch of water is also noticeable. Low clouds near the area should be considered as a possible source of error.
St. Lawrence to the Aleutian Chain	14 Apr 81	104:19:22:47	9344	#1-VIS #4-IR	N6	64P	The feature at 70 m is still present although not as well defined; Bristol Bay still lacks the structure noted before, although there is a slight SST gradient at the 60-m isobath. Clouds obscure the area over the 200-m shelf break.
St. Lawrence to the Aleutian Chain	15 Apr 81	105:05:13:45	9350	#4-IR	N6	64P	The feature at 70 m is not as distinct, and the same holds true for the gradients in Bristol Bay. Overall the water appears much cooler than previously.
Norton Sound to the Aleutian Chain, extending to slightly west of Nunivak Is.	20 Apr 81	110:18:47:17	9429	#1-VIS #4-IR	N6	64Z 6MH	An SST gradient can be seen in Bristol Bay and extending westward. The gradient lines up most closely with the 60-m isobath. A thin band of warm water can be seen along the coast, proceeding seaward there is colder water and then upon reaching approx. 50-m isobath warmer water.

APPENDIX. Continued

AREA	DATE	JULIAN DATE	PASS NUMBER	BAND	SATELLITE	TABLE	SPECIAL FEATURES
Nunivak Island to Aleutian Chain, clear in Bristol Bay and over St. Paul	22 Apr 81	112:19:43:30	9458	#4-IR	N6	64Z Zoom 2	The warm band of water is seen along the coast again; the cooler water aligns with the 50-m isobath, warming as you reach the 60-m isobath and proceedings seaward. The Alaska Stream is seen paralleling the Aleutian Chain on the Gulf side. A distinct SST gradient is seen near St. Paul approx. following the 100-m isobath. There is a colder water band which comes down along the right side of the island. Complex SST structure is seen south of the island but clouds obscure any features.
Norton Sound to just south of Pribilof Islands. Clear area extends from Cape Newenham west to St. Matthew and south of Pribilofs	8 May 81	128:20:20:07	9686	#1-VIS #4-IR	N6	64Z 6MH	Several distinct SST gradients are seen in the area around the Pribilof Islands. Most noticeable is the SST contour which follows the 70-m isobath, especially the finger-like extension. The water following this contour is warmer than the onshelf water. Cooler water surrounds St. Paul. There is also the warm band which follows the contours of the shelf break between 100 m to 3000 m; however, in the area of the 70-m canyon, an extension of this warm band follows the 70-m finger-like structure. Also there are warmer patches imposed on the warm band in a circle-like pattern. the 6MH table gives greater detail in the warm section and better distinction between cloud and water in the case of spring temperatures.

APPENDIX. Continued

AREA	DATE	JULIAN DATE	PASS NUMBER	BAND	SATELLITE	TABLE	SPECIAL FEATURES
Norton Sound to Aleutian Chain. Clear from Bristol Bay to west of St. Matthew and south of the Pribilof Islands	9 May 81	129:19:57:50	9700	#1-VIS #4-IR	N6	64Z 6MH	The most noticeable features are the SST gradients near the shelf break. In Bristol Bay only one gradient can be seen, and that is aligned with the 60-m contour. There is still a band of warmer water along the coast, but it is much thinner. The extension of warm water up the 70-m finger-like contour is still very distinct and again there is cooler water surrounding St. Paul. The warm band over the shelf break is very well pronounced, and curves around in the area near Zhemchung Canyon. On the southeast area, warmer water is imposed on the warm band and some complex structure can be seen with this portion. Again the 6MH table yields more warm water detail and gives good distinction between cloud and sea surface.
Area around the Aleutian Islands and the Pribilof Islands	27 May 81	147:19:51:13	9956		N6	64Z Zoom 2	The area around the open water is heavily contaminated with clouds — and hence the image should be considered less dependable. No structure appears.
St. Matthew to St. Paul as far east as Bristol Bay	28 May 81	148:19:27:17	9970		N6	64Z Zoom 2	Also heavy cloud contamination. However, an area of cooler water can be seen surrounding St. Paul.
Bristol Bay to Kodiak Island	17 Jun 81	168:18:32:50	10254		N6	64X Zoom 2	A large number of well defined SST gradients in Bristol Bay; most all near shore, roughly corresponding with depth contours. An area of much cooler water can be seen in the middle of the May at approx. 50 m.

APPENDIX. Continued

AREA	DATE	JULIAN DATE	PASS NUMBER	BAND	SATELLITE	TABLE	SPECIAL FEATURES
Bristol Bay to St. Paul	18 Jun 81	169:19:51:02	10269		N6	64X Zoom 2	The same inshore gradients (as described above) are seen. Along the Aleutian Chain there is a puddle of warmer water sitting between the 60-m and 100-m isobaths and extending westward to Cape Newenham. Along the 100-m contour, near Unimak Pass, small eddy-like features are seen. Again, St. Paul is surrounded by cooler water.
Western Bering Sea, Attu and Amchitka Islands of Aleutian Chain	27 Jul 81	208:20:04:20	10824	#1-VIS #3-IR #4-IR	N6	63X 64X 64V	Band 3 was included to facilitate a vapor correction; however, the image showed that for the open water temp. range, the sensor was noisy. Some clouds were black, indicating they were higher, but cool clouds; others were white, indicating lower, colder clouds. In the area near Zhemchung Canyon, approximately 3600 m, there was a large, diffuse cyclonic warm water feature. No other structure was noticeable.
Aleutian Islands from Unimak Pass to Amchitka Pass	28 Jul 81	209:19:42:30	10838	#1-VIS #4-IR	N6	64X 64Z	Clouds obscured all of a small portion of the islands near Amchitka Pass. Water on the Bering side appeared very warm with some indications of mixing with cooler water.
Bristol Bay	3 Aug 81	215:19:04:50	10923	#4-IR	N6	64X Zoom 2	The cold spot offshore of the 50-m isobath is visible. Also, SST gradients paralleling the 50-, 60-, and 70-m gradients are pronounced. The water becomes colder as one moves offshore and becomes warmer south of the pool of cooler water between the 50-70 m isobaths.

APPENDIX. Continued

AREA	DATE	JULIAN DATE	PASS NUMBER	BAND	SATELLITE	TABLE	SPECIAL FEATURES
Bristol Bay	4 Aug 81	216:18:42:03	10937	#1-VIS #3-IR #4-IR	N6	63M 63X 64X 64V Zoom 2	Band 3 has been used to determine vapor corrections, but again was noisy.
Western Bering Sea	5 Aug 81	217:06:11:42	10944	#3-IR #4-IR	N6	63X 64X	Same as above.
Western Bering Sea. Sequam I. to Attu I.	5 Aug 81	217:20:00:40	10952	#1-VIS #3-IR #4-IR	N6	63X 64X 64V	Band 3 was chosen to do a vapor correction. This image showed 70% of the area covered by black clouds, indicating they are very high. There were a few streaks of white (cooler, lower) clouds over the Bering Sea north of the islands. Although Band 3 was noisy, it still indicated cooler water temperatures around the islands from Seguam I. to Kiska I. The 64X enhancement showed cool water around the island with an eddy-like feature near Kiska I. and in Amchitka Pass. Caution must be used in discerning clouds vs. water with this table. The 64V enhancement revealed the same eddy like features. They are anticyclonic with a cool ring and warm cores. Clouds mask most all other features.